Emulating Fermi-Hubbard physics with quantum dots from few to more and how to

Hensgens, Toivo

DOI
10.4233/uuid:b71f3b0b-73a0-4996-896c-84ed43e72035

Publication date
2018

Document Version
Final published version

Citation (APA)
Hensgens, T. (2018). *Emulating Fermi-Hubbard physics with quantum dots: from few to more and how to*. [Dissertation (TU Delft), Delft University of Technology]. https://doi.org/10.4233/uuid:b71f3b0b-73a0-4996-896c-84ed43e72035

Emulating Fermi-Hubbard physics with quantum dots

from few to more and how to

Emulating Fermi-Hubbard physics with quantum dots

from few to more and how to

Proefschrift

ter verkrijging van de graad van doctor
aan de Technische Universiteit Delft,
op gezag van de Rector Magnificus prof. dr. ir. T.H.J.J. Van der Hagen,
voorzitter van het College voor Promoties,
in het openbaar te verdedigen op woensdag 10 januari 2018 om 12:30 uur

door

Toivo Hensgens

Master of Advanced Studies in Experimental and Theoretical Physics,
University of Cambridge, Verenigd Koninkrijk

geboren te Heerlen, Nederland

Dit proefschrift is goedgekeurd door de

promotor: prof. dr. ir. L.M.K. Vandersypen

Samenstelling promotiecommissie:

Rector Magnificus,	voorzitter
Prof. dr. ir. L.M.K. Vandersypen	Technische Universiteit Delft
Onafhankelijke leden:	
Prof. dr. ir. R. Hanson	Technische Universiteit Delft
Prof. dr. ir. L. P. Kouwenhoven	Technische Universiteit Delft
Prof. dr. M.I. Katsnelson	Radboud Universiteit
Prof. dr. K. Ensslin	Eidgenössische Technische Hochschule Zürich, Zwitserland
Prof. dr. D.A.M. Vanmaekelbergh	Universiteit Utrecht
Dr. M. Veldhorst	Technische Universiteit Delft

Casimir PhD Series, Delft-Leiden 2017-47, ISBN 978-90-8593-331-1

Geprint door Gildeprint, omslag door Cheyenne Hensgens

Een elektronische versie van dit proefschrift is te vinden op
http://repository.tudelft.nl/.

Our imagination is stretched to the utmost, not as in fiction,
to imagine things which are not really there, but just
to comprehend those things which are there.

Richard P. Feynman

Contents

1

Introduction

Tyger Tyger, burning bright,
In the forests of the night;
What immortal hand or eye,
Could frame thy fearful symmetry?

from *The Tyger* by William Blake

Nothing in life is to be feared,
it is only to be understood

Marie Skłodowska-Curie

1.1. Enabling the second quantum revolution

Many of the technologies we enjoy today, such as our telephones, computers and the internet, would not have been realized without a basic understanding of the quantum mechanical behavior of non-interacting particles. The physics of semiconductor materials, where the individual electrons that make up electrical current flow in a non-interacting and wave-like manner, stands out in particular. Most laser and transistor hardware, cornerstones of nearly all modern technologies, depend on it. To put the potential of this scientific genie that got out of the bottle in perspective: if advances in car manufacturing would have kept pace with the exponential Moore's law advances in computing [1] made possible by the physics of semiconductors, we would by now be able to buy new cars at less than a cent. Spending but another cent on fuel, such a car could drive us across the globe many times over at cruising velocities beyond the speed of light.

The quantum technologies we use in our day-to-day lives, however, represent only a tiny fraction of the phenomena allowed by the rich underlying physics. Sustained research and development is underway into what has been called the Second Quantum Revolution. Its goal is to unlock ever more of the potential of quantum physics as a driver for advances in computing, communication and metrology [2]. These efforts are no longer limited to university research groups and government institutes, but extend to globally active industrial players. Amongst other things, they aim to implement quantum key distribution schemes (where communication encryption is set up securely using the no-cloning law of quantum physics and relativity), quantum annealing (as a resource for the optimization codes underpinning machine learning and artificial intelligence) and universal and fault-tolerant quantum computing (for classes of otherwise classically intractable computing tasks).

What is new about these technologies is how they utilize the concept of quantum correlations, or entanglement, as particles are made to interact in controlled ways. Imagine the two of us have two marbles, one red and one blue. Imagine next that we put them in a bag, shake the bag, blindly take one each and subsequently part ways. We might not know which color of marble we have in our pockets, but the correlation is clear: when you sneak a peek and see that yours is blue, you know mine to be red. Furthermore, you are convinced that yours was blue all along, leaving little room for tricks to be played in the period between our separation and your peek. As it turns out, however, if we replace the marbles and their colour by single electrons and their internal magnetic moment, or spin, this need not be the case. Until the moment you checked for the spin of your electron, the spins were indeed correlated, but the individual ones need not have been defined yet! Instead, they found themselves to be in a so-called *entangled state* [3]. These entangled states are the yet to be fully utilized tool that quantum physics provides us with. They allow for additional tricks to be played, tricks that open up a whole world of color (such as the implementations mentioned above) to the palette of the "quantum engineer".

Even without the rules of quantum mechanics, it is well known that an increase in system size allows for an increase of complexity and for many novel and potentially useful properties to show up. This idea of *emergence* is perhaps best captured by Phil Anderson in his 1976 paper "More is Different" [4]. In it, he argues that as some well-defined system increases in size, its symmetries tend to break and novel, emergent phenomena arise. These phenomena are to be understood using vastly different theories than the one pertaining to their underlying constituents, requiring new language (or even branches of science) to be effectively described. As a living example: it takes many broken symmetries to have a cell emerge from a blob of fundamental particles. It takes many further broken symmetries to enable functional diversification at embryonic growth [5], from which finally emerges William Blake's *Tyger*, whose countenance has but one clear, albeit striking, symmetry left.

The sheer number of interacting electrons one can find in materials means they can exhibit entanglement at an enormous scale, in turn allowing the host materials to exhibit many possible novel electrical and magnetic properties. Entanglement provides the potential for exponential scaling of complexity with system size and thus for a near-infinite stack of emergent phenomena. As an example of a surprising and potentially very useful feature of materials with strongly-correlated electrons, or *quantum matter*, consider high temperature superconductors. They constitute a class of materials in which interacting electrons on their material lattice exhibit a lossless flow of current up to surprisingly high temperatures [6].

Our understanding of quantum matter, however, is severely limited by the classical (meaning conventional or non-quantum) tools at our disposal. The exact coupling mechanism that leads to high temperature superconductivity, for instance, is unknown, even though we know exactly the forces that the individual electrons feel. This ignorance greatly hinders the synthesis of materials that could exhibit superconductivity at room temperature. As Richard Feynman put it: "Nature isn't classical, dammit, and if you want to make a simulation of nature, you'd better make it quantum mechanical, and by golly it's a wonderful problem, because it doesn't look so easy" [7]. As an example, in order to compute with all states of a system of electrons on a lattice of ten-by-ten sites on a classical computing system simultaneously, we would have to make a machine that has more transistors than the number of atoms in the visible universe (estimated to be roughly 10^{80}). As we will never have access to such a machine, the potential of quantum matter to kick-start new technologies goes unused.

One potential roadmap to understanding quantum matter lies in the construction of artificial systems of interacting particles that can be made to emulate underlying models, so-called quantum simulation. Following Feynman's proposal, quantum simulation allows us to harness the knowledge that similar equations yield similar solutions. By turning the knobs of the artificial system and seeing what happens, we learn about the model under investigation. And indeed, multiple experimental platforms are employed in this ongoing effort to emulate the quantum physics of interacting particles. Some exemplary animals in the petting zoo

of tamed quantum systems include linear arrays of ions trapped in fast-changing electric fields, atoms cooled to near perfection and confined by standing wave optical light fields and arrays of coupled superconducting circuits [8].

A particularly promising, controllable system for quantum simulation is comprised of artificial lattices of conduction band electrons, confined using a combination of semiconductor band engineering and gate electrostatics. In essence, a *quantum dot array* constitutes an array of miniaturized transistors. At each individual site, a single electron can be stored and its charge and spin degrees of freedom controlled [9]. Labs around the world are working on quantum dots as building blocks for quantum computing, enthused by the potential for long-lived quantum states, all-electrical control and integration with conventional and industrial-grade nanofabrication protocols. On top of this, these arrays of electrostatically confined electrons constitute almost exactly (a scaled version of) the electronic lattices of quantum matter, and as such provide a natural platform for their emulation. Furthermore, one can hope to leverage ongoing advances in the field of using quantum dots for quantum computing, trading off some of the difficulties involved in full coherent control for ease of scaling.

However, quantum dot experiments have so far been restricted to small arrays of several sites only, limited by the intrinsic electrostatic disorder of the semiconductor substrates and imperfections in the fabrication process. Controlled scaling to larger device sizes is exactly one of the most difficult aspects of the platform [10]! Furthermore, even for the small arrays that have been realized, the control shown for quantum computing purposes constitutes only a small part of the full parameter space one would like to access. In order to utilize quantum dots as a platform for quantum simulation of quantum matter and unlock the potential for materials with novel electrical and magnetic properties, we need to find solutions to these problems.

In this thesis, I work to overcome problems of disorder and control, and with that break new ground by establishing quantum dots as a plausible platform for quantum simulations of the strongly-correlated electronic phases of quantum matter. To do so, we have adopted two approaches. A top-down approach allows us to scale to large devices easily, but without the ability to control or measure individual sites. This means that reducing disorder and inhomogeneity through clever wafer design and fabrication is paramount. A bottom-up approach utilizes the small quantum dot devices that the community has been making for qubit experiments, in which control of individual sites is both a blessing (allowing for the negation of inhomogeneity) and a curse (difficult and time consuming). We address the issue of control to the point where mapping to the relevant model is possible and efficiently calibrating larger devices becomes feasible. These results open up the inherently well-suited and scalable platform of quantum dots to emulate novel quantum states of matter.

1.2. Thesis outline

First, in **Chapter 2**, I introduce a generic model for interacting electrons on a lattice, the so-called Fermi-Hubbard model, its parameters and derivative models. Furthermore, I show how quantum dot arrays constitute a natural platform for the emulation of electron lattices by readily adhering to a generalized version of this model.

After that, I present our efforts in trying to reduce the disorder and associated inhomogeneity to the level where we can scale up the size of quantum dot arrays without the need of additional site-specific electrical control (**Chapter 3**). In this approach, we employ a capacitance spectroscopy technique that allows both global control and read-out.

In parallel, we have developed a toolbox for calibrating the more commonly used small dot arrays, whose sites have to be controlled individually. I describe these novel concepts and techniques in **Chapter 4**. They allow us to map the parameters of quantum dot arrays to those of the physical models we want to emulate.

Exactly this is done in **Chapter 5** as we emulate a finite-size analogue of the interaction-driven metal-to-insulator transition, or Mott transition. Our toolbox and the results are verified using computer calculations and serve as an example of the potential for quantum dots to emulate strongly-correlated electron systems.

Lastly, I look ahead at what can be realized in the near future using these ideas in **Chapter 6**, linking theoretical proposals to the detailed requirements, opportunities and limitations of the quantum dot platform, as well as to ongoing roadmaps for improving quantum dot systems. A conclusion is reached in **Chapter 7**.

References

[1] G. Moore, "The Future of Integrated Electronics," *Fairshild Semiconductor*, 1964.

[2] European Commission, "Quantum Technologies Flagship Intermediate Report," 2017.

[3] E. Schrödinger, "Discussion of probability relations between separated systems," *Mathematical Proceedings of the Cambridge Philosophical Society*, vol. 31, pp. 555–563, 1935.

[4] P. W. Anderson, "More is different," *Science (New York, N.Y.)*, vol. 177, pp. 393–6, 8 1972.

[5] R. Li and B. Bowerman, "Symmetry breaking in biology.," *Cold Spring Harbor perspectives in biology*, vol. 2, p. a003475, 3 2010.

[6] B. Keimer, S. A. Kivelson, M. R. Norman, S. Uchida, and J. Zaanen, "From quantum matter to high-temperature superconductivity in copper oxides," *Nature*, vol. 518, pp. 179–186, 2015.

[7] R. P. Feynman, "Simulating Physics with Computers," *Int. J. Theor. Phys.*, vol. 21, p. 467, 1982.

[8] J. I. Cirac and P. Zoller, "Goals and opportunities in quantum simulation," *Nature Physics*, vol. 8, pp. 264–266, 4 2012.

[9] L. Vandersypen, "Dot-To-Dot Design," *IEEE Spectrum*, vol. 44, pp. 42–47, 9 2007.

[10] F. A. Zwanenburg, A. S. Dzurak, A. Morello, M. Y. Simmons, L. C. L. Hollenberg, G. Klimeck, S. Rogge, S. N. Coppersmith, and M. A. Eriksson, "Silicon quantum electronics," *Reviews of Modern Physics*, vol. 85, pp. 961–1019, 7 2013.

2

Hubbard model description of quantum dots

Quantum dot lattices have the potential to emulate the poorly understood strongly-correlated electronic phases that lead to novel electrical and magnetic properties of materials, as introduced in the previous chapter. Part of what makes quantum dots so suitable is that they readily adhere to a generalized version of the model describing interacting electrons on a lattice. That so-called Fermi-Hubbard model is the focus of this chapter and is introduced in **Section 2.1**. The interaction terms can be understood in direct analogy with the theory of capacitively coupled dots and are described in **Section 2.2**. As electrons are also allowed to quantum tunnel between sites in **Section 2.3**, the mapping is complete. Finally, I discuss how from the generalized Fermi-Hubbard model other models can emerge which in themselves are of particular theoretical and experimental interest, in **Section 2.4**.

2.1. The Fermi-Hubbard model

Electronic properties of materials are typically well understood in the limits of localized and delocalized electrons. In the case of the former, electronic states closely resemble those of atomic orbitals around individual atoms, with small corrections formed by the finite overlap of adjacent orbitals. Such states are well described by tight-binding models, of which the Heitler-London model of the hydrogen molecule is a prime example [1]. The resulting electronic bands are very narrow, and will be close in energy to the orbitals of individual atoms. In the case of the latter, the atomic potentials can be seen as a mere perturbation acting on a gas of electrons, in the so-called nearly-free electron model. Bands are wide and electronic states are best described in Fourier space, as waves in a Bloch-band picture [2]. In both these limits, electronic interactions can be neglected, either because they freeze out degrees of freedom by posing insurmountable energetic hurdles for the low-energy excitations that govern the electronic properties (former) or because they are too weak to influence them significantly (latter).

It has been long clear, however, that in the intermediate case of narrow bands, Coulomb-induced electron-electron interactions cannot be neglected. In an attempt at describing the correlation effects seen for such intermediate cases, Hubbard derived a simple model that now bears his name [3]. By assuming fairly localized electronic states (which means electrons only interact when they are on the same site) and subtracting the energy offset on each site (as all unit cells are assumed to be equal) we are left with two terms only. The first term describes the delocalized nature of the electronic states given some tunneling energy t, similar to the finite overlap of adjacent orbitals in the Heitler-London model. The second term describes the on-site Coulomb repulsion, or Hubbard interaction energy U. This is the energy penalty for placing two electrons on the same site, which effectively tries to force localization. As we focus on one particular atomic orbital (a so-called single-band picture), each site i can be occupied once with a spin-up $\sigma = \uparrow$ and once with a spin-down electron $\sigma = \downarrow$, and we get:

$$H = \underbrace{-t \sum_{\langle i,j \rangle, \sigma} (c^\dagger_{i\sigma} c_{j\sigma} + \text{h.c.})}_{H_{\text{tunneling}}} + \underbrace{\frac{U}{2} \sum_i n_i (n_i - 1)}_{H_{\text{interaction}}} \tag{2.1}$$

in a second quantized picture with site-and-spin-specific electronic (Fermionic) creation and annihilation operators $c^\dagger_{i\sigma}$ and $c_{i\sigma}$ and site occupations $n_i = \sum_\sigma c^\dagger_{i\sigma} c_{i\sigma}$.

The resulting picture is deceptively simple: that of a lattice of sites that are up to doubly occupied by electrons (given they form a spin-singlet state and at a cost U) which themselves are allowed to quantum tunnel between those sites at a certain rate described by t (Fig 2.1). In the limit of $t \ll U$ interactions reign supreme, splitting the spectrum into two Hubbard bands denoting either singly or doubly occupied sites, respectively. At one electron per site (so-called half filling, in which the lower Hubbard band is fully occupied) the lattice is described by a single-particle

tight-binding picture. In the limit of $U \ll t$ we can ignore interactions altogether, regaining the all familiar band-physics.

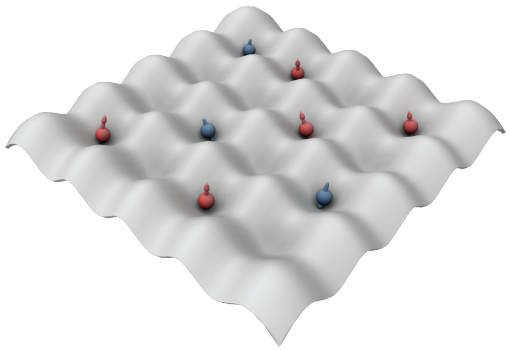

Figure 2.1: Impression of the two-dimensional Hubbard model. Two-dimensional potential lattice is shown, hosting a number of spin-up (red) and spin-down (blue) electrons. As the potential for motion of one particular electron depends on the location and spin of close by electrons, we see how electronic and magnetic properties in such a system can be governed by interactions, and emergent properties can arise.

Note the role of dimensionality on the behavior of a system described by the Hubbard model. As the number of directions in which an electron can evade interacting with neighboring electrons grows with the number of dimensions, it is not surprising that the strongest quantum correlation effects are typically found in one- and two-dimensional systems. Indeed, most of the yet-to-be-fully-understood emergent electronic and magnetic properties of materials with narrow bands result from correlation effects of electrons confined to effectively decoupled one- to two-dimensional sub-lattices [4, 5].

2.2. Theory of classically coupled quantum dots

As the name implies, the confinement potential, or lattice, for gate-defined quantum dots derives from the electrostatic control offered by gates, instead of the atomic potential of the material lattices Hubbard was trying to describe. This invalidates some of the assumptions that Hubbard took, leading us to use a slightly larger Hamiltonian to the Hubbard model in describing quantum dot systems, a resulting model that I will gradually introduce below.

First, we will ignore the tunnel coupling and describe the system of classically (capacitively) coupled quantum dots as well as introduce the concept of charge addition spectra. In the next section, we add in again the tunnel coupling, finalizing the Hamiltonian that will be prevalent throughout this thesis and showing in particular how charge addition spectra are modified by such hybridization effects. Lastly, we describe several emergent models, models that describe the low-energy excita-

tions of subsets of unfrozen degrees of freedom, given some parameter values and electron fillings.

So let us start by ignoring the tunnel coupling and changing our terminology: instead of speaking about sites on a lattice we will discuss (quantum) dots on a (quantum dot) array. In this classical limit of $t = 0$ life is easy, as we can denote the resulting states s describing the array simply by listing the charge occupations $(n_1, n_2, ..)$ of the individual dots. This ignores potential degeneracies of particular charge states due to the spin degree of freedom, but that will not concern us for now.

Unlike the potential lattice provided by atoms in a material, not all quantum dots in a gate-defined array are necessarily the same. That forces us to do some more bookkeeping, as we have to deal with the fact that any energy term becomes site-dependent ($U \rightarrow U_i$ and so on). It also means we have to add a term that Hubbard himself dropped, as it leads only to a constant offset in a perfect lattice: the site-specific detuning, which takes into account for each site the single-particle energy offset ϵ_i of the n_i electrons inhabiting it.

Furthermore, we cannot neglect Coulomb interactions between sites, an effect which is taken into account by adding an energy penalty V_{ij} when sites i and j are occupied by n_i and n_j particles, respectively. A model with such a term added is typically referred to as an *extended Hubbard model* [4]. Adding up what we have discussed so far, we get the total energy (I could write it down as a Hamiltonian, but that Hamiltonian is of course readily diagonalized in this classical limit):

$$E_s = -\sum_i \epsilon_i n_i + \sum_i \frac{U_i}{2} n_i(n_i - 1) + \sum_{i,j} V_{ij} n_i n_j \tag{2.2}$$

In the early days of quantum dots, and still now sometimes, actually, one finds experimentalists model their quantum dot systems by describing a spider web of capacitances between gates, dot potentials and the electrical ground [6]. This so-called constant interaction model might be appealing for device physicists as it directly describes the electrostatic couplings that a device design imposes, but is an inherently indirect (overly elaborate) and classical (fundamentally insufficient) method for describing the electronic states in the array itself. Only slowly did experimentalists take over the view of their more condensed-matter aware theory colleagues to model dots in a Hubbard perspective [7], with the mapping between both views formally established relatively recently [8].

Having formalized a classical model in Eq. 2.2, we can now start putting it to use. As experimentally it is the charge state of a quantum dot array exchanging electrons with adjacent reservoirs that is measured, it is the charge addition spectrum that merits our focus. As such, we are interested in some classical thermodynamics. Introducing the (electronic or *Fermi*) reservoir at chemical potential μ and temperature $k_B T$, we can describe the charge addition spectrum $\frac{\partial \langle N \rangle}{\partial \mu}$ within classical thermodynamics using simple Boltzmann-weighted sums:

$$\frac{\partial\langle N\rangle}{\partial\mu} = \frac{\langle N^2\rangle - \langle N\rangle^2}{k_B T} \quad \text{with} \quad \langle N^k\rangle = \sum_s N_s^k \exp[\frac{E_s - \mu N_s}{k_B T}] \tag{2.3}$$

where $N = \sum_i n_i$ counts the total number of electrons in the system. For $\frac{\partial\langle N\rangle}{\partial\mu} \neq 0$ the system will be allowed to exchange particles with the reservoir. In a typical measurement, we make a two-dimensional map of the charge stability as experimental voltages are changes, inducing changes in μ or the ϵ_i. Such a map is called a *charge stability diagram*, and some examples are shown below. Note that these diagrams are essentially visualizations of particular two-dimensional slices of the (higher-dimensional) charge addition spectrum.

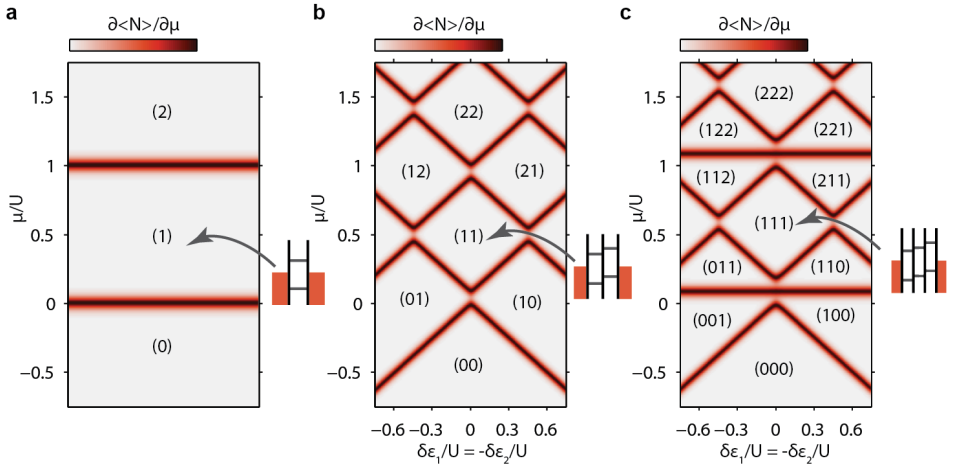

Figure 2.2: Charge stability diagrams. Simulated charge stability diagrams for a single (**a**), double (**a**) and triple quantum dot (**c**). Given a clever choice of axes, in this case potential (vertical) and distinguishable dot detunings (horizontal), identifying for what parameters different charge states are energetically preferred becomes obvious. Note that for the single-dot case shown in (**a**) there is no relevant detuning to show, and text in brackets denotes the local equilibrium charge state. Instead of these particular two-dimensional cuts in the charge stability spectrum, we can also take some set of parameters (i.e. focus on one point in charge stability, as depicted by the arrows) and vary the three detunings ϵ_i's individually, resulting in a ladder diagram representation of charge stability (inset). Rungs in the ladder depict detunings for which charge states with local occupations differing by one electron become degenerate, and thus correspond to charge addition.

We will see in Chapter 4 that the control of the quantum dot systems hinges on the measurement and interpretation of diagrams such as those shown in Fig 2.2. As an example, the size of charge states in a charge stability diagram is indicative of the interaction energies U_i. Furthermore, note that I have tried to consequently employ red colormaps for (computer) simulations, blue colormaps for experimental data,

and blue-white-red colormaps for data with both polarities and a well-defined zero (white).

2.3. Adding quantum fluctuations

As it turns out, tunnel couplings are typically much smaller than interaction effects in experiments, and as such do not influence the charge addition spectrum strongly. Nonetheless, without tunnel coupling the system is fully classical, so let us look at what happens when we add it back into the mix. This results in the following total Hamiltonian:

$$H = \underbrace{-\sum_i \epsilon_i n_i}_{H_{\text{detuning}}} \underbrace{- \sum_{\langle i,j\rangle,\sigma} t_{ij}(c^\dagger_{i\sigma} c_{j\sigma} + \text{h.c.})}_{H_{\text{tunneling}}} + \underbrace{\sum_i \frac{U_i}{2} n_i(n_i - 1) + \sum_{i,j} V_{ij} n_i n_j}_{H_{\text{interaction}}} \tag{2.4}$$

If we want to model the thermodynamic charge stability of this quantum system as it is coupled to a reservoir, we can do it using:

$$\frac{\partial \langle N\rangle}{\partial \mu} = k_B T \frac{\partial^2 \ln \mathcal{Z}}{\partial \mu^2} \quad \text{with} \quad \mathcal{Z} = \text{Tr}\{\exp[-(H - \mu N)/k_B T]\} \tag{2.5}$$

where $\mathcal{Z}$ is the partition function. Note that the Hamiltonian of Eq. 2.4 implicitly describes a single band only, whereas each physical dot can easily be filled with more than two electrons. A more complete simulation would take into account the orbital degree of freedom on each dot as well as the single-particle energy offsets associated with them [6]. It is justified from the point of view of charge stability diagrams, however, to focus on the addition of the next two electrons per dot within a single, effective, band picture [9].

The added effect of tunnel coupling hybridizes states where a single electron is free to hop between adjacent dots, and thus has most impact when these charge states are nearly degenerate. At this point, the charge states anti cross and bonding and antibonding states are formed, similar to the Heitler-London model. This serves as a starting point for a *charge qubit*, using the relative location of the electron as the unit of information. For our purposes, however, what is most important is that as the bonding state is at a lower energy than the uncoupled states, it becomes energetically more favorable in the charge stability diagram, and as such starts to occupy a larger space, effectively bending nearby charge addition lines. For a larger number of dots, this will gradually deform the charge stability into one that looks to be describing a single dot (i.e. a gradual change from diagrams such as that of Fig. 2.2c to one resembling Fig. 2.2a)

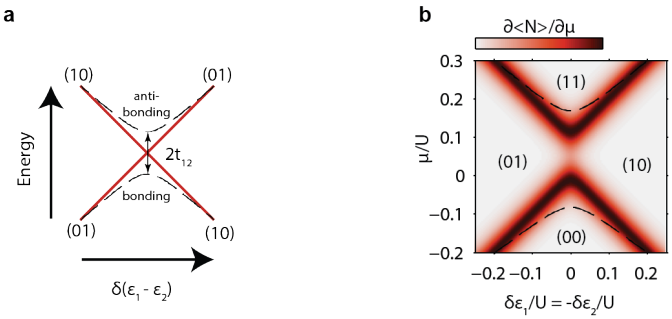

Figure 2.3: Effect of hybridization on charge stability diagrams. At increasing tunnel coupling, charge states hybridize as schematically shown in **a**. The charge states are shown in red, with the hybridized spectrum depicted with black, dashed lines. The effect on the charge stability diagram becomes apparent first at anti crossings, where two tunnel-coupled charge states are (close to) degenerate. The energy gained by the bonding state stabilizes the single-particles states (01) and (10) close to their transition, which in turn pushes out the charge addition lines at which they are degenerate with the empty (00) and doubly occupied (11) states. This effectively bends them outwards as indicated by the black, dashed lines in **b**.

2.4. Emergent models

Imagine a homogeneous lattice with strong local Coulomb repulsion, filled with one electron per site. In this case, any excitation in the charge sector would entail the creation of a double occupation at a large cost in energy. Focusing on smaller excitations, therefore, only the local spins on each site are relevant and we find ourselves describing the physics of an array of spin-1/2 particles.

This constitutes one example of an emergent model, and shows how Eq. 2.4 can be used to study different types of physics, in this case a particular model in quantum magnetism (the Heisenberg model [10]). As magnetic fields can split the local spin-up and spin-down states and virtual hopping events can lead to the coupling of these spins via so-called direct exchange, such quantum magnetism is conceptually close to the physics used to define *spin qubits* and their coupling gates [11].

In Chapter 6, we will introduce some of these emergent models in more detail, as they allow us to use the Hubbard model description of quantum dots to emulate different physical phenomena. Note that in general, one can distinguish two types of analog quantum simulation. First, one can reproduce 'textbook examples' of models that are well understood, in order to showcase the potential or give further insight (these are typically interesting single-particle models or small many-body states), but secondly, one can try to simulate less understood phases (which typically entails larger and strongly-correlated electronic states).

References

[1] W. Heitler and F. London, "Wechselwirkung neutraler Atome und homöopolare Bindung nach der Quantenmechanik," *Zeitschrift für Physik*, vol. 44, pp. 455–472, 1927.

[2] F. Bloch, "Über die Quantenmechanik der Elektronen in Kristallgittern," *Zeitschrift für Physik*, vol. 52, pp. 555–600, 7 1929.

[3] J. Hubbard, "Electron Correlations in Narrow Energy Bands," *Proceedings of the Royal Society A: Mathematical, Physical and Engineering Sciences*, vol. 276, pp. 238–257, 1963.

[4] M. Imada, A. Fujimori, and Y. Tokura, "Metal-insulator transitions," *Reviews of Modern Physics*, vol. 70, pp. 1039–1263, 10 1998.

[5] P. A. Lee, N. Nagaosa, and X.-G. Wen, "Doping a Mott insulator: Physics of high-temperature superconductivity," *Reviews of Modern Physics*, vol. 78, pp. 17–85, 1 2006.

[6] R. Hanson, L. P. Kouwenhoven, J. R. Petta, S. Tarucha, and L. M. K. Vandersypen, "Spins in few-electron quantum dots," *Reviews of Modern Physics*, vol. 79, pp. 1217–1265, 10 2007.

[7] L. Gaudreau, S. A. Studenikin, A. S. Sachrajda, P. Zawadzki, A. Kam, J. Lapointe, M. Korkusinski, and P. Hawrylak, "Stability Diagram of a Few-Electron Triple Dot," *Physical Review Letters*, vol. 97, p. 036807, 7 2006.

[8] S. Yang, X. Wang, and S. Das Sarma, "Generic Hubbard model description of semiconductor quantum-dot spin qubits," *Physical Review B*, vol. 83, p. 161301, 4 2011.

[9] X. Wang, S. Yang, and S. Das Sarma, "Quantum theory of the charge-stability diagram of semiconductor double-quantum-dot systems," *Physical Review B*, vol. 84, p. 115301, 9 2011.

[10] C. L. Cleveland and R. Medina A., "Obtaining a Heisenberg Hamiltonian from the Hubbard model," *American Journal of Physics*, vol. 44, pp. 44–46, 1 1976.

[11] D. Loss and D. P. DiVincenzo, "Quantum computation with quantum dots," *Physical Review A*, vol. 57, pp. 120–126, 1 1998.

3

Towards large quantum dot arrays with global control only

The ability of quantum dots to map onto Hubbard models of interest is only fully leveraged through the synthesis of extended arrays that have well-controlled parameters. These two qualities, however, size and control, are at direct odds. In this chapter, I describe a novel experimental technique for realizing large arrays at the cost of site-specific control. Disorder in the host material and inhomogeneity in fabrication limit not only this technique but quantum dots in general, and are described in **Section 3.1**. By using capacitance spectroscopy (**Section 3.2**), we aim to reduce the effect of disorder, as well as allowing for global measurements of the density of states. However, as described in **Section 3.3**, applying a strong and sufficiently homogeneous periodic potential required for seeing lattice physics is difficult - and our current device quality is assessed. **Section 3.4** concludes with ways in which devices can be improved[1].

[1]The work described in this Chapter can be found in ArXiv 1709.09058.

3.1. Disorder and inhomogeneity

The wave equation physics of quantum mechanical bands has been emulated on several different experimental platforms, most notably and unsurprisingly so at photonic length scales - although adding interactions as well as gauge fields are difficult on such systems [1, 2]. The relevant length scales for electronic systems in semiconductors, however, are sub-micron, at which scale the fabrication of homogeneous periodic structures becomes significantly harder. Furthermore, inherent (charge) disorder felt by electrons in imperfect host materials constitutes a background of disorder, that can overpower any periodic effect [3]. As such, realizing artificial electronic lattices has proven to be quite challenging indeed [4–6].

A notable exception is that of superlattices of graphene on hexagonal boron nitride, which shows Hofstadter's butterfly physics [7–10]. Actually, even fractional quantum Hall states on the butterfly can be observed [11], highlighting the potential of semiconductor superlattices to realize novel phases of interacting electrons.

In general, however, semiconductor heterostructures with electrostatic control using nano-fabricated gates would constitute a most promising platform, as it allows for designer lattices and voltage tunable electron density and lattice strength [12].

Manners in which inherent material disorder can be reduced, a clean and periodic gating can be achieved and read-out can be performed in two-dimensional structures will also prove to be important in assessing the feasibility of scaling of quantum information processors of quantum dots as spin qubits [13], where such disorder-negating site specific control as described in the next chapter might still be possible, but would at any rate constitute a severe experimental overhead.

3.2. Capacitance spectroscopy technique

Capacitive coupling has been long used to study 2D electronic systems [14]. In this chapter, we demonstrate a novel experimental platform that is based on the technique of capacitance spectroscopy, as pioneered by Ashoori as a graduate student, and later added on in his group to study, for instance, exchange effects in Landau levels through excited state spectroscopy [15, 16] as well as the two-dimensional dispersion of a 2DEG [17] and the observation of the vibrations of a Wigner crystal [18].

In a capacitance spectroscopy set-up, a parallel-plate capacitor is formed out of the doped back gate region of a semiconductor wafer and a fabricated top gate (see Fig 3.1). A quantum well grown between the two allows a two-dimensional electron gas (2DEG) to form as electrons tunnel in from the doped back gate, modifying the capacitance between both gates. When the density of states (DOS) in the 2DEG is large, the capacitance is defined by the distance from top gate to 2DEG. When the density of states in the 2DEG is negligible, however, the capacitance is simply described by the distance between the gates. Equivalently, we can measure the capacitance at frequencies above that of electrons tunneling between the

2DEG and the back gate, and the bare capacitance can also be found. This allows for the measurement of the charge addition spectrum of the 2DEG as function of filling and external influences (periodic potential, magnetic field,...). Furthermore, the proximity of mobile carriers in the back gate region screens disorder [12], effectively reducing both intrinsic disorder levels and reducing the impact of short-length-scale imperfections in the fabrication over any longer-length-scale periodic potential we will try to set.

The device capacitance is measured using a capacitance bridge technique, where the amplitude ratio and phase difference between measurement signals applied to the device and a reference capacitor are balanced at the bridge point (red dot in Fig 3.1c), where any remaining voltage fluctuations are amplified at different stages and read out using a lock-in amplifier. The device, reference capacitor and first amplifier are mounted on a home-built printed circuit board (PCB) that is itself mounted on the mixing chamber stage of a dilution refrigerator. Furthermore, the PCB hosts R/C filters for the D/C lines as well as bias-tees for combining D/C and A/C signals and attenuators for the A/C inputs. These attenuators were necessary as we found attenuators in the fridge to lead to ground loop issues. A high-mobility electron transistor (HEMT) is used for the first amplifier, further amplification is built at 0.7 K and at room temperature.

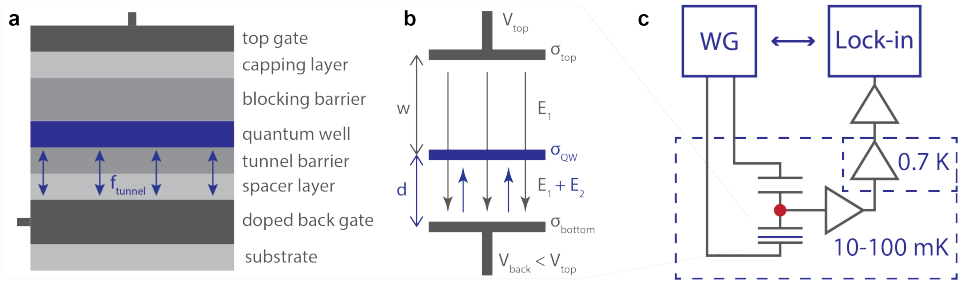

Figure 3.1: Overview of the capacitance spectroscopy technique. A schematic side (cut) view of a device made on a GaAs/AlGaAs heterostructure is shown in **a**, where a 2DEG can form in the quantum well layer as electrons tunnel in from a n-doped back gate layer. We can derive DOS information by modeling the electrostatics as charges are added to a sheet in between two parallel plate capacitor plates, as shown in **b**. The measurement itself is done at the 10 mK stage of a dilution refrigerator set-up, comparing the sample capacitance to that of a reference capacitor in a capacitance bridge (**c**). Measurement excitations are sent using a waveform generator (WG) and iteratively updated depending on the lock-in measurement outcome of the amplified bridge point (red point) voltage.

In order to balance the bridge, an iterative scheme based on a simple secant method is implemented, where the excitation on the sample side is kept at some constant phase ϕ_{sample} and amplitude V_{sample} and the phase ϕ_{ref} and amplitude V_{ref} on the reference side updated. Modeling the bridge as a linear system of complex variables $Y = AX + B$, with reference signal X, lock-in measurement Y and

bridge defined by A and B and given two slightly different inputs X_i and X_{i+1} with respective measurement outcomes Y_i and Y_{i+1}, we calculate A and B and define the next step as $X_{i+2} = -B/A$. Convergence is reached when the amplitude difference between the last two reference signals drops below some reference, typically several parts per thousand of the signal itself. From the final $X_i = V_{\text{ref}} e^{i\phi_{\text{ref}}}$ we infer the sample capacitance $C_{\text{sample}} = C_{\text{ref}} \frac{V_{\text{ref}}}{V_{\text{sample}}} \cos(\pi + \phi_{\text{ref}} - \phi_{\text{sample}})$.

The aim of this set-up is to through modulations in the capacitance derive the electronic spectrum of the 2DEG as function of density, applied field and (later in this chapter) periodic potential. In the procedure for deriving DOS from capacitance data, the device is modeled as a simple parallel plate capacitor (Fig 3.1b), where charges can be added at the quantum well layer. It follows from this schematic that the total capacitance equals $\frac{\partial Q}{\partial V} = A\frac{\partial \sigma_{\text{top}}}{\partial V} = \frac{\epsilon A}{w+d} - \frac{dA}{w+d}\frac{\partial \sigma_{\text{QW}}}{\partial V} +$ small terms that depend on changing distances and which we ignore. The realization that this is the capacitance which is measured at sufficiently low frequencies, whereas at frequencies above the tunnel rate f_{tunnel} the second term is void, allows us to infer changes in the electron density in the 2DEG using $\frac{\partial n}{\partial V} = -\frac{1}{e}\frac{\partial \sigma_{\text{QW}}}{\partial V} = \frac{1}{eA}\frac{w+d}{d}\left(C_{\text{low}} - C_{\text{high}}\right)$. See Fig 3.2 for measurements as function of frequency.

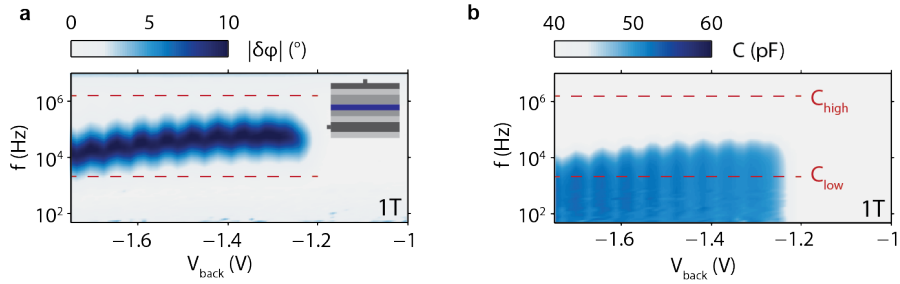

Figure 3.2: Frequency dependence of measured capacitance. Sample phase offset ($\delta\phi = \pi + \phi_{\text{ref}} - \phi_{\text{sample}}$, **a**) and capacitance (**b**) as function of applied back gate bias and measurement frequency of a device with a global metallic gate (see inset) at a perpendicularly applied magnetic field of 1 T. Oscillations in the capacitance and tunnel frequency are due to the formation of Landau levels in the integer quantum Hall effect.

It is clear that a frequency dependent capacitance indicates a non-zero DOS and as such (with changing bias) filling of the 2DEG. In order to extract the DOS, however, we also need to know how the Fermi level in the quantum well changes with changes in gate voltage, the so-called lever arm. This follows from a similar derivation: $\alpha \equiv -e\frac{\partial V}{\partial \mu} = \left(\frac{w}{w+d} + \frac{e}{\epsilon}\frac{wd}{w+d}\frac{\partial n}{\partial V}\right)^{-1}$. For a gapped system ($\delta n = 0$), we find the lever arm to simply be described by the relative distance of the quantum well location between both plates of the capacitor. The second term is due to the quantum capacitance, and becomes the dominant term after accumulation. Using the expressions for density and energy, the DOS is defined through $\frac{\partial n}{\partial \mu} = \frac{\partial n}{\partial V}\frac{\partial V}{\partial \mu} = \frac{1}{e^2 A}\frac{w+d}{d}\alpha\left(C_{\text{low}} - C_{\text{high}}\right)$.

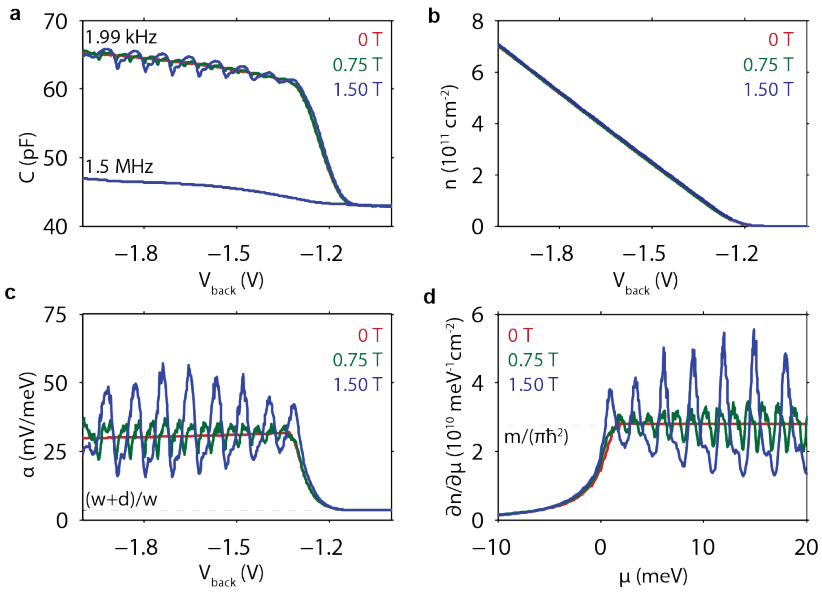

Figure 3.3: Overview of the conversion from capacitance to DOS. From the low and high frequency capacitance (**a**) one can derive (changes in) density (**b**) and lever arm (**c**). Using both, the DOS is found (**d**), where we peg the 0 T DOS after accumulation to the expected value. The same calibration is used for nonzero field values, where for increasing field strength Landau levels get resolved.

There is one unknown in the calibration of DOS, the distance d between back gate and 2DEG. The growth distance can be used as a first guess, but a better estimate can be made using either the known degeneracy or spacing of Landau levels at finite magnetic fields, or the expected value of the DOS at zero field, $\frac{m}{\pi\hbar^2} \approx 2.8\times10^{10}$ meV^{-1}cm^{-2} (Fig 3.3).

3.3. Trying to impose a periodic potential

As discussed in the previous section, capacitance spectroscopy allows for the measurement of the charge addition spectrum of a 2DEG under a global magnetic field. Here we briefly discuss two phenomena that are expected to occur when a periodic potential is applied as well (Fig 3.4). Next we describe two different device designs that would allow for a lattice potential to be applied. Several experimental imperfections of such devices have to be considered, which we do in the rest of this section.

When a weak periodic potential is applied to a 2DEG, gaps of the size of the applied potential modulation open up at the edge of the Brillouin zone, indicating the formation of a miniband that can host two additional electrons per lattice site

as described by the nearly free electron model. As confinement gets stronger with increased potential modulation, electron-electron interactions dominate and minibands split in two as electrons are filled one by one on each site. This constitutes an effective Mott transition [19, 20]. For the capacitance spectroscopy devices, we should therefore look for modulations in the capacitance at densities commensurate with the minibands, as a periodic potential is turned on. For a 200 nm periodic square grid, the expected miniband densities are $5{\times}10^9$ cm^{-2}, which coincide with a period in back gate voltage of 6 mV. The splitting of these bands in two and corresponding doubling in the periodicity would then be indicative of the Mott transition (Fig 3.4a).

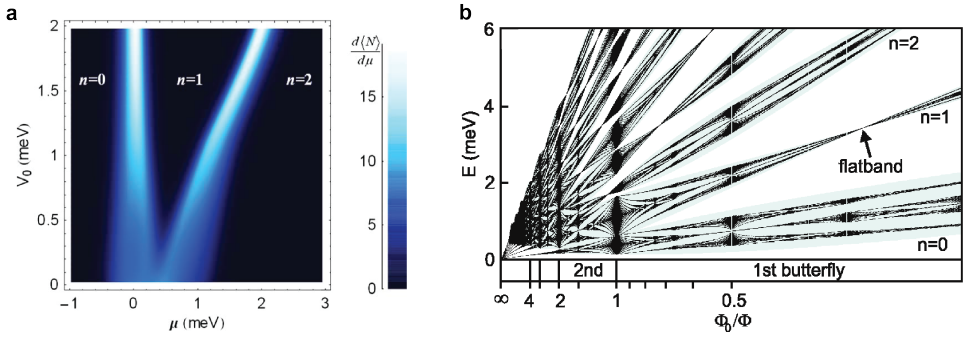

Figure 3.4: Theoretical proposals. As shown in **a**, when an imposed periodic potential (vertical) gets sufficiently strong, on-site repulsion gaps out a half-filled state with increasing Fermi level (horizontal), implying a Mott transition from a metallic nearly free electron state to a Mott insulator state (adapted from [20], a simulation on a 3x3 array with N the total number of electrons, V_0 the amplitude of the potential and n the average number of electrons per site). As shown in **b**, a small periodic potential perturbs the integer quantum Hall fan diagram by modulating the Landau level widths and opening a fractal spectrum of gaps at energies (vertical) and fields (horizontal) corresponding to the frustrated ratio between the magnetic and periodic length scales (adapted from [5]). This ratio depends on the perpendicularly applied magnetic field B and corresponds to the number of flux quanta threading each plaquette of area A as $\Phi/\Phi_0 = AB/\Phi_0$.

In a different and inherently single-particle phenomenon, the joint application of a periodic potential and perpendicularly applied magnetic field leads to a fractal butterfly spectrum [7] as the magnetic length scale describing the discrete magnetic translational symmetry of integer quantum Hall states becomes commensurate or not to the wavelength of the Bloch states on the lattice itself. Gaps open up inside the Landau levels as a repetitive function of the number of excessive flux quanta Φ_0 threading through each lattice site (Fig 3.4b). The largest gaps are expected around $k \pm 1/4$ flux quanta (with k an integer), corresponding to $52k \pm 13$ mT for a 200 nm periodic square grid.

From an experimental point of view, there are three considerations to take into account, three possible device imperfections that would lead to no visible gaps

appearing in the data: (i) the lattice strength does not exceed disorder levels, (ii) the induced modulations in density are too small to be experimentally resolved and (iii) the applied lattice potential is not sufficiently homogeneous[2]. As a start, therefore, we need to assess the disorder levels in our devices.

In the previous section, we have seen how a perpendicularly applied magnetic field modulates the density of states through the formation of Landau levels. Here, we use the visibility of the Landau levels as function of magnetic field as a heuristic metric of inherent disorder levels, given their known spacing and degeneracy (Fig 3.5). Note that for larger magnetic field, exchange enhanced Zeeman splitting becomes visible as well, highlighting that interaction effects become important for increasingly confined electrons (Fig 3.5a). In Fig 3.5b, the charge addition spectrum at low field values is shown, tracing out a Landau "fan" diagram. Gaussian fits to individual levels yield typical level broadening of 0.4-1 T. The levels get resolved at fields of roughly 0.25 T, corresponding to densities per level of 1.2×10^{10} cm^{-2} and cyclotron gaps of 0.43 meV. As a check, we have applied small changes in temperature and excitation voltage, which do not change Landau level widths. Also, we consistently measure similar results on different fabrication runs and schemes. We therefore regard these numbers in density and energy as a heuristic metric for the achievable disorder levels of particular wafers, and have striven to optimize heterostructure design to minimize them.

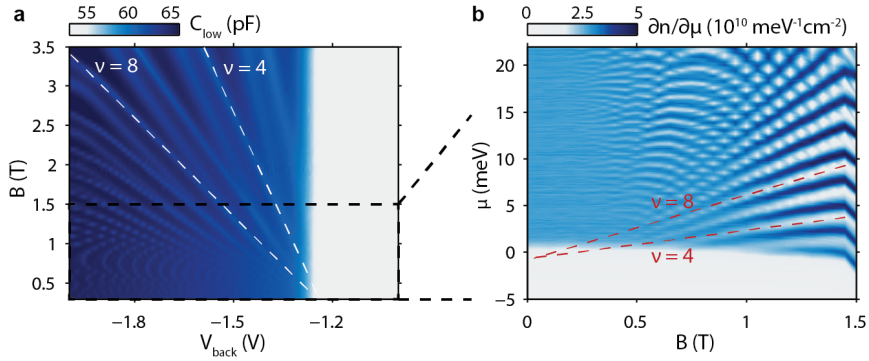

Figure 3.5: Landau fan diagram to assess intrinsic disorder level. Low frequency capacitance as function of applied back gate bias and field (**a**) for a device with a single global top gate, and the low-field regime converted to a charge addition spectrum (**b**). Landau level visibility is a hallmark of intrinsic disorder levels, given the known linear dependence of degeneracy and spacing on applied field strength. Note also how Landau levels split at fields over 2 T as exchanged-enhanced gaps open up. The gaps at filling factors $\nu = 4$ and $\nu = 8$ are indicated. At lower fields, the small Landau level spacing combined with a limited number of steps in magnetic field leads to aliasing in the image.

[2]The experimental resolution is further limited by the resolution and noise of the applied voltages and measured capacitance, but these effects are smaller than those due to device imperfections, as we will see.

Over twenty different wafers were measured in total, in various attempts to minimize their inherent disorder levels (see Appendix A). Of these, we found decreasing (increasing) the aluminum content in the tunnel (blocking) barrier to be the most successful. In order to keep the tunnel rate roughly constant, this also entails increasing the tunnel barrier thickness. As the 2DEG in these wafers is thus moved slightly further away from the doped back gate region, we hypothesize that the imperfect abruptness of the doping profile at the top interface of the back gate region, where some silicon doping atoms might have diffused into the spacer layer during growth, has the largest effect on the disorder levels.

To control both the electron filling and apply a lattice potential in the 2DEG, we have fabricated devices based on two different designs (Fig 3.6). For both designs, the gate directly on top of the heterostructure surface is patterned into a grid shape, using electron-beam lithography and evaporation and lift-off techniques (see Appendix A for further design considerations and fabrication details). An unpatterned top gate is placed on top. In the first design, these two gates are separated by a thick dielectric layer. This renders the capacitance between the gates to be negligible with respect to the device capacitance (between the grid and back gate). In the second design, the grid gate is made of a material that can be oxidized (aluminum), and is actively oxidized, such that the top gate can be placed directly on top. Given their close proximity in such a scheme, the capacitance between both gates exceeds that of the device, and from an A/C perspective they can be seen as a single gate.

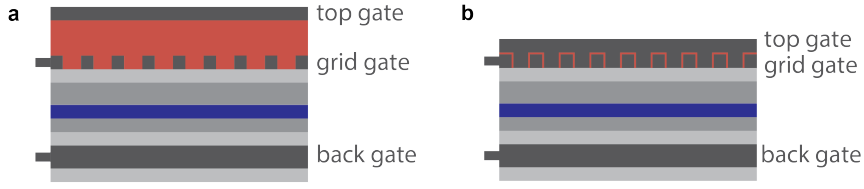

Figure 3.6: Two distinct device designs for imposing a periodic potential. Either the grid and top gate are separated by a thick dielectric (**a**), rendering their capacitance small enough to be neglected, or they are separated only by the oxidation of the first layer (**a**), in which case their capacitance is much larger than the device capacitance and the two gates can be seen as one from the perspective of the A/C measurement signal.

The critical step in device fabrication is to create the grid gates (given that these are the only sub-micron features). Perhaps surprisingly so, the limiting factor for yield and dimensionality is the grain size of the evaporated metal, and not the patterning itself (details in Appendix A). As such, we use Ti/Au(Pd) gates for both top gates in the first design, and Al only for the second design. For both, pitches of 100-200 nm can be reliably fabricated (Fig 3.7a-b). In the first design, either a > 200 nm plasma-enhanced chemical vapor deposited SiO_2 layer separates the gates, or a > 350 nm plasma-enhanced atomic layer deposited AlO_x layer, leading to a stray capacitance between the gates of several pF, typically, and no measurable con-

ductance. In the second design, the Al grid gate is oxidized using a remote oxygen plasma, leading to a stray capacitance between the gates of several hundred pF and resistances exceeding 1 GΩ.

In fabrication, it is clear that reducing the lattice dimensionality comes at a price of decreased homogeneity and fabrication yield. There are two clear limits to the lift-off process: the plaquettes of metal in the grid that have to be lift-off have to be of some minimum size (typically 40 nm by 40 nm), and the line width of the metallic lines has to be sufficient to avoid broken lines (typically 20 nm to 40 nm, depending on the metal used, see Fig 3.7c). As such, we are limited to lattice periodicities of roughly 100 nm or larger. Note that patterning a grid gate through dry etching would allow for the definition of smaller features, but is known to cause defects in the underlying substrate, and seems as of yet to be an unproven technique in the fabrication of quantum dot devices in general.

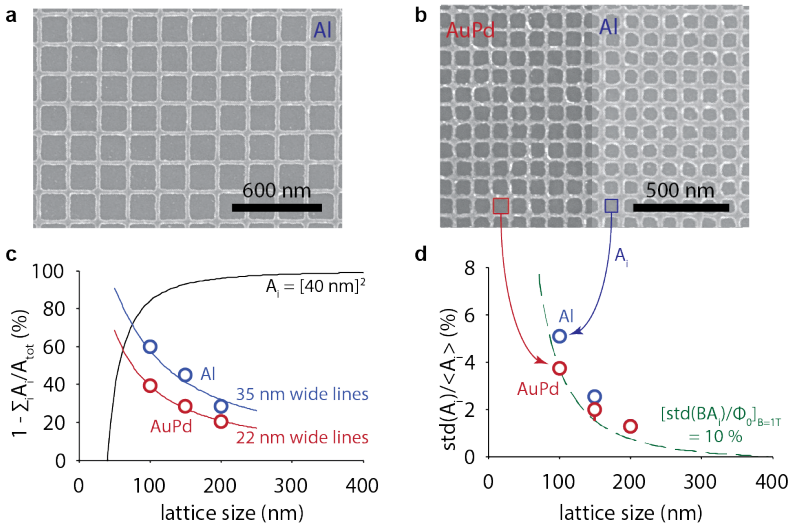

Figure 3.7: Assessment of scale and inhomogeneity of nano-fabricated grid gates. Electron micrographs of square grids at a pitch of 200 nm and 100 nm are shown in **a** and **b**, respectively, consisting of 20 nm of Al (blue) or 5/15 nm of Ti/AuPd (red). Using thresholding and contour finding techniques we extract the areas A_i of non-metal plaquettes for grids of both metals and several pitches, and plot the fraction of the surface area covered in metal (**c**) and the relative variation in plaquette areas (**d**). The black line in **c** indicates the surface covered by a grid that leaves non-metal plaquettes of 40 nm by 40 nm, whereas the blue (red) line indicates that of grids comprised of 35 nm (22 nm) lines. The dashed line in **d** shows which variations in plaquette area coincide with variations of a tenth of a threaded flux quantum at a field of 1 T.

To assess the homogeneity, we define the relative variations in the non-metal plaquettes in the grid gate as a measurable metric. These areas can be extracted from electron micrographs and indeed show a decrease in homogeneity with lat-

tice size (Fig 3.7d). Assuming that the grid shape correlates with the applied potential in the 2DEG, these variations would lead to a different amount of flux threading through each plaquette. As such, they lead to a scrambling of the butterfly spectrum in magnetic field direction, described by Hofstadter as "jiggling the graph". At sufficient inhomogeneity, therefore, one expects the added gaps to no longer be resolvable. Considering the scrambling effect on a grid at an applied field of 1 T, the experimental inhomogeneity corresponds to variations of roughly a tenth of a threaded flux quantum. Jiggling the theoretical graph by this much renders the largest gaps still resolvable. It is difficult, however, to assess whether this indicator directly translates to variations in the relevant potential applied on the 2DEG.

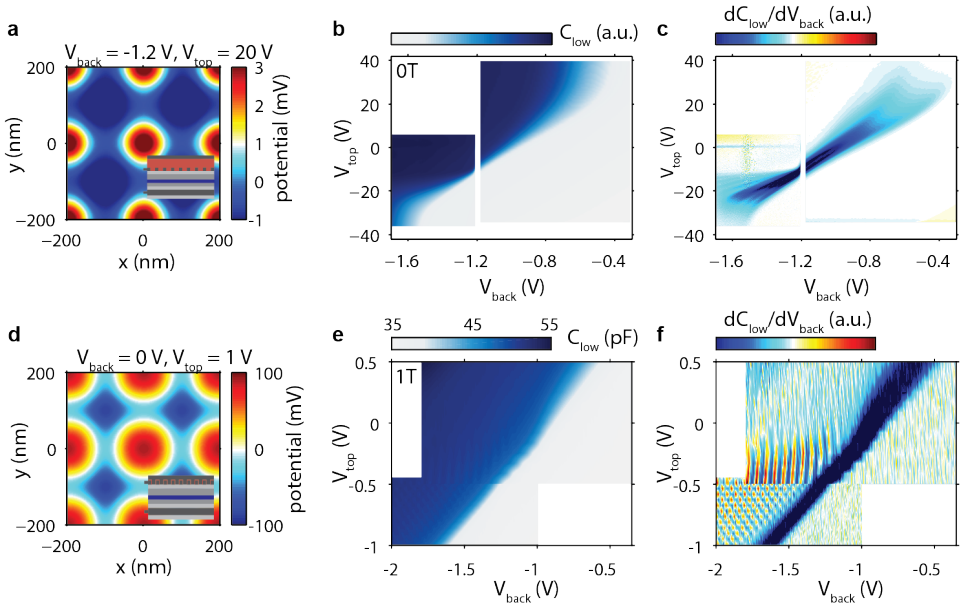

Figure 3.8: Strength of imparted periodic potential. Simulation of imparted potential in the 2DEG for both designs, with a 200 nm periodic 20 nm wide grid and a 350 nm SiO_2 spacer (**a**) or a 5 nm AlO_x spacer dielectric (**d**). For both designs, the grid gate is kept at -0.5 V. Measured capacitance is shown for devices with 200 nm periodic square grid gates based on both gate designs in **b** and **e**, respectively. Derivative of these data sets are shown in **c** and **f**.

Next, we measure the capacitance of double-layer gate devices, to assess if the applied periodic potential overcomes inherent disorder levels. The amplitude of the applied potential will depend on the design as well as on the maximum voltages that can be applied on the gates. In the measurements, we keep the voltage on the grid gate fixed, as it serves as the gate voltage of the first amplifier in the amplification chain, and change the top and back gate voltages. Electrostatic simulations show that, as expected, a much larger voltage is required on the top gate for the first design in order to set a sizable lattice potential (Fig 3.8a,d). In gen-

eral, we expect accumulation to occur in a direction that requires changes in both voltages, which is also measured experimentally (Fig 3.8b,e).

The periodic potential builds up in the perpendicular direction. As both gates are swept, we indeed find maximum voltages that can be applied. In the case of the first design, we find a saturation in the effect of the top gate at gate voltages exceeding 20 V in absolute value, a possible sign of charges building up in the dielectric or at the dielectric-semiconductor interface. For too negative voltages set to the back gate, both designs show leakage through the heterostructure from the back gate to the grid gate. The same happens in the second design for top gate voltages above 750 mV.

The onset of accumulation is broadened with changing top gate voltage for both designs, indicating that the applied potential exceeds the disorder levels of 0.4 - 1 meV (Fig 3.8c,f) at low densities, as expected from the electrostatic simulations. A clear asymmetry between positive and negative top gate voltages shows up for the first design, however, possibly as electrons accumulate either underneath the (screening) grid gate or underneath the dielectric. For the second design, we further look at the effect of gating by seeing how the Landau levels get broadened and the cyclotron gaps eventually close, concluding that the potential must exceed the Landau level splitting (which is 1.7 meV at 1 T).

In conclusion, we have assessed the inherent disorder in the wafers as well as the homogeneity of the grids, and seen that the imposed potential modulations at positive and negative top gate values overcome disorder. So far, however, no signs of butterfly gaps or the formation of minibands and subsequent Mott transition have been seen. In the case of the formation of minibands and the Mott transition, this was to be expected, given that the smallest density modulations that have been resolved (Landau levels at 0.25 T and high density on a global gate device) were still larger than those corresponding to filling a 200 nm periodic grid with one or two electrons per site, and only barely larger than those of a 100 nm grid with two electrons per site. In the case of the opening of butterfly gaps it is harder to speculate as to what forms the bottleneck, as it is hard to assess whether the imposed potential modulations in the 2DEG are more homogeneous or less so than the nano-fabricated grid shape suggest, without first results in observing the effect itself.

3.4. Outlook: room for improvement

As described above, in order to see miniband formation and the Mott metal-to-insulator transition, either the lattice dimension or the intrinsic disorder levels should be further reduced. Given the limits of the lift-off process, decreasing wafer disorder seems to be the most promising. There is room left to optimize the heterostructure, in particular to further increase (decrease) the thickness (Al content) of the tunnel barrier in order to increase the distance from 2DEG to back gate. Furthermore, the top interface of the back gate region can be made more abrupt by

reducing the growth temperature for the first couple of nanometers of the spacer layer, which has been shown to strongly reduce disorder [18].

Such a reduction in disorder levels would also lead to Landau levels that are better defined and hence observable at lower fields. Hofstadter's butterfly-induced gaps inside the Landau levels can then be searched for at lower fields as well, where the inhomogeneity-induced scrambling of the graph is less.

Although heterostructure design has to be further optimized for lattice effects to become visible, however, the potential for combining band physics with finite interactions is clear (see for instance the exhange-split Landau levels). Furthermore, time-domain measurements can be done on similar devices that would allow to probe the excitation spectrum as well [15, 16], which would be particularly interesting in studying the Mott transition.

When periodic effects become visible, capacitance spectroscopy can also be used as a relatively simple experimental platform on which scaling and homogeneity using various fabrication procedures can be studied. The fractal structure of the butterfly lends itself very well to this. As an example, the control gates for quantum dot devices intended for spin qubit measurements are fabricated with lift-off techniques similar to the ones employed here, but as groups start to seriously consider scaling [13], the more industrially viable and robust technique of dry etching is considered for imposing gate patterns. The impact of dry etching on disorder levels as well as on gate homogeneity could then be directly studied using capacitance spectroscopy measurements techniques.

References

[1] M. C. Rechtsman, J. M. Zeuner, Y. Plotnik, Y. Lumer, D. Podolsky, F. Dreisow, S. Nolte, M. Segev, and A. Szameit, "Photonic Floquet topological insulators.," *Nature*, vol. 496, pp. 196–200, 4 2013.

[2] D. Tanese, E. Gurevich, F. Baboux, T. Jacqmin, A. Lemaître, E. Galopin, I. Sagnes, A. Amo, J. Bloch, and E. Akkermans, "Fractal Energy Spectrum of a Polariton Gas in a Fibonacci Quasiperiodic Potential," *Physical Review Letters*, vol. 112, p. 146404, 4 2014.

[3] S. Goswami, M. A. Aamir, C. Siegert, M. Pepper, I. Farrer, D. A. Ritchie, and A. Ghosh, "Transport through an electrostatically defined quantum dot lattice in a two-dimensional electron gas," *Physical Review B*, vol. 85, p. 075427, 2 2012.

[4] K. Ensslin and P. Petroff, "Magnetotransport through an antidot lattice in GaAs-AlxGa1-xAs heterostructures," *Physical Review B*, vol. 41, pp. 12307–12310, 6 1990.

[5] M. Geisler, J. Smet, V. Umansky, K. von Klitzing, B. Naundorf, R. Ketzmerick, and H. Schweizer, "Detection of a Landau Band-Coupling-Induced Rearrangement of the Hofstadter Butterfly," *Physical Review Letters*, vol. 92, p. 256801, 6 2004.

[6] C. Albrecht, J. Smet, K. von Klitzing, D. Weiss, V. Umansky, and H. Schweizer, "Evidence of Hofstadter's Fractal Energy Spectrum in the Quantized Hall Conductance," *Physical Review Letters*, vol. 86, pp. 147–150, 1 2001.

[7] D. Hofstadter, "Energy levels and wave functions of Bloch electrons in rational and irrational magnetic fields," *Physical Review B*, vol. 14, pp. 2239–2249, 9 1976.

[8] C. R. Dean, L. Wang, P. Maher, C. Forsythe, F. Ghahari, Y. Gao, J. Katoch, M. Ishigami, P. Moon, M. Koshino, T. Taniguchi, K. Watanabe, K. L. Shepard, J. Hone, and P. Kim, "Hofstadter's butterfly and the fractal quantum Hall effect in moiré superlattices.," *Nature*, vol. 497, pp. 598–602, 5 2013.

[9] L. A. Ponomarenko, R. V. Gorbachev, G. L. Yu, D. C. Elias, R. Jalil, A. A. Patel, A. Mishchenko, A. S. Mayorov, C. R. Woods, J. R. Wallbank, M. Mucha-Kruczynski, B. A. Piot, M. Potemski, I. V. Grigorieva, K. S. Novoselov, F. Guinea, V. I. Fal'ko, and A. K. Geim, "Cloning of Dirac fermions in graphene superlattices.," *Nature*, vol. 497, pp. 594–7, 5 2013.

[10] B. Hunt, J. D. Sanchez-Yamagishi, a. F. Young, M. Yankowitz, B. J. LeRoy, K. Watanabe, T. Taniguchi, P. Moon, M. Koshino, P. Jarillo-Herrero, and R. C. Ashoori, "Massive Dirac fermions and Hofstadter butterfly in a van der Waals heterostructure.," *Science (New York, N.Y.)*, vol. 340, pp. 1427–30, 6 2013.

[11] G. L. Yu, R. V. Gorbachev, J. S. Tu, A. V. Kretinin, Y. Cao, R. Jalil, F. Withers, L. A. Ponomarenko, B. A. Piot, M. Potemski, D. C. Elias, X. Chen, K. Watanabe, T. Taniguchi, I. V. Grigorieva, K. S. Novoselov, V. I. Fal'ko, A. K. Geim, and

A. Mishchenko, "Hierarchy of Hofstadter states and replica quantum Hall ferromagnetism in graphene superlattices," *Nature Physics*, vol. 10, pp. 525–529, 6 2014.

[12] P. Barthelemy and L. M. K. Vandersypen, "Quantum Dot Systems: a versatile platform for quantum simulations," *Annalen der Physik*, vol. 525, pp. 808–826, 11 2013.

[13] L. M. K. Vandersypen, H. Bluhm, J. S. Clarke, A. S. Dzurak, R. Ishihara, A. Morello, D. J. Reilly, L. R. Schreiber, and M. Veldhorst, "Interfacing spin qubits in quantum dots and donors - hot, dense and coherent," *npj Quantum Information*, vol. 3, p. 34, 12 2017.

[14] V. M. Pudalov, S. G. Semenchinskii, and V. S. Edel'man, "Oscillations of the chemical potential and the energy spectrum of electrons in the inversion layer at a silicon surface in a magnetic field," *Sov. Phys. JETP*, vol. 62, no. 5, pp. 1079–1086, 1986.

[15] O. E. Dial, R. C. Ashoori, L. N. Pfeiffer, and K. W. West, "High-resolution spectroscopy of two-dimensional electron systems.," *Nature*, vol. 448, pp. 176–9, 7 2007.

[16] O. E. Dial, *PhD thesis*. 2007.

[17] J. Jang, H. M. Yoo, L. Pfeiffer, K. West, K. W. Baldwin, and R. Ashoori, "Full Momentum and Energy Resolved Spectral Function of a 2D Electronic System," *ArXiv*, p. 1701.01684, 1 2017.

[18] J. Jang, B. M. Hunt, L. N. Pfeiffer, K. W. West, and R. C. Ashoori, "Sharp tunnelling resonance from the vibrations of an electronic Wigner crystal," *Nature Physics*, vol. 1, no. December, pp. 1–6, 2016.

[19] C. A. Stafford and S. Das Sarma, "Collective Coulomb blockade in an array of quantum dots: A Mott-Hubbard approach," *Physical Review Letters*, vol. 72, pp. 3590–3593, 5 1994.

[20] T. Byrnes, N. Kim, K. Kusudo, and Y. Yamamoto, "Quantum simulation of Fermi-Hubbard models in semiconductor quantum-dot arrays," *Physical Review B*, vol. 78, p. 075320, 8 2008.

4

Efficient calibration of model parameters using local control

Progress isn't made by early risers.
It's made by lazy men
trying to find easier ways to do something.

Robert A. Heinlein

In direct contrast to the large arrays with global control described in the previous chapter, small quantum dot arrays, with site-specific control using gate voltages, are more commonplace. These are the devices intended for quantum information processing, where charge and spin degrees of freedom can be controlled and read out at a large measurement bandwidth. Engineering desired Hubbard model parameters is typically inefficient, however, limiting experiments to small parameter spaces and hindering the calibration of larger devices. In this chapter, I describe a toolbox of experimental techniques that use more of the available measurement bandwidth to efficiently set Hamiltonian parameters, a process called *tuning* (**Section 4.1**). In **Section 4.2**, I show how we can control site-specific energies by employing linear combinations of gate voltages. This in turn leads to the programmable control of chemical potential and disorder, and provides a starting point for the automated measurement of tunnel couplings (**Section 4.3**) and interaction energies (**Section 4.4**). A sufficient amount of bandwidth remains for further tools and automation to be implemented, outlined in **Section 4.5**[1].

[1]Parts of this chapter have been published in Nature **548**, 71–73 (2017).

4.1. The problem of tuning

In the small devices intended for spin qubit measurements, a quantum dot array is electrostatically defined by applying appropriate voltages to a set of gate electrodes fabricated on the surface of the semiconductor material, and read out using parallel sensing channels whose conductance is sensitive to the charge state inside the array (Fig 4.1). Below I provide a brief overview of the relevant elements of this platform.

First of all, a combination of electrical fields and band offsets between different layers of the semiconductor (or the oxide at its surface) define an energetically favorable two-dimensional plane close to the surface. Conduction band electrons at sufficiently low energies are confined to this plane and form a two-dimensional electron gas (*2DEG*). We distinguish *doped* and *undoped* substrates, where in the case of the former, a finite density of electrons is achieved through modulation doping close to the 2DEG, and in the case of the latter, gate-induced electrical fields are required to pull the conduction band edge below the Fermi level. Typical densities are on the order of 10^{11} cm^{-2}, implying a mean separation between charges of several tens of nm. As sources and/or drains for measuring electrical currents running through the 2DEG, ohmic contacts are fabricated, which galvanically connect measurement wires to the 2DEG at different locations. Finally, gate electrodes are fabricated on the surface of the semiconductor, which are also connected to measurement wires. Voltages applied to these electrodes shape the potential that conduction band electrons in the 2DEG experience and as such allow for further confinement.

One can think of this potential as a landscape or topographical map. The gate electrodes allow us to shape this landscape, albeit in a fundamentally limited (once fabricated, the gate layout is fixed) and somewhat indirect (the gates live at a finite distance) manner. Furthermore, imperfections in the material and nanofabrication mean the actual landscape is disordered. Control over the potential landscape is paramount, however, as Fermi-Hubbard parameters are controlled through detailed modulation of it. Overcoming these limitations and engineering the Hamiltonian through the application of correct gate voltages is the process called *tuning* (see Fig 4.1).

Apart from the dots themselves, device layouts are designed to allow for the definition of sensing (dot) channels. By tuning these to positions where the channel conductance is highly sensitive to the electrostatic environment, such as the pinch-off of a quantum point contact or the flank of the Coulomb peak of a sensing dot, we can identify discrete transitions in the charging of the (other) quantum dots through changes in sensing channel conductance. These are typically read out using radio-frequency reflectometry techniques at frequencies of roughly 100 MHz using homebuilt LC tank circuits on the printed circuit board [1], together with cryogenic amplification and room-temperature demodulation.

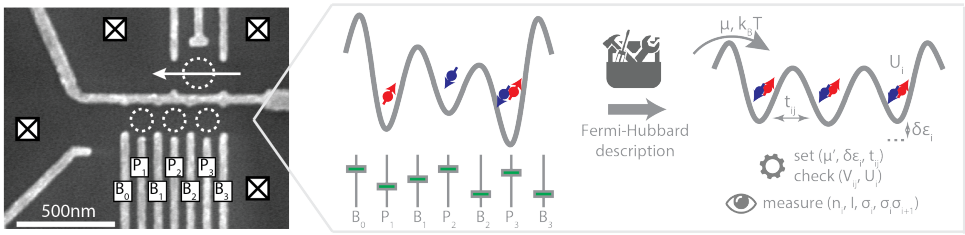

Figure 4.1: The aim of tuning: Hamiltonian engineering. Electron micrograph (left) of a triple quantum dot array, showing metallic topgates (grainy and lighter structures) on a GaAs surface (dark background). The 2DEG lives at a depth of 85 nanometer under the surface. Crossed squares indicate ohmic contacts to the 2DEG, allowing transport measurements to be done both through the device channel (three dashed circles) and the sensing dot channel (single dashed circle and arrow). The aim of the tuning process (right) is to set a desired Hamiltonian through the efficient control of voltages applied to the seven bottom-most gates.

Changes in the sensing (dot) channel conductance as probed via the phase and/or amplitude of a signal reflected off the tank circuit provide the single measurable when the quantum dot array is insulating, which it is under typical conditions. It is from this single measurable that we should try to distill the charge states n_i of the dots, as well as figure out how to control and measure relevant Hubbard parameters. Central to this are so called *honeycomb diagrams*, the experimental equivalent of the two-dimensional charge stability plots introduced in Chapter 2, where changes in the dot occupations appear as clear steps in the charge sensing signal. For an example of such a measurement, and a comparison to the plots shown before, see Fig 4.2 below.

The addition spectra introduced in Chapter 2 were mapped out by changing the chemical potential μ (of the electron reservoir) and specific on-site energy detunings $\delta\epsilon_i$ of individual dots. Experimentally, we can control the filling by changing the energy difference between the electronic states at the Fermi level of the reservoir and those of the dot array itself in two ways: either by applying bias voltages to relevant electron reservoirs that directly change their Fermi level μ, or by deforming the potential landscape of the dot array using the top gate voltages, changing the on-site energies $\delta\epsilon_i$ of the dots[2]. This latter is employed in honeycomb diagram measurements, albeit with some complications that warrant a brief discussion. First of all, we find that the physical gate voltages influence not only the local dot, but actually change the on-site energies of all of the dots to some degree. Second, as the raw data of Fig 4.2 shows, the charge sensor is sensitive

[2]On a technical note, one should realize that because the partition function is sensitive only to changes in $H - \mu N$, we can equivalently think about changes in the ϵ_i's as influencing the chemical potential directly through $\delta(\mu N) = \delta(\sum_i \epsilon_i n_i)$, which is to say, keep the reservoirs at a fixed energy and change the dot energies with respect to that energy. We can therefore map out the charge addition spectrum with top gate voltages only, whilst keeping the reservoir potentials fixed.

to changing gate voltages also, yielding a non-zero background gradient in the charge sensor signal. Countering these two complications will be the topic of section 4.2. Third, as the sensing dot is sensitive to any change in its local electric field, more transitions can appear. In particular, we find so-called *polarization lines* to appear in the experimental data. These are charge transitions where the total number of electrons in the array stays fixed, but charges rearrange between the dots, and will prove important in the determination of tunnel rates.

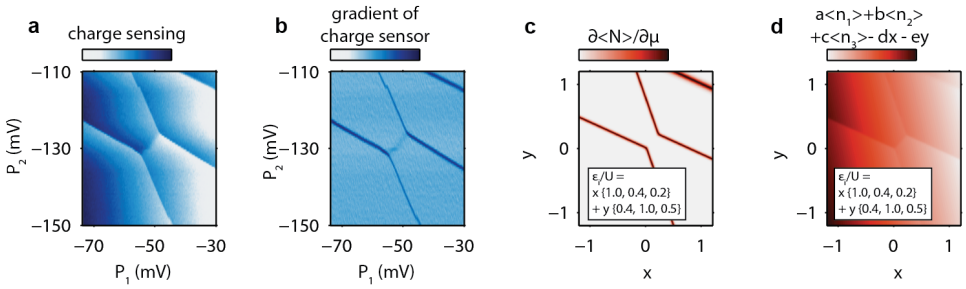

Figure 4.2: Comparing experiment to theory. Experimentally, changes in on-site energies and as such dot occupation are induced through changing plunger gate voltages. Steps in the charge sensing data indicate charge transitions, as seen in **a** and its gradient (**b**). Such a plot is reminiscent of the theoretical charge diagrams (**c**), albeit with some complications, which we model in **d**. The charge sensing data itself is a convolution of the sensing dot conductance (the flank of a Coulomb peak) and any changes in its local electric field: this will be both due to (un)wanted charge transitions or due to the direct, gradual and linear effect that changing gate voltages has on the sensing dot. Note that the polarization line is visible in all figures except **c**, as the total number of electrons remains fixed and as such $\frac{\partial \langle N \rangle}{\partial \mu} = 0$.

Some further complications become apparent as we look at a double dot honeycomb diagram covering a larger gate space in Fig 4.3. Note first that a symmetric point in the charge stability of the dots requires different gate voltages for their respective plunger gates, indicating some inhomogeneity in the quantum dot potential minima - either due to inherent disorder in the semiconductor material or fabrication imperfections. A further inhomogeneity is visible in the tunnel rates between the dots and their adjacent Fermi reservoirs. For this, I should note that this scan is made by sweeping the horizontal axis (here gate P_1) voltage. Horizontal features at some transition are indicative of charges not being able to follow this sweep, and thus of tunnel rates below the sweep rate (here roughly 100 µs, or 10 kHz). As the (00)-(01) transition shows such features, and the (00)-(10) does not, we can conclude different tunnel rates Γ_{ij} for filling the two dots[3]. Furthermore, we see that these tunnel rates are not constant. At higher electron numbers, for instance, the features are absent. The curvature of the lines around (33), which is

[3]In this particular scan, we used similar barrier gate voltages to form the barriers between the two dots and their adjacent Fermi reservoir.

indicative of charge state hybridization, shows that the same is true for the inter-dot tunnel rate t_{12}. Similarly, the charge addition energies (which depend mainly on the Hubbard U) are non-constant with filling, as we find not all charge states to be of equal size. Finally, note the reduced contrast for charge transitions at the most positive plunger voltages. This is due to the sensing dot being influenced by the plunger gates to a point where its conductivity is no longer as sensitive to the electrostatic environment.

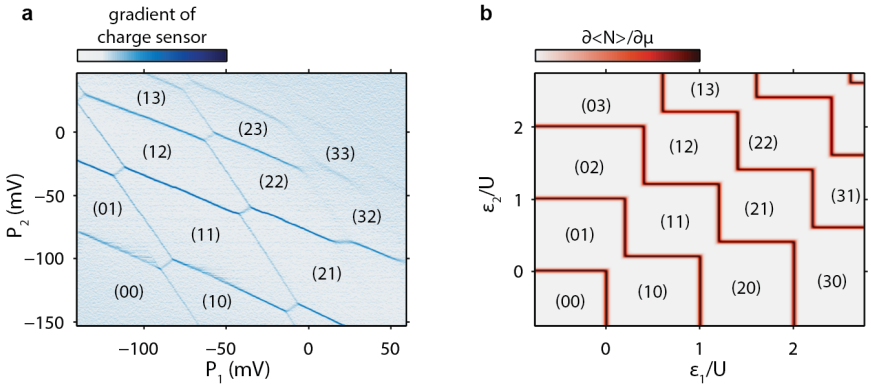

Figure 4.3: Zooming out: what goes wrong. As we focus on a large plunger gate scan of a double dot (**a**) and compare it to a theoretical charge stability diagram (**b**, with V/U = 0.2 and $k_B T/U = 0.003$), some of the difficulties involved in tuning become apparent.

On top of the plunger gates P_i as used in Fig 4.3 to change the overall chemical potential and the individual dot detuning terms, we can influence the tunnel rates using the barrier gates B_i, making the list of controllable parameters $\{\mu, \delta\epsilon_i, t_{ij}, \Gamma_{ij}\}$. This exhausts the list of available gates, though, meaning that the interaction energies $\{U_i, V_{ij}\}$ are determined by the potential landscape realized to achieve this set.

To summarize, control of the Fermi-Hubbard parameter set is achieved by modulating the potential landscape in the 2DEG using two flavors of gate electrodes, plunger and barrier gates. Main difficulties are (i) the significant cross-talk between any of the gates and the Hubbard parameters it is not meant to influence, and (ii) inherent non-linearities with large steps in gate space in general and dot occupation in particular.

4.2. Virtual gates, controlled disorder and uniform filling

Excellent mapping of small linear combinations of gate voltage changes onto on-site energy differences has been long shown to be possible [2], and is used repeatedly for experiments that aim at coherently manipulating the spin and charge degrees of freedom of electrons in quantum dots [3–5]. Focusing on specific imple-

mentations that require only small changes in gate voltages, these are not troubled by the inherent non-linearity and suffice with a pragmatic countering of specific cross-talks only. Furthermore, within the two-dimensional context of the honeycomb diagram, different slopes (and thus cross-talks) are routinely eyeballed to distinguish between different charge transitions.

In this section, we combine these two ideas. We go further by fully embracing the idea of changing linear combinations of gate voltage changes, so called *virtual gates*, and suggest a simple but universal framework in a higher-than-two dimensional space for identifying charge transitions as well as countering cross-talk on specific quantum dot energies. These virtual gates can be used to uniformly fill a quantum dot array with electrons, as well as add specific and programmable disorder in the on-site energies.

When initially tuning a quantum dot array, several different features appear, both in transport (when checking the gates initially and setting up the sensing dot) as well as in charge sensing (for the dot array once the sensing dot is formed). Examples of features are: a quantum point contact as a one-dimensional channel is formed in transport, the Coulomb peak of a sensing dot or steps in the sensing dot conductance due to changing nearby dot occupation. Because of the finite electrostatic cross-talk, all of these will shift with a change in any of the physical gate voltages. If we take one of the gates as a reference, a simple way to check this cross-talk is by scanning across such a feature as function of both this gate and all other gates. This allows for the pinpointing of where the feature is located in the 2DEG, and thus what one is looking at [6–8]. Some examples are shown in Fig 4.4 below:

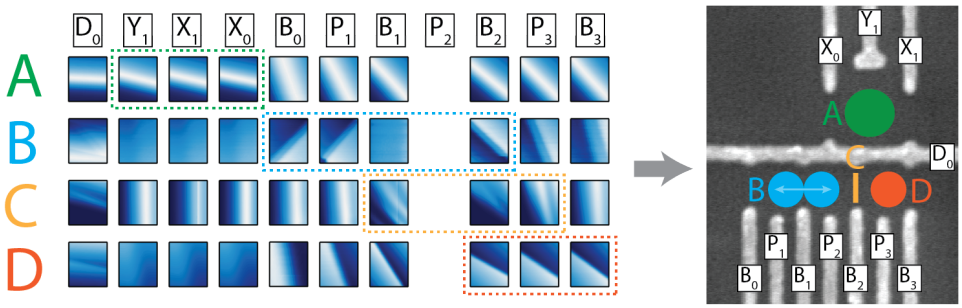

Figure 4.4: Gate influence on features indicate their origin, such as (A) a Coulomb peak in the sensing dot, (B) a polarization line between the left and middle dot, (C) the conductance through a quantum point contact formed at the tip of gate B_2 or (D) an addition line for the rightmost dot. The horizontal axis of all the sub-elements are changes in the voltage on gate P_2, whereas the vertical axis is an equal change in the gate listed for that particular column. Rows (B) and (D) indicate charge sensing data, whereas (A) and (C) are transport measurements through the sensing or dot array channel, respectively.

Determining the relative strengths in gating such a feature is as easy as recognizing the slope of the individual images, which can be robustly done without interpretation of the feature itself using image processing tools, and directly yields a row of cross-talk numbers. Note that some of this robustness can be traded in for reduced measurement time by measuring shifts in one-dimensional traces as gate voltages are changed (see [9] for example data). Because in the end we are interested in the three-dot plus sensing dot system, we choose as features for each dot a point on the higher-dimensional plane where a charge is added to that dot from a reservoir and focus on the cross-talks between these addition lines and the relevant set of gates (Fig 4.5). Again, which feature (dot) is which is obvious from the cross-talk. Because we know the charge addition of the individual dots to be linearly dependent on ϵ_i in the low tunnel coupling regime, we can write down the linear approximation of how the gates influence the dot potential energies.

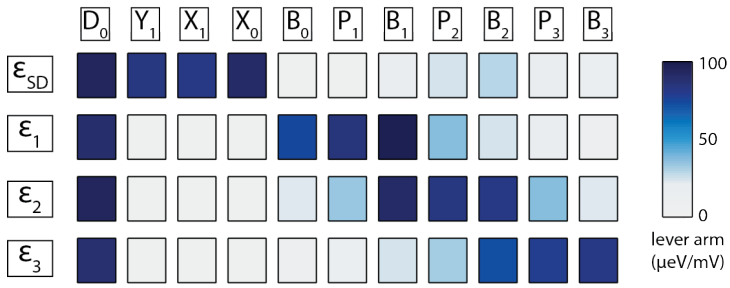

Figure 4.5: Physical gate strengths for a sensing dot + three dots system. Relative strengths have been determined with measurements similar to those of Fig 4.4. Absolute lever arms for each of the plungers in influencing their intended dot can be determined either using the temperature dependence of polarization line width measurements [10, 11], photon-assisted tunneling (used here, see [2] and section 4.3) or bias triangle measurements [12].

As devices with more dots and corresponding gates become available, the fall-off in gating strength with distance as can be seen in the rows of Fig 4.5 indicate a certain length scale for cross-talk. Expressed for instance by the number of gates that influence a particular dot by more than one per cent of the strength with which the plunger gate designed to influence it does, this length scale should be seen as one particular metric that, besides other (yet to be well defined) metrics of nonlinearity and sensitivity to fabrication imperfections of inhomogeneity in dot energies and tunnel couplings should be used in the future to qualitatively assess different device designs.

As a point of interest, the length scale for cross-talk is significantly smaller for most more recent device designs, in which more of the surface area is covered in metallic gates and long-distance electrostatic coupling is thus screened more strongly [13–15] - a possibly unforeseen advantage of the gating schemes invented

for SiMOS and SiGe-based quantum dots for different reasons[4]. In a way, we expect the design of the triple dot device measured here (single layer gates as per [16], doped GaAs wafer, deep quantum well) to constitute something of a worst-case scenario in terms of cross-talk and corresponding difficulty of gating.

A square matrix can be formed of the gate strengths measured, by adding rows that describe the physical parameters not supposed to be influenced by plunger gates (the tunnel couplings). Applying a simple matrix inversion yields our set of virtual gates. Having done this, any gate can be changed without worrying about unwanted influence on the dot energies (see Fig 4.6). This will prove especially useful for controlling tunnel coupling, as described in section 4.3. Furthermore, a continuous update of the virtual gates is found to be extremely useful in the initial tuning of the dots, as it allows for large changes in gate voltage in order to add new dots whilst keeping the occupations of previously tuned dots constant. Note furthermore that as expressed above, even for devices with many dots and given some required accuracy, only a finite number of adjacent gates will have to be taken into account in order to apply local changes, and as such the problem of inverting such a matrix to counter cross-talk will remain bounded.

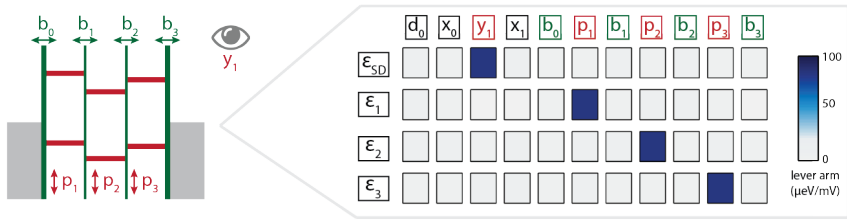

Figure 4.6: Virtual versions of the physical gates (lowercase) where the cross-talk to the (sensing) dot energy levels has been compensated for to within several per cents. Note how such a level of control is reminiscent of the schematic ladder diagram representation of charge state energy level crossings in quantum dot systems [12].

Note that although the absolute values of such (ever changing) linear combinations of physical gates are not very telling, they allow controlled changes of individual parameters[5]. Any remaining imperfection, in part because of the finite non-linearities, can be compensated for by doing repeat measurements of cross-talk using the virtual gates as a starting point, and using these linear approximations

[4](i) As the effective mass for conduction band electrons is higher in silicon devices, shorter length scales are required to achieve similar inter-dot tunnel couplings. These shorter length scales are achieved in fabrication by overlapping adjacent plunger and barrier gates, as such covering much of the surface. (ii) Due to the undoped nature of SiMOS and (most) SiGe wafers, bias cooling cannot be used to deplete the 2DEG underneath the gates, and extra depletion gates are needed to initially define a dot channel. The plunger and barrier gates run over the depletion gates in these designs, and only 'see' the wafer at exactly the locations they are meant to influence. This also reduces the cross-talk.

[5]Nonetheless, referring to physical gate voltages is still the easiest way to store and describe well-defined points in gate-space.

within small windows. As we will see in the next Chapter, it takes repeated cross-talk measurements to keep the virtual gates well-defined over large gate ranges for the triple-dot device used here. Gate designs that allow for a more linear behavior would be preferred. In particular, accumulation and depletion of the 2DEG in any part other than the array itself (e.g. underneath the gates) should be independently controllable and constant during the tuning process. Furthermore, a more well-defined one-dimensional channel would help, such that the dots move only along the axis defined by the channel and not in the direction perpendicular to it, as the gate-induced screening and thus cross-talks terms change non-negligibly in that direction. Both these considerations are best taken into account by the definition of a first layer of screening gates, the voltages on which are kept constant in the tuning process[6].

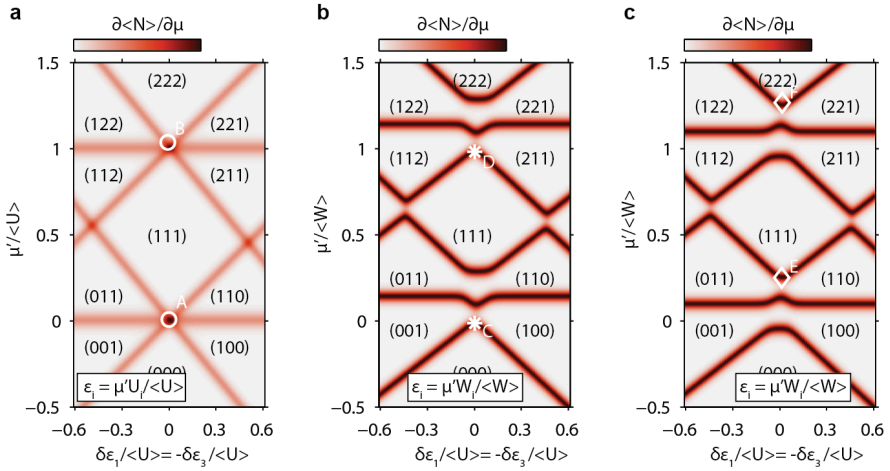

Figure 4.7: Theory of filling an inhomogeneous triple dot system. The array is filled along the center vertical, whereas along the horizontal axis the outer two dots are detuned. We distinguish the case in which $V_{ij} = 0$ (**a**) and $V_{ij} > 0$, without (**b**) or with (**c**) a small detuning in the middle dot energy. The simulations follow Eq. 2.3 with energies $U_2 = 1.05U_1 = 0.95U_3$, $V_{12} = V23 = 2V_{13} = 0.2U_2$ and $k_BT = 0.02U_2$.

Using the virtual gates, we can define a chemical potential knob that uniformly fills the array, akin to the doping parameter in Fermi-Hubbard models, as well as add programmable charge disorder. The latter is the easiest, as we have already defined $\delta\epsilon_i$ gates. For the former, we have to realize that we have to overcome the sum of local interaction energies $U_i + \sum_{i \neq j} V_{ij}$ in order to fill all dots at the same rate. For a large and homogeneous system, these terms would be the same

[6]. Such screening gates are typical for recent device designs on undoped silicon substrates [14, 15]. The high mobilities and low effective mass in GaAs, would however, combined with a gate design that has a layer of depletion gates underneath overlapping plunger and barrier gate layers, probably lead to devices with unprecedentedly reliable gate control.

everywhere, and it suffices to change all ϵ_i at the same rate. In the triple dot described here, however, this does not work. If we were to simply change all the ϵ_i by some large amount, this would not define homogeneous filling, as some dots will be filled with more electrons than others. We have to take the finite size of the array (only the middle dot has two neighbours) as well as inhomogeneity in the interaction terms (see section 5.2) into account.

Uniform filling denotes a line in the higher-dimensional gate space, which can be formed by linking up a set of well-defined points. In the case of negligible inter-site Coulomb effects ($V_{ij} = 0$), the only obvious choice consists of the points where the charge states (000) to (111), (111) to (222) and so on meet, as indicated by A and B, respectively, in Fig 4.7, and entails a change in ϵ_i at rates determined by the local Coulomb interactions U_i. A non-zero inter-site Coulomb effect, however, breaks particle-hole symmetry and moves states with more than one particle added or removed from a homogeneously filled array away in energy. As such, points A and B do not exist anymore, and we can choose to link up points C (where (000)-(100)-(010)-(001) are degenerate), D (where (111)-(211)-(121)-(112) are degenerate) and so on, or E (where (111)-(011)-(101)-(110) are degenerate), F (where (222)-(122)-(212)-(221) are degenerate) and so on.

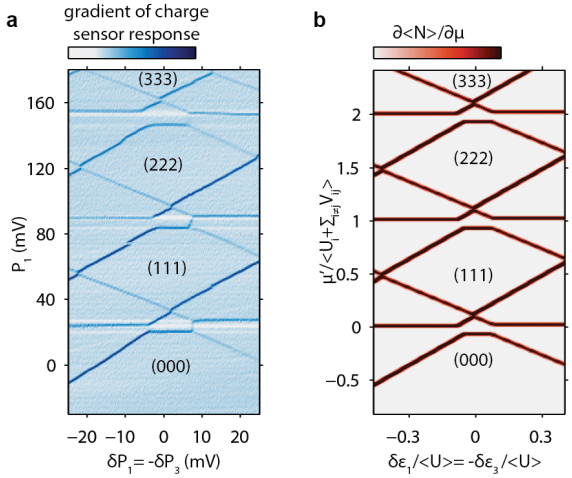

Figure 4.8: Uniform filling of the triple dot device. Charge stability diagram in which the array is homogeneously filled (**a**). Only P_1 values are shown on the vertical axes, whereas a combination of gate voltage changes is used. In **b** a theoretical diagram of a triple-dot in the classical limit ($t = 0$) is shown that is analogous to the measurement of **a**.

Fig 4.8 shows uniform filling for the triple quantum dot device. To achieve this control, an added compensation in the (virtual) barrier gates was required to account for the effect that larger wave function overlap has on increasing the tunnel coupling at higher fillings. In general, it shows how calibration of tunnel coupling as well as cross-talk (note how the different charge addition lines are not exactly par-

allel) have to be repeated for different overall fillings - a complication in the tuning process that cannot be captured using a simple linear scheme.

One further complication is that the middle dot in the array is not directly adjacent to a reservoir, so it takes a longer time to fill during measurements. In this particular diagram, however, the middle dot lines lie horizontal, and the middle dot does not have to be filled in the timescale of the horizontal experimental sweep of plunger gates 1 and 3. For larger arrays, therefore, different diagrams would be preferable to indicate and verify electron filling.

4.3. Controlling tunnel couplings

In this section I introduce and compare two different measurements for the inter-dot tunnel coupling. The previously defined virtual gates allow for repeat measurements using these techniques as function of changing barrier gate voltages, which allows us to again counter cross-talk using a simple linear scheme and yielding the independent control of individual tunnel couplings.

In a photon assisted tunneling (PAT) measurement, we check for changes in the charge sensor response across a polarization line as an AC excitation at a given frequency is turned on [2]. See Fig 4.2 for the location of polarization lines in a honeycomb diagram, and Fig 4.9 for examples and a comparison between this technique and polarization line width measurements (explained below). The detunings $\epsilon = \delta(\epsilon_i - \epsilon_j)$ and frequencies corresponding to the observed changes in measured charge sensor response map out the hybridized charge state spectrum of the double dot. The energy difference between the bonding and antibonding states at zero detuning amounts to twice the tunnel coupling, and the slope away from detuning yields the lever arm between the gate voltages changed and the energy difference between the two dots. Because of the complications of applying microwave excitations well above 40 GHz, however, this technique is limited to distinguishing tunnel couplings of up to roughly 20 GHz (83 μeV).

Alternatively, an equilibrium measurement of the width of the polarization line itself can be used to infer the tunnel coupling, as the charge hybridization widens the transition [10]. For this, some experimental complications have to be taken into account. First of all, the transition is also broadened by the effective electron temperature. Also, the charge sensor response is not a direct measurement of excess charge. A finite cross-talk between gate voltages and sensor signal V has to be taken into account, as well as a possible back-effect of the excess charge on the sensing dot, leading to different slopes on either side of the transition. To take these effects into account, we fit the data using the following equation, that handles the back-effect to first order in excess charge:

$$V(\epsilon) = V_0 + \delta V Q(\epsilon) + \left[\frac{\delta V}{\delta \epsilon}|_{Q=0} + \left(\frac{\delta V}{\delta \epsilon}|_{Q=1} - \frac{\delta V}{\delta \epsilon}|_{Q=0} \right) Q(\epsilon) \right] \epsilon \tag{4.1}$$

Excess charge on one of the dots is described by ([10]):

$$Q(\epsilon) = \frac{1}{2}\left(1 + \frac{\epsilon}{\Omega}\tanh\left(\frac{\Omega}{2k_B T_{\text{eff}}}\right)\right) \tag{4.2}$$

where $\Omega = \sqrt{\epsilon^2 + 4t_{ij}^2}$ and, for the triple quantum dot array in the set-up used for this work, we find an effective temperature $k_B T_{\text{eff}} \approx 6.5$ μeV (1.6 GHz). This scheme works for tunnel rates that are larger than the effective electron temperature, and neglects any inherent nonlinearity in (the flank of the Coulomb peak to which the) charge sensor (is tuned).

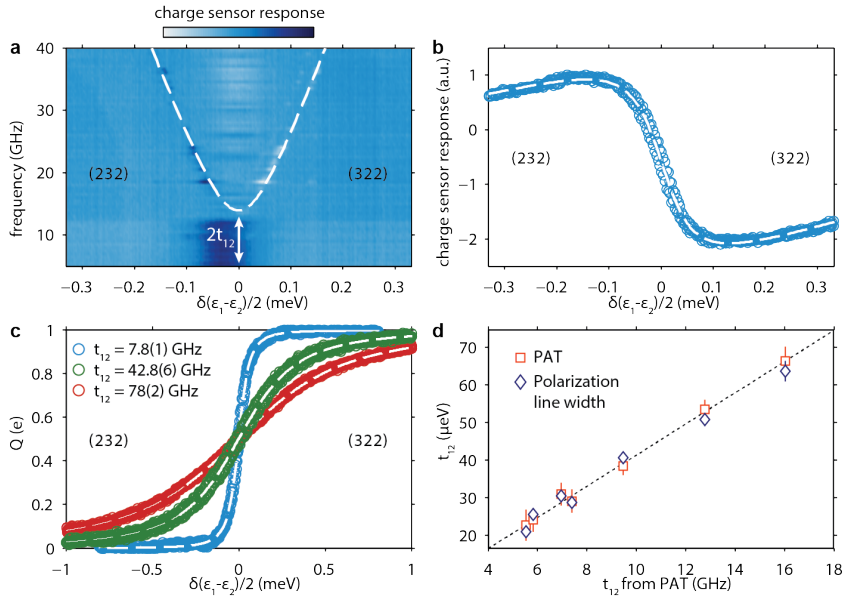

Figure 4.9: PAT and Pol measurement techniques: explanation and comparison. The difference between the charge sensor response with and without applying the AC excitation in a PAT measurement shows the hybridized charge spectrum in **a**, whereas the width of the transition itself depends on effective electron temperature and tunnel coupling (**b**). Excess charge as function of detuning for different tunnel couplings is shown in **c**, indicating that this method works up to tunnel couplings several times higher than those obtainable using PAT. A comparison between the two techniques is made in **d**. The data is well explained assuming a constant lever arm between gate P_2 and ϵ_2 of 83(1) μeV/mV.

Tunnel coupling measurements are typically seen as a large effort, and repeat measurements, when made at all, are few and far between. One reason for this is that in the higher-dimensional charge stability of the array, one has to find the right polarization line indicative of a charge jumping between two specific dots, and stay there as other gate voltages are changed, most notably the barrier gate that is

meant to influence that particular tunnel coupling. When using physical gate voltages only, that means that repeated charge stability measurements are necessary just to regain the polarization line. Using well-defined virtual gates, however, we are free to change (virtual) barrier gate voltages without changing our location in charge stability, and repeat measurements become more straightforward. Having access to repeat measurements, in turn, allows us to reduce also the cross-talk that (virtual) barrier gates have on other tunnel couplings. We first realize that unlike the dot energies, tunnel rates t_i will depend exponentially on changes in the potential landscape and as such on (all, virtual) barrier gate voltages b_i:

$$t_i = t_i^0 \times 2^{\sum_j b_j/\alpha_{ij}} \tag{4.3}$$

in which α_{ij} describe the couplings - they are defined as the voltage change in gate b_j that causes a doubling of t_i. As a practical example, let us write out Eq. 4.3 for the linear three dot system, which has two tunnel couplings:

$$\begin{pmatrix} \log_2[t_1/t_1^0] \\ \log_2[t_2/t_2^0] \end{pmatrix} = \begin{pmatrix} 1/\alpha_{11} & 1/\alpha_{12} \\ 1/\alpha_{21} & 1/\alpha_{22} \end{pmatrix} \begin{pmatrix} b_1 \\ b_2 \end{pmatrix} \tag{4.4}$$

These cross-talks are best measured at relatively large tunnel coupling values and using polarization line measurements, as they entail simple one-dimensional scans and repeat measurements are thus fast (tunnel coupling measurement rates of 1 Hz can be achieved). In assessing the feasibility of scaling, note that the same boundedness on cross-talk length as discussed for the virtual plunger gates applies here as well. If we require m points for a sufficiently accurate fit of the exponential dependence, and have to take k adjacent tunnel couplings into account at any point, it follows that $(1 + k(m-1))$ tunnel coupling measurements are required. With $m = 10$ and $k = 6$, a single minute of characterization measurements per tunnel coupling suffices.

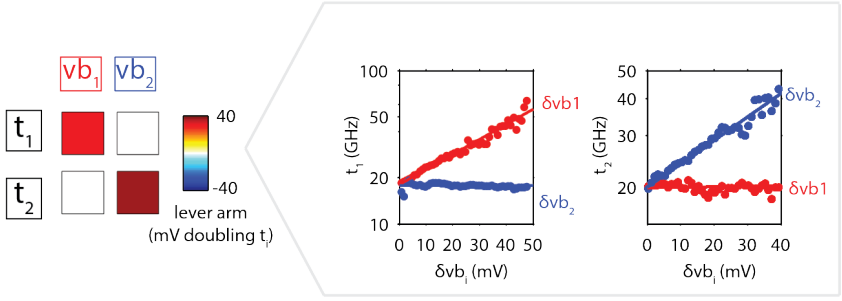

Figure 4.10: Controlling one tunnel coupling at a time. Compensating for the cross-talk measured in Fig 4.4, we can define barrier gates vb_i that influence only one tunnel coupling at a time. (add meV to x-label!)

And again we can negate cross-talk effects by defining a linear combination of gates, in this case of virtual barrier gates that influence one single tunnel coupling at a time (Fig 4.10). Such a virtual barrier gate is particularly relevant in the operation of quantum dots as spin qubits. It allows to turn the exchange interaction effect between one particular pair of adjacent spins on and off without influencing adjacent spins or coupling to (inherently less coherent) charge degrees of freedom, and as such defines a two-qubit gate with increased robustness to charge noise [4, 5]. In order to achieve a certain on-off ratio in exchange, it entails pulses with a certain height, given the measured barrier lever arms. A ratio of 900, for instance, would entail a tunnel rate change of factor 30 (as exchange goes with tunnel rate squared) and pulses on the gates of 150-200 mV - large steps, given finite pulse rise times and the potential for heating under repeated operation.

It will be interesting to see how homogeneous such operation voltages will prove to be for larger arrays, as well as their dependence on device design. As an example, anything between similar to five times stronger sensitivity of tunnel coupling to barrier gate voltages has been reported on first experiments with overlapping gate designs on undoped SiGe wafers (the voltage change that doubles tunnel coupling is roughly 10 mV in [17], 30 mV in [5] and 6 mV in [13], with the device designs for the last two nominally identical).

Similarly, one can define a global tunnel coupling knob, a linear combination of gate changes that increases all tunnel couplings at the same rate. As t/U defines the relevant interaction strength, such control will prove relevant for probing interaction-driven effects, such as in the experiment described in Chapter 5.

We have so far though omitted the problem of measuring the tunnel rates for electrons that jump between the dots and the Fermi reservoirs, which we typically tune to be in the several (tens of) kHz. A relatively simple measurement that can be added to this framework is one where the real-time hopping of electrons at the transition is observed [18], which would also allow for the measurement of slower inter-dot tunneling rates - although decoherence rates have to be taken into account to extract coherent tunnel rates [19, 20].

4.4. Measuring interaction energies

Note again that in current gate designs there is no independent control over the interaction energies - they just are what they are, depending on the number of electrons and the potential landscape that is set. For a full understanding of our Hamiltonian, however, it is imperative that we find a way to measure them. Luckily, this becomes fairly trivial using virtual gates that can add offsets in on-site energies. See Fig 4.11 for an example. The spacing between parallel charge addition lines yields the on-site interactions, whereas the jump in a charge addition line as an adjacent dot is filled yields their inter-site repulsion.

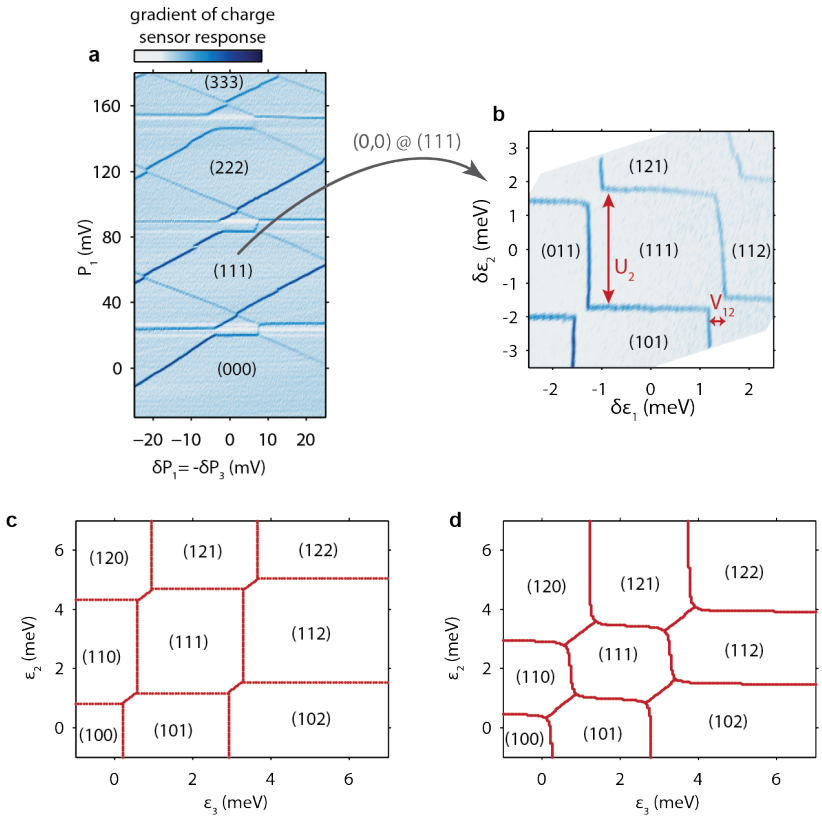

Figure 4.11: Extracting interaction energies from charge stability diagrams. Given some charge occupation, such as the (111) state shown in **a**, the interaction energies can be found by focusing on the parallel (single-dot) and crossing (double-dot) features as the relevant dot energies are changed (**b**). Note also how such a measurement employs virtual gates to closely resemble a naive theoretical picture. Also shown are theoretical triple dot charge stability diagrams at low ($t = 0.006,\ U_1 = 3.98,\ U_2 = 3.48,\ U_3 = 2.70,\ V_{12} = 0.41,\ V_{23} = 0.35,\ V_{13} = 0.11$ in **c**) and higher ($t = 0.17,\ U_1 = 2.92,\ U_2 = 2.39,\ U_3 = 2.53,\ V_{12} = 0.55,\ V_{23} = 0.47,\ V_{13} = 0.27$ in **d**) tunnel coupling (all energies in meV). In both cases we can extract the interaction energies from the simulated data to within 5 % using the method shown in Fig 4.11.

Two things complicate this picture. First of all, as discussed in Chapter 2, single-dot lines bend at increased tunnel couplings, and as such we expect this technique to break down at large tunnel coupling. For tunnel couplings up to $t/U \approx 0.1$ though, we have verified that no large errors build up (Fig 4.11c,d). Furthermore, we require electron addition from the reservoir to be possible, something that will break down for larger arrays. A different scheme has to be used there, one that focuses not on charge addition but on polarization lines between neighboring dots [21].

4.5. There is plenty of room in a coax

The charge state of an array can be measured using an RF sensing dot with suitable signal-to-noise ratio at rates of over 1 MHz. We therefore know that there is a lot that can be measured and/or calibrated in a short time, given the proper electronic input. As has been shown before [22], this means that a two-dimensional honeycomb diagram of 100 by 100 points can easily be measured in real-time, at refresh rates of over 1 Hz, which is now routinely used. Harnessing this bandwidth is however limited to measurements employing gates that have bias-tees and coaxial cables connected, as twisted pair wires employed for DC bias voltages are typically filtered to lower cut-off frequencies and would at any rate suffer from large cross-talk.

However, the increased dimensionality of the charge stability of ever larger quantum dot devices asks for a revision of the central use of two-dimensional honeycomb diagram. Charge addition lines and polarization lines are in fact planes in a higher-dimensional space, defined by a single point and a normal vector (which is exactly the row of numbers measured in a cross-talk measurement). Because of plot crowding as well as the loss of direct contact to a Fermi reservoir, furthermore, overview diagrams such as Fig 4.8 will have to make way for ladder diagram plots [12], which at least for linear arrays still allow for the visualization of close by charge transitions.

A ladder measurement is nothing but a set of one-dimensional measurements where the dot detunings are swept about their DC value (see Fig 4.12 for examples of such a measurement, taken at several points in the charge stability of a double quantum dot). The differentiated charge sensor signal clearly indicates where charge transitions take place, which are furthermore clearly identified given their occurrence in a particular ladder (loading from reservoir) or adjacent ladders (inter-dot transition). Given the small number of measurement points in total (as compared to a two-dimensional plot) they can easily be done in real-time.

Note that for a longer linear array, additional dots can be added with little overhead, both visually and in terms of measurement time. Compensating for sensing dot shifts in the one-dimensional scans would clearly be beneficial too, and given the known charge sensor derivative allow us to calibrate the color bar of the ladders to show the induced energy shifts in the sensing dot, further simplifying the real-time identification of visible charge transitions. Additionally, we can show the measured data from multiple nearby charge sensors for each dot, further adding to ease of use and scalability. As an example, that means that polarization lines would be clearly distinguishable due to the opposite step on neighboring sensors, as an electron moving away from one sensing dot would inevitably move towards the other sensor.

Note also that the idea of virtual gates, when embraced fully, can simplify the initial tuning of quantum dots. Already formed dots will stay as is during the addition of further ones, as cross-talk is negated for. One could even keep checking the

charge addition lines of previous dots in real-time using one-dimensional traces as discussed above. This, then, means that there is no reason that after setting up the sensing dots, remaining initial tuning cannot be done in minutes, as compared to the weeks or even months that many in the field accept as reasonable. All that needs doing is writing the code, and the first steps have already been made [23].

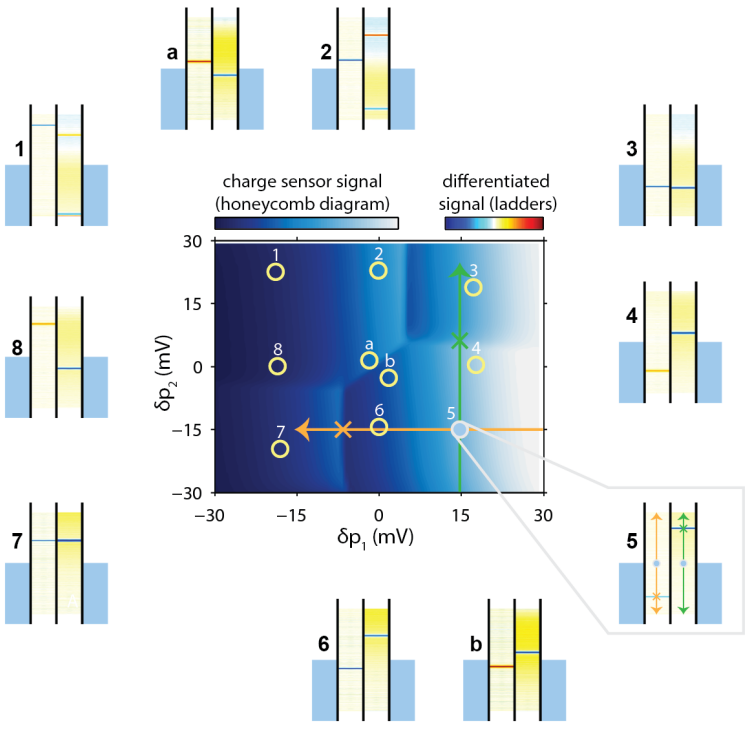

Figure 4.12: Measuring a double dot using ladder diagrams. Charge stability diagram of a double dot. Virtual plunger gates corresponding to dot 1 and 2 are swept on the horizontal and vertical axis, respectively. Circles indicate locations in gate space where two simple 1D traces in the same virtual plunger gates were measured, with location 7 indicating an empty array. Note that ladders 1 and 2 show the second charge addition line for dot 2. Also, ladders 2, 4, 6 and 8 show one addition and one polarization line, whereas a and b show the same polarization line for both dots. The path that the ladders at point 5 trace are indicated in the charge stability diagram (orange for dot one, green for dot 2), with the one transition both ladders encounter indicated with crosses for both.

A more formidable obstacle is the reliable fabrication of larger devices on Si substrates [15], and the inherent difficulties these have with respect to the GaAs substrate used here, such as higher effective mass (meaning smaller length scales are required in fabrication) and potentially small valley splittings [24].

To assess these larger devices, we have to define relevant metrics, some of which

have been alluded to in this Chapter. Spread in pinch-off voltages for plunger and barrier gates (1) are obvious ones, and should be followed by measurements of the length-scale of gate-dot cross-talks (2). With charge sensing set up and the device tuned to the single-electron regime (constant dot energies and tunnel couplings), the voltages required to get there (3) are important, as are the lever arms for virtual plunger (4) and barrier (5) gates in changing dot energies and tunnel rates, respectively. It is only when the spread in voltages is sufficiently small (especially for barrier gates, as too high tunnel rates mean individual dots are no longer well-defined) that one can measure the metrics of final interest, the variations in potential energy offsets (6) and tunnel rates (7) given some fixed voltage for all plungers and some fixed voltage for all barriers.

But who knows - perhaps we are but several breakthroughs in fabrication away from measuring (6) to be fractions of a charging energy and (7) to vary by less than an order of magnitude, and in turn, rendering the techniques described in this Chapter irrelevant.

References

[1] C. Barthel, M. Kjærgaard, J. Medford, M. Stopa, C. M. Marcus, M. P. Hanson, and A. C. Gossard, "Fast sensing of double-dot charge arrangement and spin state with a radio-frequency sensor quantum dot," *Physical Review B*, vol. 81, p. 161308, 4 2010.

[2] T. H. Oosterkamp, T. Fujisawa, W. G. van der Wiel, K. Ishibashi, R. V. Hijman, S. Tarucha, and L. P. Kouwenhoven, "Microwave spectroscopy of a quantum-dot molecule," *Nature*, vol. 395, pp. 873–876, 10 1998.

[3] K. D. Petersson, J. R. Petta, H. Lu, and A. C. Gossard, "Quantum Coherence in a One-Electron Semiconductor Charge Qubit," *Physical Review Letters*, vol. 105, p. 246804, 12 2010.

[4] F. Martins, F. K. Malinowski, P. D. Nissen, E. Barnes, S. Fallahi, G. C. Gardner, M. J. Manfra, C. M. Marcus, and F. Kuemmeth, "Noise Suppression Using Symmetric Exchange Gates in Spin Qubits," *Physical Review Letters*, vol. 116, no. 11, pp. 1–5, 2016.

[5] M. D. Reed, B. M. Maune, R. W. Andrews, M. G. Borselli, K. Eng, M. P. Jura, A. A. Kiselev, T. D. Ladd, S. T. Merkel, I. Milosavljevic, E. J. Pritchett, M. T. Rakher, R. S. Ross, A. E. Schmitz, A. Smith, J. A. Wright, M. F. Gyure, and A. T. Hunter, "Reduced Sensitivity to Charge Noise in Semiconductor Spin Qubits via Symmetric Operation," *Physical Review Letters*, vol. 116, no. 11, pp. 1–6, 2016.

[6] K. Nabors and J. White, "FastCap: a multipole accelerated 3-D capacitance extraction program," *IEEE Transactions on Computer-Aided Design of Integrated Circuits and Systems*, vol. 10, no. 11, pp. 1447–1459, 1991.

[7] F. A. Mohiyaddin, R. Rahman, R. Kalra, G. Klimeck, L. C. L. Hollenberg, J. J. Pla, A. S. Dzurak, and A. Morello, "Noninvasive Spatial Metrology of Single-Atom Devices," *Nano Letters*, vol. 13, pp. 1903–1909, 5 2013.

[8] R. Jochemsem, *Estimating the locations of quantum dots using cross capacitance measurements as a tool for efficient tuning*. BSc thesis, 2017.

[9] M. Houck, *The use of virtual gates and 1D traces to scalably characterize and control quantum dot arrays*. BSc thesis, 2017.

[10] L. DiCarlo, H. J. Lynch, A. C. Johnson, L. I. Childress, K. Crockett, C. M. Marcus, M. P. Hanson, and A. C. Gossard, "Differential Charge Sensing and Charge Delocalization in a Tunable Double Quantum Dot," *Physical Review Letters*, vol. 92, p. 226801, 6 2004.

[11] L. Janssen, *Scalable toolbox for quantum simulations in a GaAs triple dot array*. MSc thesis, 2016.

[12] R. Hanson, L. P. Kouwenhoven, J. R. Petta, S. Tarucha, and L. M. K. Vandersypen, "Spins in few-electron quantum dots," *Reviews of Modern Physics*, vol. 79, pp. 1217–1265, 10 2007.

[13] M. G. Borselli, K. Eng, R. S. Ross, T. M. Hazard, K. S. Holabird, B. Huang, A. A. Kiselev, P. W. Deelman, L. D. Warren, I. Milosavljevic, A. E. Schmitz, M. Sokolich, M. F. Gyure, and A. T. Hunter, "Undoped accumulation-mode Si/SiGe quantum dots," *Nanotechnology*, vol. 26, p. 375202, 9 2015.

[14] M. Veldhorst, C. H. Yang, J. C. C. Hwang, W. Huang, J. P. Dehollain, J. T. Muhonen, S. Simmons, A. Laucht, F. E. Hudson, K. M. Itoh, A. Morello, and A. S. Dzurak, "A two-qubit logic gate in silicon," *Nature*, vol. 526, 2015.

[15] D. Zajac, T. Hazard, X. Mi, E. Nielsen, and J. Petta, "Scalable Gate Architecture for a One-Dimensional Array of Semiconductor Spin Qubits," *Physical Review Applied*, vol. 6, p. 054013, 11 2016.

[16] J. Medford, J. Beil, J. M. Taylor, S. D. Bartlett, A. C. Doherty, E. I. Rashba, D. P. DiVincenzo, H. Lu, A. C. Gossard, and C. M. Marcus, "Self-consistent measurement and state tomography of an exchange-only spin qubit," *Nature Nanotechnology*, vol. 8, pp. 654–659, 9 2013.

[17] D. M. Zajac, A. J. Sigillito, M. Russ, F. Borjans, J. M. Taylor, G. Burkard, and J. R. Petta, "Quantum CNOT Gate for Spins in Silicon," *ArXiv*, p. 1708.03530, 8 2017.

[18] J. M. Elzerman, R. Hanson, L. H. Willems van Beveren, B. Witkamp, L. M. K. Vandersypen, and L. P. Kouwenhoven, "Single-shot read-out of an individual electron spin in a quantum dot," *Nature*, vol. 430, pp. 431–435, 7 2004.

[19] "Electron counting in quantum dots," *Surface Science Reports*, vol. 64, pp. 191–232, 6 2009.

[20] F. R. Braakman, P. Barthelemy, C. Reichl, W. Wegscheider, and L. M. K. Vandersypen, "Long-distance coherent coupling in a quantum dot array," *Nature Nanotechnology*, vol. 8, pp. 432–437, 4 2013.

[21] H. Flentje, B. Bertrand, P.-A. Mortemousque, V. Thiney, A. Ludwig, A. D. Wieck, C. Bäuerle, and T. Meunier, "A linear triple quantum dot system in isolated configuration," *Applied Physics Letters*, vol. 110, p. 233101, 6 2017.

[22] J. Stehlik, Y.-Y. Liu, C. Quintana, C. Eichler, T. Hartke, and J. Petta, "Fast Charge Sensing of a Cavity-Coupled Double Quantum Dot Using a Josephson Parametric Amplifier," *Physical Review Applied*, vol. 4, p. 014018, 7 2015.

[23] T. A. Baart, M. Shafiei, T. Fujita, C. Reichl, W. Wegscheider, and L. M. K. Vandersypen, "Single-spin CCD," *Nature Nanotechnology*, vol. 11, pp. 330–334, 1 2016.

[24] F. A. Zwanenburg, A. S. Dzurak, A. Morello, M. Y. Simmons, L. C. L. Hollenberg, G. Klimeck, S. Rogge, S. N. Coppersmith, and M. A. Eriksson, "Silicon quantum electronics," *Reviews of Modern Physics*, vol. 85, pp. 961–1019, 7 2013.

5

Quantum simulation of collective Coulomb blockade

The tools described in the previous chapter allow us to map the physical parameters of a small quantum dot array onto those of the Hubbard model. That exact concept is employed in this chapter. In particular, I will show how the experimentally accessible parameter space of filling and delocalization maps onto the physics of collective Coulomb blockade (**Section 5.1**) for a triple quantum dot device. This serves three main purposes. First, it is an exploration of the experimentally accessible phase space of the Hubbard model for a typical device (**Section 5.2**). Second, it allows us to verify the toolbox of the previous chapter by comparing the results to classical simulations (**Section 5.3**). Lastly, it serves as a clear example that quantum dots can indeed be used to emulate the physics of strongly-interaction quantum states of matter, discussed in more detail in **Section 5.4**.[1]

[1]Parts of this chapter have been published in Nature **548**, 71–73 (2017).

5.1. A finite-size analogue of the Mott transition

Metal-insulator transitions have been widely observed and described in a large variety of solid state systems [1]. As a first guess of whether a material should conduct or not, the number of valence electrons per unit cell can be counted, as it indicates whether one expects a partially or fully filled band at the Fermi level. To the surprise of two physicists working at a light bulb factory in Eindhoven in 1937, however, NiO_2 does not follow this rule: one expects to find a conducting, partially filled $3d$ band, but nonetheless insulating behavior was observed [2]. It was quickly suggested, by Nevill Mott, that a simple band physics description might not suffice here, as electronic (Coulomb) interactions could be forcing localization and the resulting insulating behavior [3].

Perhaps surprisingly so, eighty years since, the interaction-driven transition between a metallic state and a (Mott) insulating state is still an active topic of research. Proof-of-principle experimental work has shown how two-site Mott physics can be simulated on a programmable quantum processor [4], but the requirement or error correction leads to a large experimental overhead. Analog quantum simulation efforts, on the other hand, are typically limited by residual entropy of the system, restricting correlations in span and strength [5]. In the early years of gate-defined quantum dots, it was realized that the Mott transition can be studied in small quantum dot systems also, by varying the relative strength of tunnel coupling (delocalization) to that of the charging effects (Coulomb interaction-induced localization) [6].

As a theoretical example of CCB in a triple dot system, we consider a simplified Hubbard model that stays close to the original proposal [6]. In this simplified model (Fig 5.1a), each dot has two orbitals separated by level spacing Δ, all parameters are constant over the different sites and the inter-site Coulomb coupling is neglected. CCB can be seen clearly in the charge addition spectrum as the relative tunnel coupling strength is increased (Fig 5.1b). At low tunnel couplings, we find four distinct peaks in the charge addition spectrum at $\mu = 0$, U, $U + \Delta$ and $2U + \Delta$. Note that the first two peaks are similar to points A and B in Fig 4.7a, and all four correspond to filling each dot in the array simultaneously with one additional electron. This is the well-known classical Coulomb blockade, which arises from the classical charging effect (Hubbard U) of each dot.

When we turn on tunnel coupling, quantum fluctuations start to compete with classical charging effects, splitting the peaks into minibands and reducing the gaps at uniform filling. Coulomb blockade of individual dots is lost, and the gap at half filling becomes of a collective nature, akin to the gap describing charge excitations in a Mott insulator. As tunnel coupling is increased even more, we find nonzero $\partial \langle N \rangle / \partial \mu$ even at uniform filling, as the gap starts to yield to temperature.

Experimentally, it is long known that the two extremes of low and high tunnel coupling can be reached for gate-defined quantum dots [7–10]. The Coulomb blockade regime at low tunnel coupling is where individual dots can be well controlled,

and as such has been the focus of the last chapter as well as the typical working condition for spin qubit experiments. Similarly, a regime in which a large dot (typically with a large and unknown number of electrons) is formed that spans several lithographically defined locations, is also quite common. Indeed, such a configuration is sometimes used as intermediary state in the initial tuning of quantum dots [11]. A controlled transition between both regimes, with a small and known number of electrons occupying each dot, will be the focus of this Chapter. This not only showcases the Hamiltonian engineering described in the previous Chapter, but also maps out a typical experimentally accessible Fermi-Hubbard phase space for quantum dots, and as such, forms a good start for a discussion into how quantum dots can be used to emulate Fermi-Hubbard physics in general.

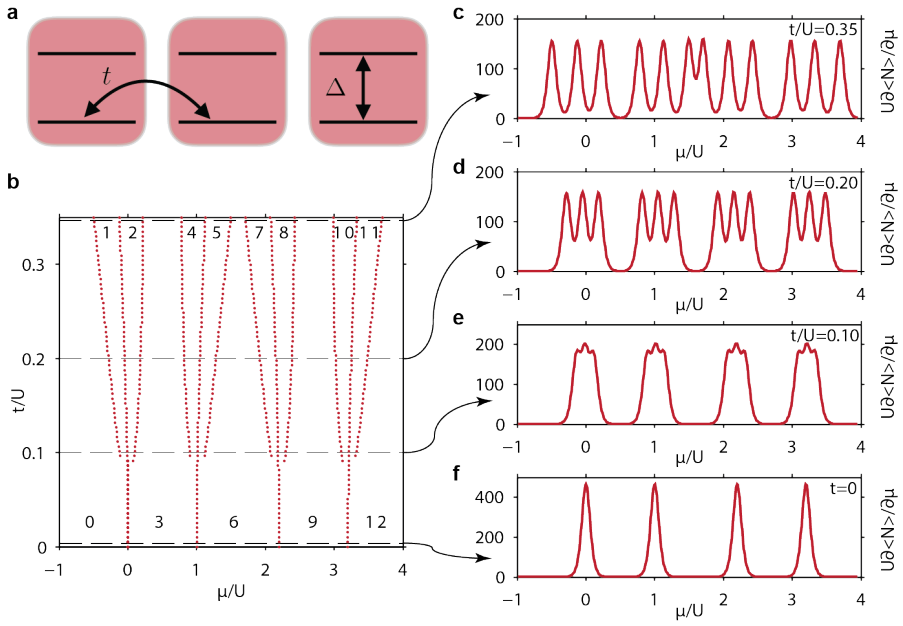

Figure 5.1: Simple model of CCB. Cartoon diagram of a simplified triple dot system is shown in **a**. The tunnel couplings t_{ij} and on-site interactions U_i are taken to be constant, the intersite interactions V_i are neglected and a finite level splitting Δ is defined between the first and second orbital. We use $\Delta/U = 0.2$ and $k_B T/U = 0.04$. Peaks in the charge addition spectrum are shown in red in **b**, **c**-**f** shown cuts at different values of t/U. Numbers indicate total number of electrons in the array when the chemical potential is placed in the respective gap. This simple model is based on [6].

5.2. The experimental phase space of a triple quantum dot array

An overview addition spectrum similar to that of Fig 5.1b amounts to measuring the experimentally accessible phase space of a triple quantum dot. Here, I first

describe a strategy for navigating such a gate space, which revolves around controlling the filling and delocalization, whilst measuring the Coulomb interaction parameters in the process [12]. Next, I outline how the full overview addition spectrum is put together.

As the tools described in the previous Chapter focus on small changes in gate space, we divide the diagram of Fig 5.1b into four minibands, and focus on one at a time. In the first miniband, the first three electrons are added to the array. In the second miniband the next three are added, and so on. This is similar to the concept of homogeneous filling described in the previous chapter and shown in Fig 4.8. Note that the inter-site Coulomb already splits the three peaks even at zero tunnel coupling, as shown again for the third miniband in Fig 5.2a. The middle dot detuning has to be chosen to minimize the width of the miniband (see Fig 5.2b), and the two tunnel couplings tuned to be a similar value. Once achieved, we note down the voltages of the three points highlighted in red in Fig 5.2 that are needed to follow the charge addition lines in the overview diagram.

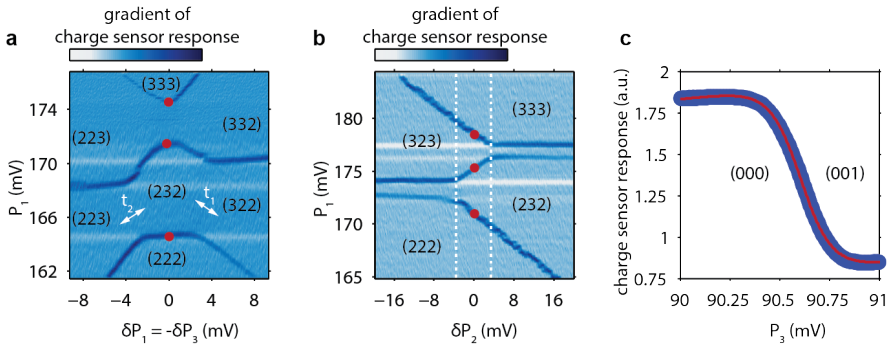

Figure 5.2: Miniband width and electron temperature. A zoom-in on a miniband is shown in **a**, in this case the from (222) to (333). The relevant anti crossings for measuring the tunnel couplings and inter-site Coulomb couplings are highlighted by the white arrows. As the energy level of the middle dot (horizontal line in **a**) is changed, the overal width of the miniband (vertical in **a**) is no longer due to only the inter-site Coulomb and tunnel coupling effects, but is increased by unwanted disorder in one of the dot potentials. In order to check that this is not the case, the middle dot energy can be varied and the width minimized (indicated by a P_2 tuning in between the vertical dashed lines in **b**). Red points indicate the sought after transition points for the overview diagram, of which the gate voltages required are stored. The width of a charge addition line, as shown in **c**, indicates the effective electron temperature, which is typically found to be 70-75 mK (6.0-6.5 μeV).

Next, we re-measure the cross-talk between all gates and the three dots, that allow us to reliably go from changing gate voltages to dot detunings, and use these to measure the inter-site and on-site Coulomb couplings. The relevant on-site interactions for our description within a single-band Fermi-Hubbard model as described in section 5.3 are those of the (111) state for the first two and the (333) state for the last two minibands. With the gate voltages, cross-talks and Hamiltonian

parameters for a certain value of the average tunnel coupling known, we can increase the tunnel couplings to a larger but equal value and re-measure cross-talk and interaction energies, progressively working our way up the miniband.

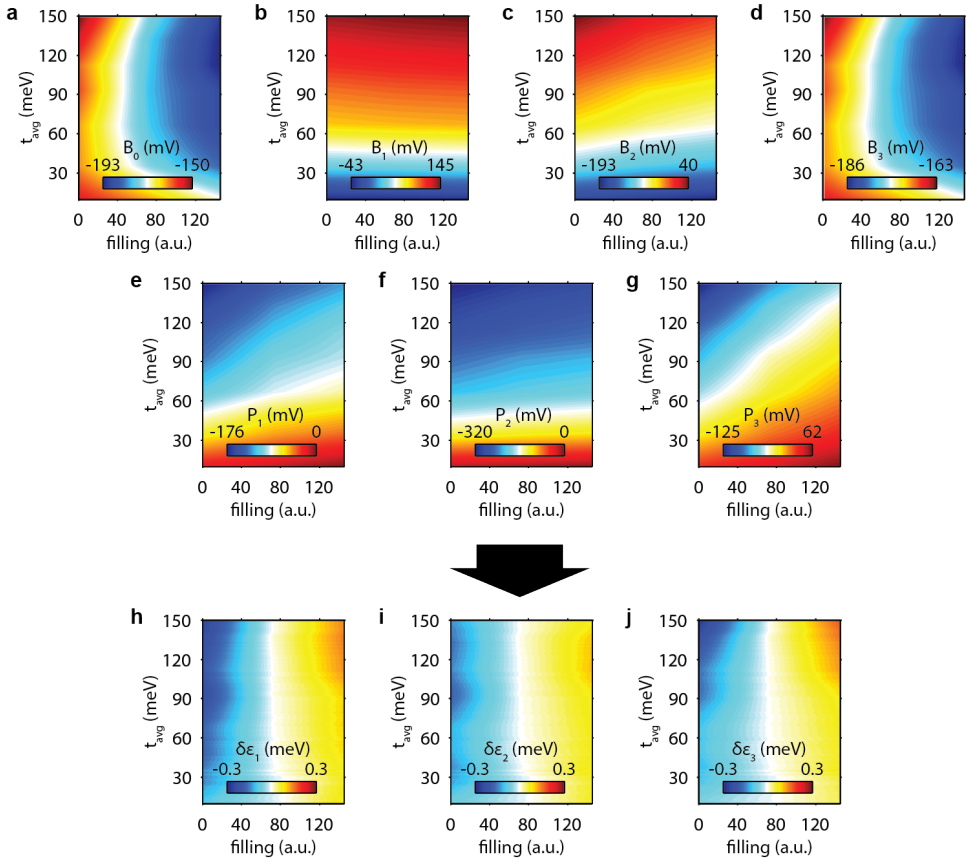

Figure 5.3: Gate voltages of second miniband. The gate voltages that are used to traverse the second miniband are shown in **a**-**g** as function of average tunnel coupling and filling. The filling axis is chosen to have charge state (111) on the left and (222) at the right, with the three charge addition lines defining this miniband at values of roughly 40, 80 and 120, respectively. As the cross-talks have also been measured at several particular tunnel couplings, we can derive the exact detunings that correspond to the filling axis as function of the seven gate voltages, shown in **j**-**l**. We define $\delta\epsilon_i = 0$ at the middle transition.

Having repeated this set of measurements for as large a range as possible in tunnel coupling, we now have a library of stored gate voltages that correspond with certain well-calibrated points in the overall diagram. By linearly interpolating with tunnel coupling, a set of voltages is made to continuously map out each individual miniband (Fig 5.3). As the cross-talk terms have also been repeatedly measured,

the required gate voltages can be converted to changes in the site-specific detunings $\delta\epsilon_i$, taking the middle transition as a reference (Fig 5.3h-j).

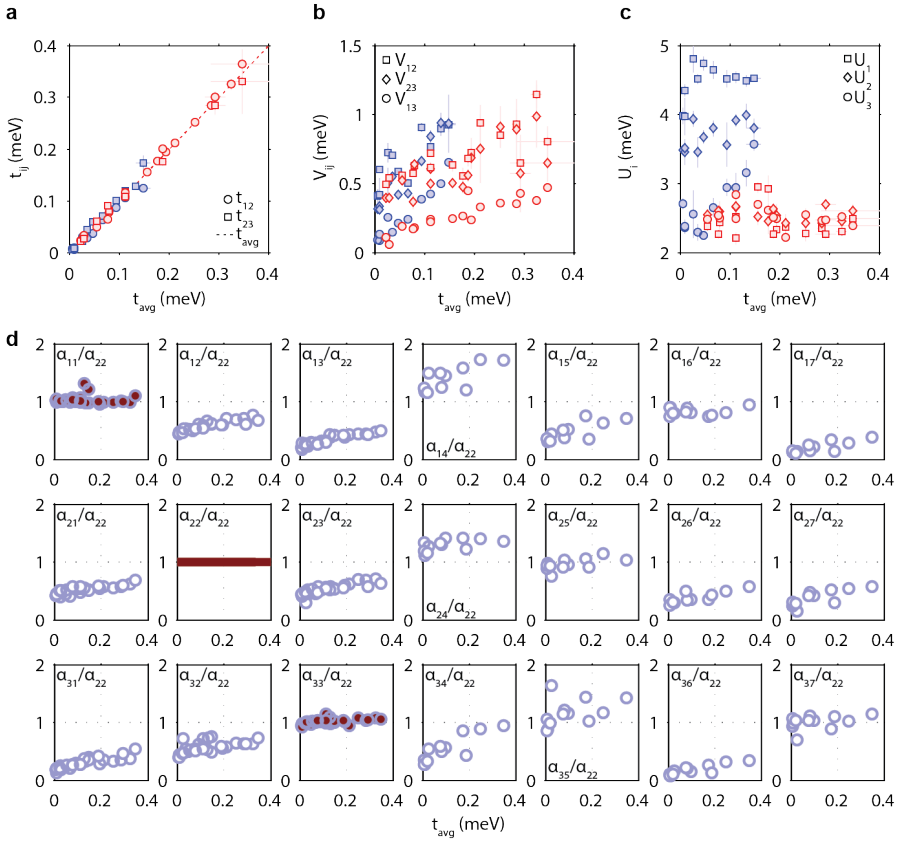

Figure 5.4: Measured energies. Calibrated tunnel coupling values (**a**) and measured inter-site Coulomb (**b**) and on-site Coulomb energies (**c**) as function of the average tunnel coupling. Blue points indicate the first two minibands, red points the third and fourth miniband. For the on-site interactions, this means blue points are measured in the (111) charge state and red points in the (333) charge state. Measured cross-talks α_{ij} between gate j of (P_1,P_2,P_3,B_0,B_1,B_2,B_3) and dot i are shown in **d**, also as function of the tunnel couplings. No visual distinction is made between the different minibands.

In tuning the individual minibands, we found some regimes in tunnel coupling hard to reach. For the first and second minibands, for example, tunnel couplings were limited to 30 μeV and 150 μeV, respectively. At larger tunnel couplings, either (i) only one of the two tunnel coupling could be further increased and at expense of the other tunnel coupling, (ii) the voltages themselves became too large (too strong local fields can lead to a rearrangement of charges in the doping layer) or (iii) too large voltage differences between adjacent gates were required, that can

lead to leakage. If future experiments are aimed at larger tunnel couplings at low fillings, the lithographically defined dot-to-dot separation should be made smaller by design. With more than six electrons in the array, on the other hand, we found that the smallest tunnel rates were unachievable, which is probably due to the larger wave function overlap of the more extended dots [13].

These limits in achievable tunnel rates are not surprising, as this particular triple dot design [14] is optimized for spin qubit measurements that focus on the regime with around 10 μeV tunnel coupling and one electron per site [15, 16]. In order to increase the overall range in which we can tune the tunnel rates regardless of filling, a design where gating is not achieved from the side, but directly from the top, would be preferred. In such a gate design, the relevant plunger and barrier gates will also be separated from each other and the heterostructure by dielectrics, further increasing the maximum gate voltages that can be applied [17, 18]. Note furthermore that the voltages required on the different gates are quite distinct, showcasing the need for tuning protocols as described in the previous Chapter, to overcome the inherent inhomogeneity and disorder.

Fig 5.4 shows the measured tunnel couplings, interaction energies and cross-talk terms for the four minibands. Note that inter-site energies increase with tunnel coupling, which is most likely due to changing dot locations. On-site energies remain fairly constant with tunnel coupling, but their values depend on the number of electrons in the dot already, and at one electron per dot, differ substantially between the different dots. Such remaining inhomogeneity is beyond gate control, and might be of concern for quantum simulation proposals where both local holon and doublon excitation energies are typically assumed to be constant across the array. For our current purposes however, it is not a concern, as the methods of the last Chapter allow us to account for this inhomogeneity.

As calibrating large changes in the ϵ_i directly is hard given the inherent non-linearities, we fix the middle transitions of the minibands and plot the minibands at distances corresponding to the measured interaction energies at low tunnel coupling. It can be seen in Fig 5.1 that this is justified for the effect of tunnel coupling on band bending for these values of $t/U < 0.2$. However, it neglects changes in the interaction energies with tunnel coupling as shown in Fig 5.4b-c. We choose ϵ_3 as the variable in which we express the filling, and plot the resulting overview in Fig 5.5.

The main effect of increased tunnel coupling is a widening of the minibands and an accompanying reduction of the gaps at half filling, analogous to the reduction of the Mott gap. Given the finite size of the array, these gaps do not close completely, as a finite capacitance exists for the resulting 'large dot' at high tunnel coupling. As all Hamiltonian parameters are calibrated or measured, we can compare the measured transitions to Fermi-Hubbard theory (red points in Fig 5.5). Details of this calculation are shown in section 5.3. The agreement validates the experimental tools for Hamiltonian engineering discussed in the previous Chapter, and shows how detailed mapping of a quantum dot array to a desired Hubbard model is possible.

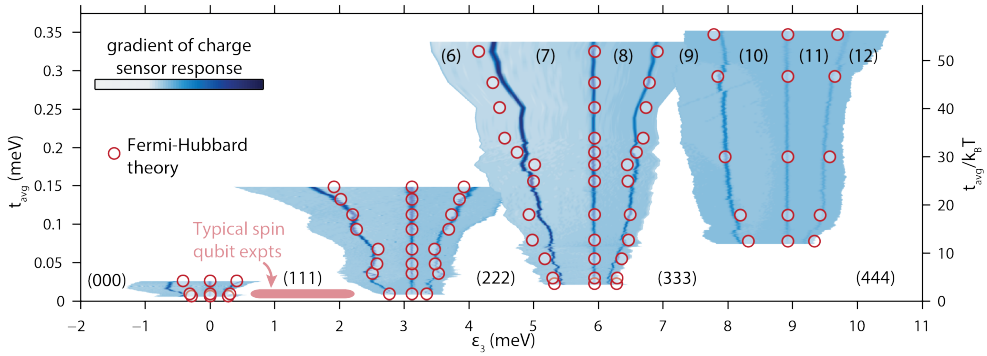

Figure 5.5: Collective Coulomb blockade transition. The experimentally accessed phase space is mapped out in continuous charge sensing, with addition lines showing up in dark blue. The spacings between the bands are taken from the low tunnel coupling values of the interaction energies, and are taken to be constant with tunnel coupling. Simulated locations of the transitions are shown in red, for the same values of average tunnel coupling where the tuning was done and the energies measured.

5

To clearly distinguish the CB regime at low and CCB regime at high tunnel coupling, we focus on the half-filled band with three electrons per site and measure both in charge sensing and transport through the quantum dot array (Fig 5.6).

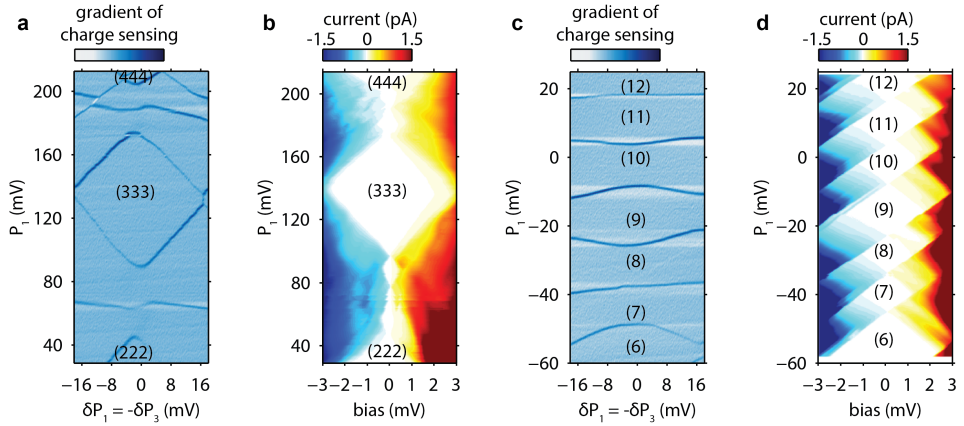

Figure 5.6: Low and high tunnel coupling regimes in charge and transport. Charge stability diagrams at low ($t/U < 0.02$, **a**) and high ($t/U > 0.15$, **c**) tunnel coupling. Transport data in both low and high tunnel coupling regimes are also shown in **b** and **d**, respectively. A combination of gates is swept in the vertical direction (see section 4.2), but only P_1 values are shown. Bias is applied for 60% on the leftmost and 40% on the rightmost reservoir.

The distinct slopes of the charge addition lines in the low tunnel coupling regime

indicate the three isolated dots. This individual nature is all but gone at large tunnel couplings, indicating the incipient formation of a single large dot (compare Fig 5.6a,c). A similar effect is seen in transport, where Coulomb diamonds appear along the zero detuning line at applied bias. In the case of isolated dots, the largest Coulomb diamonds correspond to homogeneously filled states such as (333), whereas smaller Coulomb diamonds elsewhere indicate that significantly less bias is required for current to flow when the Fermi level is placed inside a miniband (Fig 5.6b). At high tunnel couplings, this distinction is all but gone, and the Coulomb diamonds indicating charge addition become more independent of filling, as expected for a single, large dot (Fig 5.6d).

5.3. Verifying the toolbox with classical simulations

We perform numerical calculations in line with the experiments by focusing on individual minibands at certain tunnel couplings, and taking local values of the interaction energies into account[2]. Both the first two and the last two minibands are simulated independently using an effective single-band Hubbard Hamiltonian (see Eq. 2.4 and [20]).

First of all, we have to find the correct (ϵ_1,ϵ_2,ϵ_3)-line that corresponds to horizontal changes in Fig 5.5 and takes the homogeneous filling into account. This is done by identifying and linking the two points (for n and $n' = n+1$) where (n,n,n) is degenerate with ($n+1$,n,n), (n,$n+1$,n) and (n,n,$n+1$). Next, we search for the charge transitions residing on this line, and write down their ϵ_i's (see Table 5.1). To clarify the difference with changing all ϵ_i uniformly, we also show the calculated transitions when the array is filled along (μ,μ,μ) with $\mu = \frac{1}{N}\sum_i \epsilon_i n_i$. The data is clearly not described by such uniform filling.

Table 5.1: Transition points for a triplet dot system with parameters $t = 0.29, U_1 = 2.26, U_3 = 2.48, V_{12} = 0.65, V_{23} = 0.57, V_{13} = 0.43$. The column headings $N_1 \rightarrow N_2$ indicates that the data for each column are for the transition from a total of N_1 particles to N_2 particles. ϵ_i ($i = 1, 2, 3$) are the 'local' chemical potentials on each dot, while μ is the 'uniform' chemical potential. The last two columns compare the theoretical (Th.) and experimental (Exp.) width of the fourth miniband, that from 9 to 12 electrons. All energies are given in meV.

	$6 \rightarrow 7$	$7 \rightarrow 8$	$8 \rightarrow 9$	$9 \rightarrow 10$	$10 \rightarrow 11$	$11 \rightarrow 12$	(Th.)	(Exp.)
ϵ_1	6.38	7.13	8.05	9.78	10.56	11.51	1.73	1.67
ϵ_2	7.46	8.37	9.48	11.58	12.53	13.68	2.10	1.91
ϵ_3	6.66	7.44	8.40	10.22	11.04	12.04	1.82	1.74
μ	6.62	7.34	8.98	10.10	11.02	13.26	3.16	-

From these calculated values, the theoretical width of the miniband can be ex-

[2] The theoretical work and computer simulations described in this section were performed by X. Li and S. Das Sarma at the University of Maryland as part of [19].

tracted (see Table 5.2). This still leaves one degree of freedom, the relative position of the middle transition. The middle transition is typically halfway, but can shift somewhat depending on the detailed middle dot detuning (see Fig 5.2b). To overlay the simulated miniband widths on our data, we use values for the relative location of the middle transition of (0.5,0.6,0.65,0.6) for the four minibands, respectively.

Table 5.2: Comparison of the experimental (Exp.) and theoretical (Th.) width of the fourth miniband. Theoretical widths take the interaction energies measured at the specific tunnel coupling values into account. All energies are in meV.

t	ϵ_1 (Th.)	ϵ_1 (Exp.)	ϵ_2 (Th.)	ϵ_2 (Exp.)	ϵ_3 (Th.)	ϵ_3 (Exp.)
0.08	1.00	1.00	1.16	1.13	1.02	0.99
0.11	1.16	1.09	1.43	1.46	1.23	1.37
0.19	1.58	1.54	1.82	1.76	1.62	1.53
0.29	1.73	1.76	2.10	2.07	1.82	1.74
0.35	2.04	2.18	2.35	2.43	1.91	1.96

5.4. Discussion: what has this example told us?

The work described in this Chapter (as summarized in Fig 5.5) entails an exercise in the control described in the previous Chapter as well as the exploration of its limits.

In terms of control: tuning across a phase space such as that of Fig 5.2 took some time, but was done using a process that can be sped up significantly more. Already over the course of measuring the data in this Chapter, we got more efficient, but substantial follow-up steps in automation and control are in progress. Typical errors in control and energy measurements that we settled for were $\sigma(t_i)/t$ **and** $\sigma(\delta\epsilon_i)/U$ $<$ **5 per cent**, but can in principle be reduced further by more repeat measurements (mainly to capture remaining non-linearities) to the limit of the inherent thermal broadening. Note also that we found the required gate voltages to be surprisingly robust. Drifts in gate space for this particular device are easily correctable even on the timescale of months. Furthermore, as mentioned several times in this and the previous Chapter, overlapping gate designs should make the control even easier. First, such designs separate the functions of depleting parts of the 2DEG and that of influencing the potential in the section where the dot array will form. Second, they allow for the definition of a more controlled one-dimensional channel, which might furthermore help in decreasing non-linearities that arise due to a movement of the dots in the direction perpendicular to the channel. Last, such gate designs show significantly less cross-talk [17].

In terms of the limits in the controllable parameter space, let us look at the tunability of different terms in the Fermi-Hubbard Hamiltonian. We shall take the mean on-site interaction energy as a reference, but will also refer to the measured electron temperature. Fig 5.2 shows the controlled relative strength of interactions versus delocalization, or t/U**, from 0 to 0.14 (0 - 54** $k_B T$**)**, as well as the simultaneous

control of filling μ/U **from -1 to 4 (-300 - 1200 $k_B T$)**. Practical limits on the latter are due to unwanted remaining disorder of the device. In this case, an unwanted dot shows up for larger fillings (it can be seen in the top-left of Fig 5.6a as it anti crosses a middle dot line.). Practical limits on the former are perhaps more relevant. As described in this Chapter, several practical effects, most of which are design-related, limit the achievable tunnel rates. On top of these, note how the toolbox described in the previous Chapter starts to break down for larger tunnel couplings, as it gets progressively harder to distinguish individual sites.

Site-specific detunings can also be applied, and as such also disorder in on-site energies imprinted. The homogeneous filling defining $\delta\epsilon_i = 0$ and used for Fig 5.2 constitutes a good starting point, and adding disorder $\sigma(\delta\epsilon_i)/U$ **in the range of -2 to 2 (-600 - 600 $k_B T$)** is fairly straightforward, as also indicated by the measurements for the interaction energies. This range should more than suffice for studying disorder-(co)driven localization effects [1].

Important for the realization of correlated phases, these energies can all be made sufficiently larger than temperature. As per some estimates, a superconducting phase can be stabilized with $t/k_B T = 20$ in the 2D Hubbard model [21]. One has to keep in mind, however, that these large energy scales also mean short time scales. Although the large energies with respect to temperature are convenient for realizing correlation effects in steady state without requiring adiabatic initialization [22], the corresponding time scales for charge excitations are in the picosecond regime, and as such will be hard to measure. A reduction in electron temperature (measured here to be 70-75 mK) by a factor 5 or so might be possible by careful filtering and shielding [23], but a reduction in charge noise that leads to an increase in coherence times for charge excitations would be even more welcome (unexpectedly lower charge noise levels have recently been measured [24]).

Another implicit number is obviously sample size, as described by the number of sites $N_s = 3$. For larger devices, one could measure the scaling behavior on the reduction of the Mott gap at half filling with tunnel coupling. In a one-dimensional array of dots (where multiple orbitals per site exist) and in the thermodynamic limit, a quantum phase transition is indeed expected at a finite t/U [25]. In order to see the gap fully close and witness the subsequent metallic behavior in the CCB phase, either a larger device or a higher temperature is needed.

More worrying perhaps for future experiments is the remaining and uncontrollable inhomogeneity in the interaction terms. As a matter of example, in the single-electron regime for this device, $\sigma(U_i)/U_i > 25$ **per cent**. For overlapping gate designs in SiGe, however, this relative spread in charging energies has been measured to be less than 10 per cent [18]. If this is an important number, one can consider working with a larger number of electrons per dots. For the measurements shown here, for instance, $\sigma(U_i)/U_i < 5$ **per cent** in the (333) regime.

Overall, the results highlight how quantum dots can be used to emulate the Hubbard model over a large range of effective interaction strengths and with well defined dot occupation in the regime where quantum correlations are strong [6, 26–

28]. The next Chapter takes these numbers and considerations to assess the feasibility of several theoretical proposals for quantum simulations using gate-defined quantum dots.

References

[1] M. Imada, A. Fujimori, and Y. Tokura, "Metal-insulator transitions," *Reviews of Modern Physics*, vol. 70, pp. 1039–1263, 10 1998.

[2] J. H. d. Boer and E. J. W. Verwey, "Semi-conductors with partially and with completely filled 3d-lattice bands," *Proceedings of the Physical Society*, vol. 49, pp. 59–71, 8 1937.

[3] N. F. Mott and R. Peierls, "Discussion of the paper by de Boer and Verwey," *Proceedings of the Physical Society*, vol. 49, pp. 72–73, 8 1937.

[4] R. Barends, L. Lamata, J. Kelly, L. García-Álvarez, A. G. Fowler, A. Megrant, E. Jeffrey, T. C. White, D. Sank, J. Y. Mutus, B. Campbell, Y. Chen, Z. Chen, B. Chiaro, A. Dunsworth, I.-C. Hoi, C. Neill, P. J. J. O'Malley, C. Quintana, P. Roushan, A. Vainsencher, J. Wenner, E. Solano, and J. M. Martinis, "Digital quantum simulation of fermionic models with a superconducting circuit," *Nature Communications*, vol. 6, p. 7654, 7 2015.

[5] A. Mazurenko, C. S. Chiu, G. Ji, M. F. Parsons, M. Kanász-Nagy, R. Schmidt, F. Grusdt, E. Demler, D. Greif, and M. Greiner, "A cold-atom Fermi–Hubbard antiferromagnet," *Nature*, vol. 545, pp. 462–466, 2017.

[6] C. A. Stafford and S. Das Sarma, "Collective Coulomb blockade in an array of quantum dots: A Mott-Hubbard approach," *Physical Review Letters*, vol. 72, pp. 3590–3593, 5 1994.

[7] L. P. Kouwenhoven, F. W. J. Hekking, B. J. van Wees, C. J. P. M. Harmans, C. E. Timmering, and C. T. Foxon, "Transport through a finite one-dimensional crystal," *Physical Review Letters*, vol. 65, pp. 361–364, 7 1990.

[8] F. R. Waugh, M. J. Berry, D. J. Mar, R. M. Westervelt, K. L. Campman, and A. C. Gossard, "Single-Electron Charging in Double and Triple Quantum Dots with Tunable Coupling," *Physical Review Letters*, vol. 75, pp. 705–708, 7 1995.

[9] C. Livermore, C. H. Crouch, R. M. Westervelt, K. L. Campman, and A. C. Gossard, "The Coulomb Blockade in Coupled Quantum Dots," *Science (New York, N.Y.)*, vol. 274, pp. 1332–5, 11 1996.

[10] S. D. Lee, K. S. Park, J. W. Park, J. B. Choi, S.-R. E. Yang, K.-H. Yoo, J. Kim, S. I. Park, and K. T. Kim, "Single-electron spectroscopy in a coupled triple-dot system: Role of interdot electron-electron interactions," *Physical Review B*, vol. 62, pp. R7735–R7738, 9 2000.

[11] A. Bogan, L. Bergeron, A. Kam, P. Zawadzki, S. Studenikin, L. Gaudreau, and A. Sachrajda, "Strategies for tuning a linear quadruple quantum dot array to the few electron regime," *Applied Physics Letters*, vol. 109, no. 17, p. 173108, 2016.

[12] L. Janssen, *Scalable toolbox for quantum simulations in a GaAs triple dot array*. MSc thesis, 2016.

[13] J. G. Pedersen, C. Flindt, A.-P. Jauho, and N. A. Mortensen, "Influence of confining potentials on the exchange coupling in double quantum dots," *Physical Review B*, vol. 81, p. 193406, 5 2010.

[14] J. Medford, J. Beil, J. M. Taylor, S. D. Bartlett, A. C. Doherty, E. I. Rashba, D. P. DiVincenzo, H. Lu, A. C. Gossard, and C. M. Marcus, "Self-consistent measurement and state tomography of an exchange-only spin qubit," *Nature Nanotechnology*, vol. 8, pp. 654–659, 9 2013.

[15] T. A. Baart, P. T. Eendebak, C. Reichl, W. Wegscheider, and L. M. K. Vandersypen, "Computer-automated tuning of semiconductor double quantum dots into the single-electron regime," *Applied Physics Letters*, vol. 108, p. 213104, 5 2016.

[16] T. Baart, T. Fujita, C. Reichl, W. Wegscheider, and L. Vandersypen, "Coherent spin-exchange via a quantum mediator," *Nature Nanotechnology*, vol. 12, pp. 26–30, 2016.

[17] M. G. Borselli, K. Eng, R. S. Ross, T. M. Hazard, K. S. Holabird, B. Huang, A. A. Kiselev, P. W. Deelman, L. D. Warren, I. Milosavljevic, A. E. Schmitz, M. Sokolich, M. F. Gyure, and A. T. Hunter, "Undoped accumulation-mode Si/SiGe quantum dots," *Nanotechnology*, vol. 26, p. 375202, 9 2015.

[18] D. Zajac, T. Hazard, X. Mi, E. Nielsen, and J. Petta, "Scalable Gate Architecture for a One-Dimensional Array of Semiconductor Spin Qubits," *Physical Review Applied*, vol. 6, p. 054013, 11 2016.

[19] T. Hensgens, T. Fujita, L. Janssen, X. Li, C. J. Van Diepen, C. Reichl, W. Wegscheider, S. D. Sarma, and L. M. K. Vandersypen, "Quantum simulation of a Fermi-Hubbard model using a semiconductor quantum dot array," *Nature*, vol. 548, pp. 70–73, 2 2017.

[20] X. Wang, S. Yang, and S. Das Sarma, "Quantum theory of the charge-stability diagram of semiconductor double-quantum-dot systems," *Physical Review B*, vol. 84, p. 115301, 9 2011.

[21] P. A. Lee, N. Nagaosa, and X.-G. Wen, "Doping a Mott insulator: Physics of high-temperature superconductivity," *Reviews of Modern Physics*, vol. 78, pp. 17–85, 1 2006.

[22] U. Farooq, A. Bayat, S. Mancini, and S. Bose, "Adiabatic many-body state preparation and information transfer in quantum dot arrays," *Physical Review B*, vol. 91, p. 134303, 4 2015.

[23] F. Mueller, R. N. Schouten, M. Brauns, T. Gang, W. H. Lim, N. S. Lai, A. S. Dzurak, W. G. van der Wiel, and F. A. Zwanenburg, "Printed circuit board metal powder

filters for low electron temperatures," *Review of Scientific Instruments*, vol. 84, p. 044706, 4 2013.

[24] X. Mi, X. Mi, J. V. Cady, D. M. Zajac, P. W. Deelman, and J. R. Petta, "Strong coupling of a single electron in silicon to a microwave photon," *Science*, vol. 2469, 2016.

[25] P. Schlottmann, "Metal-insulator transition in an Hubbard-like model with degeneracy in one dimension," *Physical Review B*, vol. 45, pp. 5784–5789, 3 1992.

[26] E. Manousakis, "A Quantum-Dot Array as Model for Copper-Oxide Superconductors: A Dedicated Quantum Simulator for the Many-Fermion Problem," *Journal of Low Temperature Physics*, vol. 126, pp. 1501–1513, 3 2002.

[27] T. Byrnes, N. Kim, K. Kusudo, and Y. Yamamoto, "Quantum simulation of Fermi-Hubbard models in semiconductor quantum-dot arrays," *Physical Review B*, vol. 78, p. 075320, 8 2008.

[28] P. Barthelemy and L. M. K. Vandersypen, "Quantum Dot Systems: a versatile platform for quantum simulations," *Annalen der Physik*, vol. 525, pp. 808–826, 11 2013.

6

Towards quantum simulations of classically intractable models

Yesterday's sensation is today's calibration,
and tomorrow's background.

Richard P. Feynman

The work shown in the previous Chapters showcases the potential for quantum simulation experiments using artificial lattices of interacting electrons confined in semiconductor materials. Does that bring Feynman's dream of solving open problems in physics through direct emulation within reach, using these devices? I attempt to answer that question here. The small number of sites in current quantum dot arrays is a clear issue, but there are also some less obvious experimental difficulties and complexities (**Section 6.1**). What advances can we expect from the sustained effort of improving quantum dot devices and control (**Section 6.2**) in attempts to build quantum processors employing its emergent spin physics (**Section 6.3**)? Given these considerations, opportunities for emulating *many-body localization* physics in linear arrays are discussed in **Section 6.4**. And although large two-dimensional systems seem out of reach, quasi-one-dimensional systems such as ladders are feasible using current quantum dot fabrication techniques. In **Section 6.5**, I describe how these can already give insight into open questions in the description of doped Mott insulators.

6.1. Complications

In this section I will discuss some intricacies in employing quantum dots as simulators for Hubbard physics that we could avoid discussing for the work described in the previous Chapters, but that are important to take into consideration for future work. First, we will write down a more complete Hamiltonian that takes orbital degrees of freedom and magnetic fields into account. Second, we summarize the achievable energies for the parameters of this model, as well as the levels of disorder after tuning and their sensitivity to gate voltage changes. This last point is relevant as electrons in a quantum dot array do not form a fully isolated system; electrical and magnetic noise couple in and lead to dissipation and dephasing effects. Lastly, we will discuss scaling at a device level, and argue that two-dimensional arrays with site-specific control are unachievable.

We have already seen that given the less localized wave functions of electrons in dots as compared to those of coupled atomic orbitals, they are described by a more extended Hubbard model. As such, for quantum dots the orbital quantization (whose characteristic energy spacings grow inversely proportional to the later dimension squared) is typically smaller than on-site interactions (that grow inversely proportional to the lateral dimension). Although quantum dots get filled similarly to atomic orbitals (in an orderly manner, starting from the lowest orbital [1]) one has to keep in mind that orbital splittings are typically smaller than the on-site repulsion.

For a thorough description at all relevant energy scales, we should therefore use a multi-band Hamiltonian. In the case of the experiment of the last Chapter, for instance, this might mean that as we consider scaling the experiment to longer arrays, the closing of the charge excitation gap in the regime with one electron per site might behave qualitatively differently from that with three or five, and that a complete calculation of the expected transitions would have to take all orbitals into account simultaneously [2]. The added complexity means that fewer dots are needed to make simulating such a transition classically intractable, but it also means that the system does not behave like the simple single-band Hubbard model one might prefer to study. Furthermore, an equally efficient manner for measuring these orbitals as was employed for the interaction energies would be needed to match theory and experiment [3].

As we write down a multi-band Hamiltonian, tunneling and interaction terms should take into account both inter- and intra-orbital effects, the need for which we have implicitly encountered in the previous Chapter as the addition energies in (111) and (333) were seen to differ. I add a Zeeman term that describes the energy cost of aligning (or not) the electron spins along the quantization axes defined by the local magnetic fields. In this term, g is the electron g-factor, μ_B is the Bohr magneton and σ_i the spin operator that describes the total spin on site i, which feels the local field $\vec{B}_i$.

Let us now put everything together. For sake of clarity, I sum up the parts of the Hamiltonian that are controlled by experimentally applied fields on the first line.

These entail the local electric fields that are controlled by gate voltages (assuming orthogonal control as described in Chapter 4 is achieved, we can describe the local influence of virtual plunger gates p_i and barrier gates b_{ij}) and the global magnetic field $\vec{B}_{\text{ext}}$. Local engineering of Zeeman energies is also possible to some extent, and will be discussed in section 6.3. Putting everything together, we get:

$$\begin{aligned} H = &\underbrace{-\sum_i \epsilon_i \hat{n}_i}_{H_{\text{detuning}}} \underbrace{- \sum_{\langle i,j\rangle,\alpha,\alpha',\sigma} t_{ij\alpha\alpha'}[\hat{c}^\dagger_{i\alpha\sigma}\hat{c}_{j\alpha'\sigma} + \text{h.c.}]}_{H_{\text{tunneling}}} + \underbrace{\frac{g\mu_{\text{B}}}{2}\sum_i \vec{B}_i\sigma_i}_{H_{\text{Zeeman}}} \\ &\underbrace{\sum_{i,\alpha}\frac{U_{i\alpha\alpha}}{2}\hat{n}_{i\alpha}[\hat{n}_{i\alpha}-1] + \sum_{i,\alpha,\alpha'\neq\alpha}\frac{U_{i\alpha\alpha'}}{2}\hat{n}_{i\alpha}\hat{n}_{i\alpha'} + \sum_{i,j}V_{ij}\hat{n}_i\hat{n}_j}_{H_{\text{interaction}}} + \underbrace{\sum_{i,\alpha}\Delta_{i\alpha}\hat{n}_{i\alpha}}_{H_{\text{orbital}}} \end{aligned} \tag{6.1}$$

where α describes the orbital degree of freedom, $\Delta_{i\alpha}$ keeps track of the extra energy of an electron inhabiting orbital α on site i and dot occupations n_i sum over both σ and α.

One of the largest effects of orbitals seen in charge stability is that of decreasing the charging energy $E_c(N)$ required to add an electron to a dot with N electrons already present. Using the Hamiltonian above, we find for filling the first three orbitals ($\alpha = 0, 1, 2$) of a single dot that $E_c(1) = U_{11}$, $E_c(2) = U_{12} + \Delta_1$, $E_c(3) = (2U_{12}+U_{22})/3$, $E_c(4) = (U_{13}+U_{23})/2+(\Delta_2-\Delta_1)$ and $E_c(5) = (U_{33}+2U_{13}+2U_{23})/5$. An independent measurement of the orbital splittings would thus allow one to extract the orbital-dependent on-site repulsions of up to the last fully filled orbital. This would then allow for the fitting of charge stability diagrams over larger ranges of filling[1].

Note that despite the additions to the single-band extended Hubbard Hamiltonian used in the previous Chapters, Eq. 6.1 still has many underlying assumptions. For instance, we ignore the dependence on the orbital degree of freedom of the inter-site Coulomb terms, detunings and g-factor, the spin-orbit effect in general and assume an isotropic g-factor [4].

As was seen in the last chapter, there are limits to the degree of homogeneity we can reach with the tuning process, as well as in the interaction-energies. I list the values we found below, as well as typical numbers for how static these are with changes in the control fields, in particular the closest gate voltage. The effect of a global magnetic field on these parameters has not been measured here, but in particular the effect of the perpendicular component on confinement and therefore orbital splittings [5] and tunnel rates [6] is known to be large. The global magnetic field, however, is typically kept constant for long periods of time during measurements, and some corresponding retuning with changing field values taken for granted.

[1] The constant interaction model, as the name suggests, does not take such multi-band effects as changes in the interaction energy with filling into account.

Table 6.1: Assessment of parameters and gate dependencies. Fermi-Hubbard model parameters and dependence on gate voltages, using the device measured in the previous Chapters as an example. For the orbital splitting, we take the energy difference between the ground and first excited orbital. Note that (1) any tunnel coupling apart from nearest-neighbor can be ignored, and that the remaining inhomogeneity in tunnel coupling is mostly due to the accuracy of the tunnel coupling measurements used for tuning. The Zeeman term and its sensitivity (2) will be discussed in section 6.3. The fall-off of inter-site Coulomb with distance (3) should be assessed in more detail in larger devices. Here I list the nearest-neigbor value.

parameter	typical size (meV)	inhomogeneity after tuning	sensitivity to gate voltage (1 mV on nearby gate)
ϵ_i	-5 - 15	< 1 %	80 μeV
t_{ij}	0.01 - 0.3[1]	< 5 %	2 %
$\mu_B[gB]_i$	0 - 0.5		0 - 0.4 μeV[2]
U_i	2 - 5	25 %	< 1 μeV
V_{ij}	0.3 - 1[3]	10 %	8 μeV
Δ_i	1	?	?

6

Conduction band electrons in the semiconductor host device do not yield a fully isolated system. Electric field fluctuations arise due to charge noise in the material, interfaces and on the gate voltages, a certain phonon occupation exists at finite temperatures and fluctuations in the global, external field as well as on nearby nuclear spins couple to the system. As such, dissipation channels exist for both spin and charge degrees of freedom, and coherent superpositions can dephase due to fluctuating energy spacings. The largest effect is charge noise, which, when denoted as an rms voltage fluctuation on gates, is typically found to be several tens of μV depending on device and set-up [7–9]. A look at Table 6.1 makes it clear, then, that dephasing via detuning (ϵ_i) will usually be the most dominant contribution. Typical dephasing times for charge excitations are then also the shortest at under a nanosecond, although they can be extended to several nanoseconds when working with superpositions that are insensitive to ϵ_i in first order, such as the bonding and anti-bonding state at a polarization line [7].

These classical fluctuations, when described as an effective electron temperature, further indicate that initialization might not always yield a pure state - a finite amount of classical entropy will remain. Certain pure states can be adiabatically initialized [10], but a detailed look at the adiabaticity of such an initialization will be necessary at a case-by-case basis. It is however still here that quantum dots excel, with comparatively large energies with respect to effective temperature. In the experiments described in the previous Chapter, for instance, $t/k_BT > 50$ was reached.

Furthermore, other limits on experimental timescales (or corresponding frequencies) exist. Applied excitations are practically limited to several tens of GHz (with pulse rise times typically on the order of a fraction of a nanosecond), meaning that,

for instance, the 80 GHz tunnel couplings measured in the previous chapter cannot be effectively quenched. Obtained charge measurement bandwidths (at reasonable signal-to-noise-ratios) in GaAs devices with RF reflectometry on a sensing dot channel are on the order of MHz, a bandwidth which is yet to be realized in a silicon-based device.

Lastly, a comment should be made on scaling. Whereas current gate designs for linear arrays are copy-and-paste-able [11–13] with size limited by the yield of the fabrication and the number of control lines required, no such designs exist for going beyond linear arrays. Small plaquettes, including triangular and square designs, have been realized [14–16], but those still rely on a fan-out of gates to all sides. In principle, the fabrication recipes used for some of these devices [15, 16] but also the multi-layer gate stacks used for Si devices [17] suffice for realizing designs with the potential to define ladders of quantum dots, but so far, no measurement has shown how a single dot can have controllable tunnel rates to more than two direct neighbors. The problem of fan-out for gates indicates furthermore that large two-dimensional lattices with site-specific control are out of reach, as they require a number of layers in the fabrication that grows linearly with dimension, whereas three or four layers is the limit of what can be done whilst maintaining the tight spacing of the gates required for tunnel-coupled dots, even using state-of-the-art industrial fabrication processes [18].

Having established some limitations to keep in mind whilst proposing future experiments, let us now show how expected improvements at the device and control level and the focus on emergent models (where we can start ignoring many degrees of freedom and corresponding parameters) can still provide an interesting route forward.

6.2. Expected future advances

The spin physics of electrons in quantum dots has been proposed as a platform for gate-controllable quantum computing [19], and a large effort in the field of gate-defined quantum dots is indeed geared towards this goal in an attempt to leverage the potential for scalability provided by the compatibility with conventional CMOS nanofabrication techniques [20, 21], the long coherence times for individual spins in purified silicon substrates [17] and a potential robustness to modest increases in temperature [21].

Moving to silicon-based substrates, however, comes at the expense of reduced mobilities and increased effective masses as compared to GaAs substrates [22]. To counter these effects, a clearly defined channel and a tight spacing of neighbouring dots (and resulting gate-to-gate distances) is required. The alterations in gate designs that have been developed to achieve this are relevant for our current discussion, as they might greatly simplify the process of tuning.

To understand this, we must first realize that most currently used device designs on silicon substrates are undoped, and therefore require gates to accumulate in-

stead of deplete electrons in part of the 2DEG. As a first example, a strained silicon quantum well sandwiched by silicon-germanium layers can be grown epitaxially, defining a quantum well at some depth underneath the surface. As charge stability was found to be an issue when such heterostructures also used modulation-doped layers [22], most experiments are performed on undoped heterostructures. In a second method, a 2DEG is formed directly underneath the oxide that forms at the surface of an intrinsic silicon wafer [23]. A third method worth considering is that of patterned silicon grown on an insulator. The substrate can then be used as a bottom gate, and the silicon layer where the dots form is patterned to define a channel without added gate electrostatics required [20].

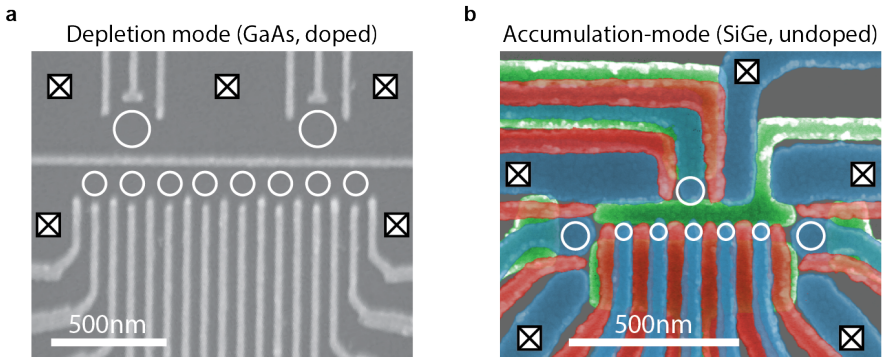

Figure 6.1: Comparing gate designs. Electron micrograph of an 8-dot gate layout (**a**) akin to that of the 3-dot device used in this work and false-color picture overlying gate micrographs of the three gate layers of a 5-dot gate layout (**b**, courtesy of N. Kalhor) designed for undoped SiGe. Fermi reservoirs contacted by ohmic contacts are shown with the crossed white box, whereas white circles indicate intended (sensing) dot locations. In a single-layer gate GaAs device such as in (**a**), bias cooling is used to deplete underneath the gates, which already loosely defines a channel. In the triple-layer SiGe design shown in (**b**), the different layers have different functions. The bottom layer (green) screens the effect of top layers from accumulating at unwanted locations, and can be further used to clearly define the relevant channels. The top layers form the local barriers (red) and plungers or accumulation regions (blue).

In depletion-mode devices with a single layer of gates such as the triple-dot device used in the previous Chapters, gates serve two purposes. First of all, they allow for a loose definition of the dot and sensing dot channels via the application of bias cooling voltages. By cooling down the device with positive voltages applied to the gates, the doping layer underneath the gates becomes more negatively charged, charges that get frozen below the ionization temperature of the silicon dopants (roughly 70 K) and continually impose depletion underneath the gates during subsequent operation. Second, they allow for the control of the potential landscape in the dot and sensing dot channels, influencing energy offsets and tunnel barriers. Because of this dichotomous function, however, these gates cannot be made to

run over the section of the 2DEG they are designed to influence during the tuning process, increasing cross-talk and limiting the amount of orthogonal control that can be achieved even with compensation of cross-talk (given the finite window for voltages that can be applied before leakage occurs)[2].

In accumulation-mode devices, however, these two tasks are split by design. Gates do run over the section of the 2DEG they are meant to influence (Fig 6.1), and the gate leads made unimportant as to allow to better define a one-dimensional channel through either the placement of a dielectric [12, 26] underneath the leads, a separate layer of screening gates [17], or by defining a channel in the semiconductor itself [20]. This has the potential for better gate control. Note, however, that a process with a first layer of screening gates could also be implemented on doped GaAs devices (which would then effectively serve as depletion gates). This, especially given the high mobilities and larger length scales that will suffice, could allow for very well-controlled devices.

Although a similar assessment to that of Table 6.1 remains to be fully done for larger devices and different gate designs on both GaAs and silicon-based substrates, the potential for increased dot homogeneity despite decreased 2DEG mobility has started to become more apparent, with for instance inhomogeneities in on-site Coulomb interactions of under 10 % measured for individually formed dots in a 9-dot linear array in SiGe [26] (the first orbital excited states were also measured in the same work, with a relative spread of roughly 15 % found).

The more confined dots in silicon have typically even higher orbital energies, but working in silicon comes at the expense of it being an indirect band-gap semiconductor, whose conduction band electrons reside in one of six different valley states. The band-engineering and electrostatics of a dot in a 2DEG break spatial symmetries and therefore the degeneracy of these valleys, although the gap between the lowest two remains smaller than that to the first orbital excited state [17]. Given the potential for spin qubits, however, there is a large effort at getting consistently large valley splittings (of over 100 μeV).

In general, GaAs is probably a better-suited platform for quantum simulation experiments that focus on the charge sector, as charge noise is found to be comparable, but the higher mobilities and proven high achievable tunnel couplings [11, 27] are clearly important factors here. The greatly improved spin coherence in silicon (and in particular purified silicon), on the other hand [17], make it readily preferred for emulations that focus on coherent evolution in the spin sector.

An important open question at the moment is what the dominant sources of charge noise are in quantum dot devices, and how it can be reduced. Some devices measured have already shown surprisingly narrow charge qubit linewidths [28], and these might yield clues as to its origin. In general, however, as device yield im-

[2] Single-layer gate devices with an added accumulation gate running across the dot array and a dielectric placed underneath the gates have been realized in GaAs, and show good control of the potential landscape [24, 25]. Spacings and cross-talk can be further reduced, however, by using multiple gate layers.

proves and characterization measurements become more common in the path towards scaling, one can hope to find systematic correlations that give further insight. The distinction between the effective electron temperature of a galvanically contacted Fermi reservoir and that of inter-dot transitions is an example, with the latter becoming more important as scaled-up devices have less contact with reservoirs, and reservoirs themselves can be fully depleted in accumulation-mode devices once the correct number of electrons is loaded onto the array. Such dependencies might hint at electrical noise on the gates or ohmic contacts to be the dominant source. In parallel, ongoing work on better semiconductor host material, dielectric layers and interfaces might bear fruit.

Lastly, expected advances in negating the experimental complexities involved with issues such as packaging, calibration and measurement of larger devices are worth mentioning. The need for more automated calibration tools is now widely realized, with clear paths forward known (some of which are described in the previous Chapters). Furthermore, increasing standardization of programming tools (such as the Python-based data acquisition framework QCoDeS) and control electronics as well as the reliability and ease of use of dilution refrigerators make that researchers find more time to specialize in the control of devices as compared to setting up the peripherals. Current experimental modus operandi can readily scale to linear arrays of several tens of dots without yet requiring any large engineering hurdles to be overcome.

6.3. Emergent quantum magnetism: spin physics

The emergent spin physics of a fixed number of electrons trapped in a quantum dot array obviously resembles the concepts used in the field of spin qubits. To introduce the subject in a way that allows for discussing the feasibility of future experiments, I will again write down an effective Hamiltonian and discuss its limits in control and homogeneity.

Assume each dot is occupied with a single electron, with the charge states deep in Coulomb blockade. Charge excitations and corresponding Hubbard parameters U,ϵ,V will then only play a role in second order (virtual) tunneling processes, with the remaining unfrozen degrees of freedom being the site-specific spins σ_i[3]. Because of Pauli blockade, such delocalization processes (in which an electron joins one of its neighbors, and one of them quickly returns to the emptied dot) are only possible when the spins are in a singlet-configuration, reducing the overall energy. As Pauli blockade has no spatially-defined quantization axis, this yields an effective isotropic (Heisenberg) exchange coupling between neighboring spins, in direct analogy to the direct (kinetic) exchange effect in materials.

In this simple picture, the virtual process requires two hopping events, with the intermediate state (the spins on the same site) at expense of an on-site repulsion U. As such, one expects a nearest-neighbor exchange coupling $J_{ij} \propto t_{ij}^2/U$, with

[3] Furthermore assume large enough orbital and valley splittings, so these can also be neglected.

typically employed values up to hundreds of MHz. The cost of double occupancy can be reduced by detuning the single-particle energies between the dots, meaning that the effective exchange coupling will depend on the location in the charge stability diagram. Only at the so-called symmetric operation point are the effective couplings insensitive to detuning to first order. In detunings where the equilibrium charge state has two electrons residing on the same dot, the spin triplets are allowed only with one of the electrons in an excited orbital/valley state, yielding an effective exchange coupling that depends on the smallest orbital/valley splitting [29]. Such exchange is also less sensitive to detuning, but is typically too large (too fast) to be useful in experiments.

Besides the exchange coupling of adjacent spins, we have to take the site-specific Zeeman term into account. I split it into two pieces: a global term, that can be seen as a mean Zeeman splitting and is tunable by an external magnetic field, and a 'disorder'-term, which takes site-specific effects into account:

$$H = \underbrace{\sum_{\langle i,j \rangle} J_{ij}\sigma_i\sigma_j}_{H_{\text{exchange}}} + \underbrace{\frac{g\mu_{\text{B}}}{2}\sum_i \langle \vec{B}_i \rangle \sigma_i}_{H_{\text{potential}}} + \underbrace{\frac{g\mu_{\text{B}}}{2}\sum_i \delta\vec{B}_i\sigma_i}_{H_{\text{designer-disorder}}} \tag{6.2}$$

From this equation, it is clear that the mean magnetic field $\langle \vec{B}_i \rangle$ can be seen as something like a chemical potential term for spin, that defines an overall quantization axis. At an externally applied field of 1 T, this is the largest term at 5 GHz (GaAs) or 28 GHz (Si), overcoming thermal fluctuations and polarizing all spins in equilibrium. The effective exchange term in double occupancy, however, can be even larger, providing a ways to adiabatically initialize regardless of external field. This can be done by initializing in charge states with variable amounts of double occupancy, yielding unpolarized (202020..) to partially polarized (20112011..) to fully (1111..) polarized spin states [10].

The last term warrants further discussion. Site-specific variations can occur both on the g-factor and the magnetic field. Variations in g-factor are typically small, and might be slightly dependent on gate voltages [30]. In GaAs, the Overhauser field induced by background nuclear spins yields significant variations $\delta\vec{B}_i$ in local magnetic fields (on the order of several mT [4]). Variations in local field can, however, also be engineered, using micro-magnets placed on the device. Micro-magnets will induce not only a static field offset, but also magnetic field gradients (typically on the order of tenths of mT/nm to several mT/nm, see the supplementary info of [31] for general design considerations). Because of these gradients, voltage-induced shifts in the effective dot location (on the order of nm/V, depending on gate design and corresponding shallowness of the confinement potential) will also have an influence on the Zeeman energy. This means that charge noise can couple to the spin degree of freedom and limit coherence times [32], but also that we can engineer using gate voltages the site-specific disorder term. Assuming voltage ranges of several tens of mV are acceptable as to stay reasonably close to

the charge symmetry point, we can tune Zeeman disorders over several (tenths of) MHz.

As larger devices become available, a similar phase-space (as function of $J/\mu_B gB$, $k_B T/\mu_B gB$ and $\sigma(\mu_B[gB]_i)/\mu_B gB$) and parameter assessment to that of the previous Chapter (and Table 6.1) should be done for this Heisenberg Hamiltonian, showing access to disordered, anti-ferromagnetic and polarized phases[4]. Equivalently, these emergent spin systems require a toolbox akin to that described in Chapter 4 for the charge stability, with a particular focus on scalable spin-to-charge conversion [29, 33–35] and efficient measurements of on-site Zeeman splittings [34, 36] and exchange-couplings [11]. Such tools, however, will also be needed and developed in the context of spin qubits.

Diverse proposals exist for experiments on well-controlled Heisenberg chains, that are often discussed with potential uses for quantum information processing in mind. As an example, the adiabatic transfer of spin through spin chains has been theoretically studied [10, 37, 38]. Initial experimental work that shows coherent coupling via a mediator has already been done, using either an empty [9] or highly-occupied dot [25]. As such coupling mechanisms come with different requirements and limitations, they might prove useful for realizing (parts of) scalable quantum information processors, but for now these measurements are perhaps better seen as emulators of quantum magnetism, reminiscent of oxygen p-band mediated superexchange coupling in ceramic materials [39].

The eigenvalues and eigenvectors of the anti-ferromagnetic Heisenberg spin chain have been long known, following Bethe's ansatz [40]. Similarly, low energy excitations such as single flipped spins in a polarized chain are easily described (in this case in terms of spin waves). Emulating this textbook physics would yield further confidence in the experimental set-up, but does not yet go towards classical intractability. An experimentally accessible way, however, to nonetheless put strain on classical methods and test them is to quench the chain [41], forcing a description to take the coherent evolution of many states into account.

Lastly, I note that the effective evolution of a spin chain under non-Heisenberg models can also be realized through the process of trotterization [42]. Experimental implementation is not very forgiving for imperfect single- and two-qubit gates however, making implementation quite challenging. As such, an initial and probably limited demonstration of arbitrary spin models (see [43] as an example of such a demonstration, in this case in a linear ion trap) would serve more as a showcase of improved spin qubit control than as an efficient (direct) emulation of quantum magnetism.

[4] Dimerization can also be of interest, defining artificial sub-lattices with, for example, twice as large a unit cell by alternating the strength of exchange coupling terms.

6.4. Simulating many-body localization

Materials can be made electrically insulating when a critical amount of disorder is introduced, as described by Anderson [44]. More recently, the combination of electronic interactions and disorder was shown to lead to a very particular type of localization dubbed many body localization [45], where many-body effects also play a role. A clear feature of an isolated many-body localized state is that it fails to thermalize, showing non-ergodic evolution. As the name suggests, many-body localized states are strongly-correlated, with detailed modeling limited to one-dimensional chains of roughly twenty particles [46].

A canonical example of this physics is the Anderson-Hubbard model, the simple Hubbard model with site-specific disorder added. As the previous Chapters have shown, implementing such a Hamiltonian in a quantum dot array can be done. As discussed in the previous section, however, the quantum dot system is not very isolated when it comes to charge excitations. Overcoming the dephasing of charge degrees of freedom requires tunnel coupling and disorder to be large, which is doable, but means experimental timescales become too short to be workable. As an example, quenching a certain initialized state (for instance prepared in equilibrium) to start evolving under the desired Hamiltonian will, because of the finite rise times of pulses, be adiabatic instead of diabatic, with the same happening as this Hamiltonian is switched off for read-out.

Such physics, however, can be mapped onto the spin degrees of freedom via the Jordan-Wigner transformation [47]. Disorder in single-particle energy offsets becomes disorder in the local magnetic fields, or Zeeman energies. As discussed in the previous section, a configuration with gate-programmable disorder on the range of (tens of) MHz is feasible. Exchange couplings can be tuned to be of the same order, and both will induce evolution effects that are much faster than the timescale for dissipation, in particular on purified silicon substrates [17].

I sketch a measurement below (Fig 6.2) that is close to a previously performed experiment in the charge sector of a linear atomic lattice [48]. It would allow to search for the many-body localized state by distinguishing between ergodic and non-ergodic behavior on a Heisenberg spin chain formed with electrons in quantum dots.

This proposal relies on a simple micromagnet design combined with some control of the dot location within the single electron regime to realize the disordered Heisenberg chain of Eq 6.2. Local magnetic fields are given by:

$$\vec{B}_i = \underbrace{\vec{B}_{\text{ext}} + \vec{B}^0_{\mu\text{mag}}}_{\langle \vec{B}_i \rangle} + \underbrace{\frac{\partial \vec{B}_{\mu\text{mag}}}{\partial z}(\delta z_i + \sum_i \frac{\partial z_i}{\partial V_i}\delta V_i)}_{\delta \vec{B}_i} \tag{6.3}$$

in which $\vec{B}_{\text{ext}}$ is the external, global magnetic field, $\vec{B}^0_{\mu\text{mag}}$ the average micromagnet

field felt by the dots and the third term approximates the deviations due to varying dot location as described in the previous section. Given strong vertical confinement and the symmetry along the axis of the array, we focus on the z direction, adding a static contribution described by dot location disorder δz_i and a dynamic contribution due to varying dot location with changes in gate voltages δV_i away from the charge symmetry point.

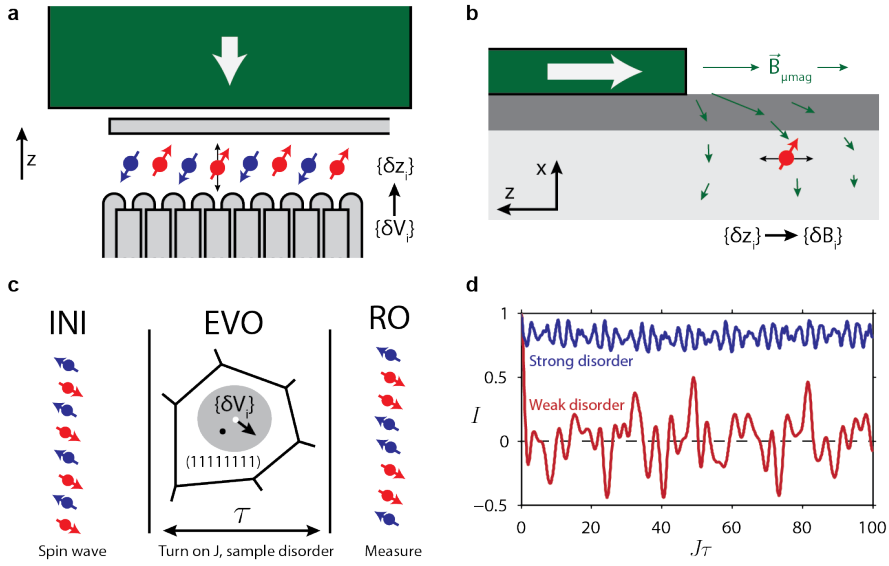

Figure 6.2: (Non)-Ergodic behaviour and many-body localization in a quantum-dot based Heisenberg spin chain with controllable disorder. Overview of micromagnet placement and sample design, seen from the top (**a**) and side (**b**). Gate voltages V_i induce small changes in dot locations z_i, which in turn makes the spins feel modified local magnetic fields δB_i. The measurement scheme is shown in **c**. An initialized spin wave evolves for a time τ under exchange and disorder, with the latter controlled by small changes in gate voltages V_i. The black dot indicates the charge symmetry point, the white dot the point in gate space where all Zeeman splittings are equal. Measuring the spin projection of (one or more) spins allows distinguishing ergodic vs. non-ergodic behavior by measuring the diffusion of energy via changes in the local spin states. As observable we define an imbalance $I(\tau) = \frac{1}{8}\sum_i (-1)^i \sigma_i(\tau)$. The initial state has $I = 1$, averaging over random states yields $A = 0$ and the inverted starting state has $I = -1$. Simulation of the evolution of an 8-spin array are shown in **d**, done by V. Michal with specific disorders $g\mu_B \delta B_i/2J = W(0.96, 0.11, -0.52, 0.63, -0.66, -0.17, 0.96, 0.23)$ and disorder strengths $W = 0.1$ (weak disorder, red) and $W = 5$ (strong disorder, blue). Note that the mean (global) magnetic field need not be defined as it does not influence the evolution, and that the long-lived out-of-equilibrium spin wave state under strong disorder serves as hallmark of the MBL phase.

Simulating the magnetostatics of a Co micromagnet that magnetizes to 1.8 T and

given dot locations 100 nm away and 100 nm below the edge of the magnet, we find $\vec{B}^0_{\mu\text{mag}} = (261, 0, -232)$ mT and $\partial\vec{B}_{\mu\text{mag}}/\partial z = (-1, 0, 0.5)$ mT/nm. The ratio of inherent disorder in dot locations and tunability of those using gate voltages depends on channel confinement, gate design and material quality and is yet to be measured and optimized for extended arrays. Although no good numbers exist for individual quantities (in particular on homogeneity), the ability to tune Zeeman energies over the range of MHz to tens of MHz has been shown [32]. Exchange couplings can be tuned to match, with evolution driven by both terms considerably larger than dissipation times (which are on the order of hundreds of milliseconds in purified silicon [17]).

More elaborate experiments have been done in linear arrays of trapped ions, that use control and measurement tools developed for quantum information processing to access further hallmarks of the MBL state such as the distribution of energy level spacings and the long-term entanglement growth [49] (a disordered Ising Hamiltonian with tunable, long-range couplings is realized). Further experiments could focus on the coherent time evolution of the system under a periodic drive. Such a non-equilibrium Floquet system can show long-lived, sub-harmonic correlations, a phase that has been dubbed a 'discrete time crystal' [50, 51]. Also here, a coherent time-evolution experiment would serve as a showcase of spin qubit control, following an experiment performed in a linear array of trapped ions [52].

6.5. Simulating (doped) Mott insulators

As will have become clear in the previous sections, experiments that focus on emergent spin physics in general and on coherent time evolution of those in particular will have to compete with proof-of-concept experiments done on other qubit platforms. The direct mapping of quantum dots to the Fermi-Hubbard model, however, allows to directly emulate models in which spin and charge degrees of freedom play a joint role, models that are much harder to simulate in generic qubit platforms.

Proof-of-principle digital quantum simulations of Fermi-Hubbard physics have indeed been performed (see [53] for an example in which a two-site Fermi-Hubbard model is simulated using a superconducting quantum circuit), but will remain to be quite limited for the foreseeable future due to the inherent difficulty of anticommutativity and the additional overhead required for error correction. At the same time, classical tools that try to circumvent the exponential growth in complexity are fundamentally limited. Let me give some examples and discuss in more detail.

Mean-field techniques which rely on a semi-classical treatment, such as Hartree-Fock [54] and density functional theory [55] are accurate in high spatial dimensions, but struggle in 1D and 2D, where quantum fluctuations are important. Stochastic methods such as Monte Carlo, on the other hand, have a hard time generating the quasi-probability distributions that are non-positive or even complex that are required for fermionic systems, known as the sign problem [56]. A particularly pow-

erful class of numerical techniques is based on Tensor Network states, where a computationally manageable variational Ansatz based on an entanglement representation allows capturing many-body properties to a certain extent [57]. These techniques work best when tight constraints exist on the entanglement content of low-energy states. This is remarkably often the case[5], as the low-energy eigenstates of gapped Hamiltonians with local interactions are known to obey the so-called area-law for entanglement entropy growth with system size, and evolution under a Hamiltonian with local interactions have been found to only be able to evolve from a small subset of states to all over the Hilbert space in a time that grows exponentially in system size [59]. All of which is of course in line with intuition that the exponential growth with complexity is only really realized when a large amount of entanglement exists, such as can for example be found at a quantum phase transition, following a quench or in a system with built-in frustration [60].

It is thus here that potential for quantum dots as platform for quantum simulation is the clearest, leveraging the direct analogy with the Hubbard model close to the Mott transition (where fluctuations in charge and spin are expected to be strong) and using the large energy scales with respect to temperature, allowing it to serve as a simulation platform to further aforementioned theoretical and numeric approaches. Actually, it would be a useful exercise to take a token many-body problem on a small lattice and map out the results of different approximate techniques next to a full diagonalization [61], regarding an experiment as just another approximate technique with its own approximations and imperfections. An example of an experiment that requires joint access to spin and charge degrees of freedom would be a simulation of the so-called t-J model [62], describing a half-filled Hubbard band with a small amount of holes added. In particular, Nagaoka ferromagnetism can be realized in a 2x2 array with a total of three electrons [63], showing not only the interplay of charge and spin degrees of freedom, but also the phase-inducing effects of a magnetic field, as flux is threaded through the plaquette. Comparing for instance the overall magnetization in equilibrium over the phase space of t/U and $B_\perp$ (and/or $\mathsf{k_B}T$) with a full diagonalization result as well as different numerical techniques would allow for a direct comparison and detailed discussion.

As another example, the collective Coulomb transition shown experimentally in the previous Chapter contained up to twelve electrons and was compared to effective single-band Hubbard model. Such a single-band Hubbard model is known to break down at larger tunnel couplings, and a multi-band Hubbard model would already be quite challenging to compute. A simple proposal would be to redo the same experiment in a larger array, with up to as many electrons as possible. An experiment in which the eight-dot device shown in Fig 6.1 is filled with up to four electrons per site, for instance, would require more thought to be sufficiently accurately described in theory. It would be interesting to see if the uncertainties in some of the theoretical approaches (such as a single-band assumption) exceed those of the measurement itself.

[5] Efficient approximability, however, is not guaranteed, see for example [58].

Whether Feynman's goal of learning new physics can be reached using these experiments is hard to say. Nonetheless, as these types of experiments, their scale and complexity evolve, it serves to think about what observables and models would make most sense to compare to theory. On the short term, using experiments as additional simulation tools to train functionals for density functional theory or compare different Tensor Network representations, that can subsequently be employed for comparable problems, might seem like the most realistic path forward. It requires, though, to start a more thorough discussion with specialists in many-body physics in general and numerical tools in particular, to look at what models and observables would be most interesting. As example, measuring charge addition lines is an indirect measurement of compressibility, an observable of typical theoretical interest close to the Mott transition, as it becomes hard to compute [64, 65]. Other examples could be specific heats and (higher-order) correlation functions, whose extraction from measurement might be less straightforward. At the same time, related to the discussion above, measures of entanglement have grown in interest, to benchmark the non-classicality of states and the degree to which efficient classical tools exist [58, 66–68].

With such general considerations in mind, the experimental realization of Hubbard ladders close to half filling seems like a promising line of inquiry. Both from a theoretical and experimental point of view ladders can be approached as quasi one-dimensional, while still allowing for characteristics of the two-dimensional Hubbard model to emerge [69–71]. From an experimental perspective, ladder designs need a manageable number of gate layers. Using the fabrication processes of the device in Fig 6.1b, on GaAs substrates and given its corresponding reasonable length scales, ladder designs can be readily realized. Indeed, the realization of plaquettes of dots [14–16] and ongoing measurements towards Nagaoka's ferromagnetism can be seen as a natural point on the way to a ladder structure. From a theoretical perspective, the quasi one-dimensional nature is crucial for allowing the implementation of the Jordan-Wigner transform and an accurate description using Tensor Network techniques, in particular the density matrix renormalization group (DMRG) [57]. There therefore exists a numerical tool that can be used to benchmark experiments up to some point.

Weakly doped ladders are known to have a gapped spin mode and a single gapless charge mode, serving as a precursor phase to two different ordered phases in the two-dimensional limit, either a superconducting or a charge-density-wave phase. The question of which phase dominates boils down to finding whether the ladder system has stronger density-density or superconducting (singlet-singlet) correlations. DMRG calculations have found a fast decay of the superconducting correlations, in disagreement with earlier analytical work and in turn in disagreement with more recent and advanced DMRG work, which finds a sufficiently slow decay in the superconducting correlations to favor the superconducting state over the density wave [72]. Measuring the correlations in an experimentally realized weakly doped Hubbard ladder of quantum dots would thus be a helpful additional benchmark, providing a new tool in the discussion of doped Mott insulators.

References

[1] S. Tarucha, D. G. Austing, T. Honda, R. J. van der Hage, and L. P. Kouwenhoven, "Shell Filling and Spin Effects in a Few Electron Quantum Dot," *Physical Review Letters*, vol. 77, pp. 3613–3616, 10 1996.

[2] P. Schlottmann, "Metal-insulator transition in an Hubbard-like model with degeneracy in one dimension," *Physical Review B*, vol. 45, pp. 5784–5789, 3 1992.

[3] A. Hofmann, V. Maisi, C. Gold, T. Krähenmann, C. Rössler, J. Basset, P. Märki, C. Reichl, W. Wegscheider, K. Ensslin, and T. Ihn, "Measuring the Degeneracy of Discrete Energy Levels Using a GaAs / AlGaAs Quantum Dot," *Physical Review Letters*, vol. 117, p. 206803, 11 2016.

[4] R. Hanson, L. P. Kouwenhoven, J. R. Petta, S. Tarucha, and L. M. K. Vandersypen, "Spins in few-electron quantum dots," *Reviews of Modern Physics*, vol. 79, pp. 1217–1265, 10 2007.

[5] W. Hansen, T. Smith, K. Lee, J. Brum, C. Knoedler, J. Hong, and D. Kern, "Zeeman bifurcation of quantum-dot spectra," *Physical Review Letters*, vol. 62, pp. 2168–2171, 5 1989.

[6] R. Hanson, I. T. Vink, D. P. DiVincenzo, L. M. K. Vandersypen, J. M. Elzerman, L. H. W. van Beveren, and L. P. Kouwenhoven, "Determination of the tunnel rates through a few-electron quantum dot," *arXiv*, p. 0407793, 7 2004.

[7] K. D. Petersson, J. R. Petta, H. Lu, and A. C. Gossard, "Quantum Coherence in a One-Electron Semiconductor Charge Qubit," *Physical Review Letters*, vol. 105, p. 246804, 12 2010.

[8] X. Wu, D. R. Ward, J. R. Prance, D. Kim, J. K. Gamble, R. T. Mohr, Z. Shi, D. E. Savage, M. G. Lagally, M. Friesen, S. N. Coppersmith, and M. A. Eriksson, "Two-axis control of a singlet-triplet qubit with an integrated micromagnet.," *Proceedings of the National Academy of Sciences of the United States of America*, vol. 111, pp. 11938–42, 8 2014.

[9] T. Baart, T. Fujita, C. Reichl, W. Wegscheider, and L. Vandersypen, "Coherent spin-exchange via a quantum mediator," *Nature Nanotechnology*, vol. 12, pp. 26–30, 2016.

[10] U. Farooq, A. Bayat, S. Mancini, and S. Bose, "Adiabatic many-body state preparation and information transfer in quantum dot arrays," *Physical Review B*, vol. 91, p. 134303, 4 2015.

[11] J. Medford, J. Beil, J. M. Taylor, S. D. Bartlett, A. C. Doherty, E. I. Rashba, D. P. DiVincenzo, H. Lu, A. C. Gossard, and C. M. Marcus, "Self-consistent measurement and state tomography of an exchange-only spin qubit," *Nature Nanotechnology*, vol. 8, pp. 654–659, 9 2013.

[12] M. G. Borselli, K. Eng, R. S. Ross, T. M. Hazard, K. S. Holabird, B. Huang, A. A. Kiselev, P. W. Deelman, L. D. Warren, I. Milosavljevic, A. E. Schmitz, M. Sokolich, M. F. Gyure, and A. T. Hunter, "Undoped accumulation-mode Si/SiGe quantum dots," *Nanotechnology*, vol. 26, p. 375202, 9 2015.

[13] D. M. Zajac, T. M. Hazard, X. Mi, K. Wang, and J. R. Petta, "A reconfigurable gate architecture for Si/SiGe quantum dots," *Applied Physics Letters*, vol. 106, no. 22, 2015.

[14] R. Thalineau, S. Hermelin, A. D. Wieck, C. Bäuerle, L. Saminadayar, and T. Meunier, "A few-electron quadruple quantum dot in a closed loop," *Applied Physics Letters*, vol. 101, p. 103102, 9 2012.

[15] M. Seo, H. K. Choi, S.-Y. Lee, N. Kim, Y. Chung, H.-S. Sim, V. Umansky, and D. Mahalu, "Charge Frustration in a Triangular Triple Quantum Dot," *Physical Review Letters*, vol. 110, p. 046803, 1 2013.

[16] A. Noiri, K. Kawasaki, T. Otsuka, T. Nakajima, J. Yoneda, S. Amaha, M. R. Delbecq, K. Takeda, G. Allison, A. Ludwig, A. D. Wieck, and S. Tarucha, "A triangular triple quantum dot with tunable tunnel couplings," *Semiconductor Science and Technology*, vol. 32, p. 084004, 8 2017.

[17] M. Veldhorst, J. C. C. Hwang, C. H. Yang, a. W. Leenstra, B. de Ronde, J. P. Dehollain, J. T. Muhonen, F. E. Hudson, K. M. Itoh, A. Morello, and a. S. Dzurak, "An addressable quantum dot qubit with fault-tolerant control-fidelity," *Nature Nanotechnology*, vol. 9, no. 12, pp. 981–985, 2014.

[18] S. Natarajan, M. Agostinelli, S. Akbar, M. Bost, A. Bowonder, V. Chikarmane, S. Chouksey, A. Dasgupta, K. Fischer, Q. Fu, T. Ghani, M. Giles, S. Govindaraju, R. Grover, W. Han, D. Hanken, E. Haralson, M. Haran, M. Heckscher, R. Heussner, P. Jain, R. James, R. Jhaveri, I. Jin, H. Kam, E. Karl, C. Kenyon, M. Liu, Y. Luo, R. Mehandru, S. Morarka, L. Neiberg, P. Packan, A. Paliwal, C. Parker, P. Patel, R. Patel, C. Pelto, L. Pipes, P. Plekhanov, M. Prince, S. Rajamani, J. Sandford, B. Sell, S. Sivakumar, P. Smith, B. Song, K. Tone, T. Troeger, J. Wiedemer, M. Yang, and K. Zhang, "A 14nm logic technology featuring 2nd-generation FinFET, air-gapped interconnects, self-aligned double patterning and a 0.0588 μm2 SRAM cell size," in *2014 IEEE International Electron Devices Meeting*, pp. 1–3, IEEE, 12 2014.

[19] D. Loss and D. P. DiVincenzo, "Quantum computation with quantum dots," *Physical Review A*, vol. 57, pp. 120–126, 1 1998.

[20] S. De Franceschi, L. Hutin, R. Maurand, L. Bourdet, H. Bohuslavskyi, A. Corna, D. Kotekar-Patil, S. Barraud, X. Jehl, Y.-M. Niquet, M. Sanquer, and M. Vinet, "SOI technology for quantum information processing," in *2016 IEEE International Electron Devices Meeting (IEDM)*, pp. 1–13, IEEE, 12 2016.

[21] L. M. K. Vandersypen, H. Bluhm, J. S. Clarke, A. S. Dzurak, R. Ishihara, A. Morello, D. J. Reilly, L. R. Schreiber, and M. Veldhorst, "Interfacing spin qubits in quantum

dots and donors - hot, dense and coherent," *npj Quantum Information*, vol. 3, p. 34, 12 2017.

[22] F. A. Zwanenburg, A. S. Dzurak, A. Morello, M. Y. Simmons, L. C. L. Hollenberg, G. Klimeck, S. Rogge, S. N. Coppersmith, and M. A. Eriksson, "Silicon quantum electronics," *Reviews of Modern Physics*, vol. 85, pp. 961–1019, 7 2013.

[23] S. J. Angus, Andrew J. Ferguson, A. S. Dzurak, , and R. G. Clark, "Gate-Defined Quantum Dots in Intrinsic Silicon," *Nano Letters*, vol. 7, pp. 2051–2055, 2007.

[24] F. Martins, F. K. Malinowski, P. D. Nissen, E. Barnes, S. Fallahi, G. C. Gardner, M. J. Manfra, C. M. Marcus, and F. Kuemmeth, "Noise Suppression Using Symmetric Exchange Gates in Spin Qubits," *Physical Review Letters*, vol. 116, no. 11, pp. 1–5, 2016.

[25] F. K. Malinowski, *Noise suppression and long-range exchange coupling for gallium arsenide spin qubits*. 2017.

[26] D. Zajac, T. Hazard, X. Mi, E. Nielsen, and J. Petta, "Scalable Gate Architecture for a One-Dimensional Array of Semiconductor Spin Qubits," *Physical Review Applied*, vol. 6, p. 054013, 11 2016.

[27] T. Hensgens, T. Fujita, L. Janssen, X. Li, C. J. Van Diepen, C. Reichl, W. Wegscheider, S. D. Sarma, and L. M. K. Vandersypen, "Quantum simulation of a Fermi-Hubbard model using a semiconductor quantum dot array," *Nature*, vol. 548, pp. 70–73, 2 2017.

[28] X. Mi, X. Mi, J. V. Cady, D. M. Zajac, P. W. Deelman, and J. R. Petta, "Strong coupling of a single electron in silicon to a microwave photon," *Science*, vol. 2469, 2016.

[29] J. R. Petta, A. C. Johnson, J. M. Taylor, E. A. Laird, A. Yacoby, M. D. Lukin, C. M. Marcus, M. P. Hanson, and A. C. Gossard, "Coherent Manipulation of Coupled Electron Spins in Semiconductor Quantum Dots," *Science*, vol. 309, no. 5744, 2005.

[30] V. P. Michal, T. Fujita, T. A. Baart, J. Danon, C. Reichl, W. Wegscheider, L. M. K. Vandersypen, and Y. V. Nazarov, "Non-linear and dot-dependent Zeeman splitting in GaAs/AlGaAs quantum dot arrays," p. 1709.08971, 9 2017.

[31] M. Pioro-Ladriere, T. Obata, Y. Tokura, Y.-s. Shin, T. Kubo, K. Yoshida, T. Taniyama, and S. Tarucha, "Electrically driven single-electron spin resonance in a slanting Zeeman field," *Nature Physics*, vol. 4, pp. 776–779, 2008.

[32] J. Yoneda, K. Takeda, T. Otsuka, T. Nakajima, M. R. Delbecq, G. Allison, T. Honda, T. Kodera, S. Oda, Y. Hoshi, N. Usami, K. M. Itoh, and S. Tarucha, "A >99.9%-fidelity quantum-dot spin qubit with coherence limited by charge noise," p. 1708.01454, 8 2017.

[33] J. M. Elzerman, R. Hanson, L. H. Willems van Beveren, B. Witkamp, L. M. K. Vandersypen, and L. P. Kouwenhoven, "Single-shot read-out of an individual electron spin in a quantum dot," *Nature*, vol. 430, pp. 431–435, 7 2004.

[34] T. A. Baart, M. Shafiei, T. Fujita, C. Reichl, W. Wegscheider, and L. M. K. Vandersypen, "Single-spin CCD," *Nature Nanotechnology*, vol. 11, pp. 330–334, 1 2016.

[35] J. Gray, A. Bayat, R. K. Puddy, C. G. Smith, and S. Bose, "Unravelling quantum dot array simulators via singlet-triplet measurements," *Physical Review B*, vol. 94, p. 195136, 11 2016.

[36] T. Otsuka, T. Nakajima, M. R. Delbecq, S. Amaha, J. Yoneda, K. Takeda, G. Allison, T. Ito, R. Sugawara, A. Noiri, A. Ludwig, A. D. Wieck, and S. Tarucha, "Single-electron Spin Resonance in a Quadruple Quantum Dot," *Scientific Reports*, vol. 6, no. 31820, 2016.

[37] S. Yang, A. Bayat, and S. Bose, "Spin-state transfer in laterally coupled quantum-dot chains with disorders," *Physical Review A*, vol. 82, p. 022336, 8 2010.

[38] N. Chancellor and S. Haas, "Using the J1-J2 quantum spin chain as an adiabatic quantum data bus," *New Journal of Physics*, vol. 14, p. 095025, 9 2012.

[39] H. Kramers, "L'interaction Entre les Atomes Magnétogènes dans un Cristal Paramagnétique," *Physica*, vol. 1, pp. 182–192, 1 1934.

[40] H. Bethe, "Eigenwerte und Eigenfunktionen der linearen Atomkette," *Zeitschrift für Physik*, vol. 71, pp. 205–226, 3 1931.

[41] P. Calabrese and J. Cardy, "Time Dependence of Correlation Functions Following a Quantum Quench," *Physical Review Letters*, vol. 96, p. 136801, 4 2006.

[42] S. Lloyd, "Universal Quantum Simulators," *Science (New York, N.Y.)*, vol. 273, pp. 1073–8, 8 1996.

[43] B. P. Lanyon, C. Hempel, D. Nigg, M. Müller, R. Gerritsma, F. Zähringer, P. Schindler, J. T. Barreiro, M. Rambach, G. Kirchmair, M. Hennrich, P. Zoller, R. Blatt, and C. F. Roos, "Universal Digital Quantum Simulation with Trapped Ions," *Science*, vol. 334, no. 6052, 2011.

[44] P. W. Anderson, "Absence of Diffusion in Certain Random Lattices," *Physical Review*, vol. 109, pp. 1492–1505, 3 1958.

[45] D. Basko, I. Aleiner, and B. Altshuler, "Metal–insulator transition in a weakly interacting many-electron system with localized single-particle states," *Annals of Physics*, vol. 321, no. 5, pp. 1126–1205, 2006.

[46] D. M. Basko, I. L. Aleiner, and B. L. Altshuler, "Possible experimental manifestations of the many-body localization," *Physical Review B*, vol. 76, p. 052203, 8 2007.

[47] P. Jordan and E. Wigner, "Über das Paulische Äquivalenzverbot," *Zeitschrift für Physik*, vol. 47, no. 9-10, pp. 631–651, 1928.

[48] M. Schreiber, S. S. Hodgman, P. Bordia, H. P. Lüschen, M. H. Fischer, R. Vosk, E. Altman, U. Schneider, and I. Bloch, "QUANTUM GASES. Observation of many-body localization of interacting fermions in a quasirandom optical lattice.," *Science (New York, N.Y.)*, vol. 349, pp. 842–5, 8 2015.

[49] J. Smith, A. Lee, P. Richerme, B. Neyenhuis, P. W. Hess, P. Hauke, M. Heyl, D. A. Huse, and C. Monroe, "Many-body localization in a quantum simulator with programmable random disorder," *Nature Physics*, vol. 12, pp. 907–911, 6 2016.

[50] D. V. Else, B. Bauer, and C. Nayak, "Floquet Time Crystals," *Physical Review Letters*, vol. 117, p. 090402, 8 2016.

[51] N. Yao, A. Potter, I.-D. Potirniche, and A. Vishwanath, "Discrete Time Crystals: Rigidity, Criticality, and Realizations," *Physical Review Letters*, vol. 118, p. 030401, 1 2017.

[52] J. Zhang, P. W. Hess, A. Kyprianidis, P. Becker, A. Lee, J. Smith, G. Pagano, I.-D. Potirniche, A. C. Potter, A. Vishwanath, N. Y. Yao, and C. Monroe, "Observation of a discrete time crystal," *Nature*, vol. 543, pp. 217–220, 3 2017.

[53] R. Barends, L. Lamata, J. Kelly, L. García-Álvarez, A. G. Fowler, A. Megrant, E. Jeffrey, T. C. White, D. Sank, J. Y. Mutus, B. Campbell, Y. Chen, Z. Chen, B. Chiaro, A. Dunsworth, I.-C. Hoi, C. Neill, P. J. J. O'Malley, C. Quintana, P. Roushan, A. Vainsencher, J. Wenner, E. Solano, and J. M. Martinis, "Digital quantum simulation of fermionic models with a superconducting circuit," *Nature Communications*, vol. 6, p. 7654, 7 2015.

[54] P. Echenique and J. L. Alonso, "A mathematical and computational review of Hartree–Fock SCF methods in quantum chemistry," *Molecular Physics*, vol. 105, pp. 3057–3098, 12 2007.

[55] R. Jones, "Density functional theory: Its origins, rise to prominence, and future," *Reviews of Modern Physics*, vol. 87, pp. 897–923, 8 2015.

[56] M. P. Nightingale and J. Umrigar, *Quantum Monte Carlo Methods in Physics and Chemistry*. Springer, 1999.

[57] R. Orus, "A practical introduction to tensor networks: Matrix product states and projected entangled pair states," *Annals of Physics*, vol. 349, pp. 117–158, 10 2014.

[58] N. Schuch, M. M. Wolf, F. Verstraete, and J. I. Cirac, "Entropy Scaling and Simulability by Matrix Product States," *Physical Review Letters*, vol. 100, p. 030504, 1 2008.

[59] D. Poulin, A. Qarry, R. Somma, and F. Verstraete, "Quantum Simulation of Time-Dependent Hamiltonians and the Convenient Illusion of Hilbert Space," *Physical Review Letters*, vol. 106, p. 170501, 4 2011.

[60] J. I. Cirac and P. Zoller, "Goals and opportunities in quantum simulation," *Nature Physics*, vol. 8, pp. 264–266, 4 2012.

[61] J. K. Cullum and R. A. Willoughby, *Lanczos Algorithms for Large Symmetric Eigenvalue Computations Volume 1*. 2002.

[62] J. Spałek, "t-J Model Then and Now: a Personal Perspective from the Pioneering Times," *Acta Physica Polonica A*, vol. 111, p. 409, 2007.

[63] Y. Nagaoka, "Ferromagnetism in a Narrow, Almost Half-Filled," *Physical Review*, vol. 147, p. 392, 7 1966.

[64] G. Kotliar, S. Murthy, and M. J. Rozenberg, "Compressibility Divergence and the Finite Temperature Mott Transition," *Physical Review Letters*, vol. 89, p. 046401, 7 2002.

[65] P. M. Duarte, R. A. Hart, T.-L. Yang, X. Liu, T. Paiva, E. Khatami, R. T. Scalettar, N. Trivedi, and R. G. Hulet, "Compressibility of a Fermionic Mott Insulator of Ultracold Atoms," *Physical Review Letters*, vol. 114, p. 070403, 2 2015.

[66] L. Amico, R. Fazio, A. Osterloh, and V. Vedral, "Entanglement in many-body systems," *Reviews of Modern Physics*, vol. 80, pp. 517–576, 5 2008.

[67] R. Horodecki, P. Horodecki, M. Horodecki, and K. Horodecki, "Quantum entanglement," *Reviews of Modern Physics*, vol. 81, pp. 865–942, 6 2009.

[68] J. Eisert, M. Cramer, and M. B. Plenio, "Colloquium: Area laws for the entanglement entropy," *Reviews of Modern Physics*, vol. 82, pp. 277–306, 2 2010.

[69] E. Dagotto, J. Riera, and D. Scalapino, "Superconductivity in ladders and coupled planes," *Physical Review B*, vol. 45, pp. 5744–5747, 3 1992.

[70] E. Dagotto and T. M. Rice, "Surprises on the Way from One- to Two-Dimensional Quantum Magnets: The Ladder Materials," *Science*, vol. 271, pp. 618–623, 2 1996.

[71] R. Noack, S. White, and D. Scalapino, "The ground state of the two-leg Hubbard ladder a density-matrix renormalization group study," *Physica C: Superconductivity*, vol. 270, pp. 281–296, 10 1996.

[72] M. Dolfi, B. Bauer, S. Keller, and M. Troyer, "Pair correlations in doped Hubbard ladders," *PHYSICAL REVIEW B*, vol. 92, p. 195139, 2015.

7

Conclusion

The work shown in this thesis has illustrated how problems of disorder and control can be solved as to allow using quantum dot systems to emulate the many-body physics of interacting fermions on a lattice. I have focused on both a top-down fabrication approach to scaling that attempts to minimize disorder from the onset as well as on a bottom-up approach that focuses on efficient site-specific control to negate disorder. The latter specifically aligns with the rapid advances in the field of quantum dot systems in general, with proof-of-principle experiments done and further efforts underway. I have no doubt that the level of complexity of quantum simulation realizations using dots will increase fast, keeping in mind the insights that our work has taught us, with which I conclude here.

Disorder in heterostructures and fabrication currently limits the definition of two-dimensional arrays of quantum dots with global control only. Even in GaAs structures designed to reduce the effect of disorder and optimize homogeneity [1], we found intrinsic disorder levels to be too high to capacitively measure periodic effects and the formation of large arrays of dots [2]. In particular, it is hard to quantify inhomogeneity with limited input from measurements. This is not the case for bottom-up approaches, where the potential for scaling can be assessed more thoroughly before attempts are made (more below).

There is much room for improvement in Hubbard Hamiltonian engineering of site-controlled quantum dots with current technology. Given the expeditious nature of charge sensing measurements [3] of transitions in dot occupations and their well-known mapping to Hubbard terms [4], many elements are in place to negate the previously inhibiting effects of gate cross-talk and remaining inhomogeneity. These allow for the orthogonal control of a number of Hamiltonian terms equal to the number of control gates, yielding site-specific control of single-particle energies (doping and disorder) and tunnel coupling (relative interaction strength) over a large phase space [5].

To leverage these improvements in pushing to experiments with larger numbers of dots, standardization and specialization are important. A technological push consolidating the best of individual set-ups and measurements can be expected from ongoing efforts in spin qubits, although the precise designs and requirements for simulations might be slightly different. Unlike current experiments involving only one or few dots, this involves the definition of clear metrics in control and homogeneity [6], that describe both device and set-up performance. I see reductions in charge noise (current bottleneck in coherent control) and consistently solid charge sensing (say, signal-to-noise ratio for measuring the closest-by inter-dot transition at an effective bandwidth of 1 MHz) as important drivers.

Regardless of that outcome, though, classical intractibility seems within reach. Frankly, it does not take many quantum degrees of freedom for computers to get a hard time for full diagonalization [7], and the Hubbard model describing dots has many (site, orbital and spin). Furthermore, linear arrays of several tens of dots can be controlled within current modus operandi (gate designs, wiring and control electronics) and control requirements for simulations in the spin sector are significantly less stringent than those for fault-tolerant spin qubit control.

Further thought is required, however, as to go towards experiments that really add to collective knowledge of emergent quantum phenomena. An impressive amount of control has by now been shown for a range of tamed quantum systems, including but not limited to trapped ions, atomic lattices and superconducting platforms. Nonetheless, it has proven hard to employ this fledgling quantum hardware to extend our knowledge of many-body systems [8]. In the case of quantum dots, it would be a pitfall to realize elaborate toy models that are experimentally convenient just as to show off advances in control, in part because many such experiments have been done in the above-mentioned platforms, but also because they fail to cash in on the inherent advantages of quantum dots in readily realizing the strongly-correlated Fermi-Hubbard model and the resulting proximity to many condensed-matter problems of interest. Already early on, it therefore makes sense to assess in collaboration with theorists just where small quantum dot arrays can make a difference, be it in studying the thermalization of isolated, disordered many-body systems, benchmarking numerical tools in describing weakly doped Hubbard ladders and their emergent superconducting pairing [9], or something else.

References

[1] P. Barthelemy and L. M. K. Vandersypen, "Quantum Dot Systems: a versatile platform for quantum simulations," *Annalen der Physik*, vol. 525, pp. 808–826, 11 2013.

[2] T. Hensgens, U. Mukhopadhyay, P. Barthelemy, R. Vermeulen, R. Schouten, S. Fallahi, G. C. Gardner, C. Reichl, W. Wegscheider, M. J. Manfra, and L. M. K. Vandersypen, "Capacitance spectroscopy of gate-defined electronic lattices," *arXiV*, p. 1709.09058, 9 2017.

[3] C. Barthel, M. Kjærgaard, J. Medford, M. Stopa, C. M. Marcus, M. P. Hanson, and A. C. Gossard, "Fast sensing of double-dot charge arrangement and spin state with a radio-frequency sensor quantum dot," *Physical Review B*, vol. 81, p. 161308, 4 2010.

[4] S. Yang, X. Wang, and S. Das Sarma, "Generic Hubbard model description of semiconductor quantum-dot spin qubits," *Physical Review B*, vol. 83, p. 161301, 4 2011.

[5] T. Hensgens, T. Fujita, L. Janssen, X. Li, C. J. Van Diepen, C. Reichl, W. Wegscheider, S. D. Sarma, and L. M. K. Vandersypen, "Quantum simulation of a Fermi-Hubbard model using a semiconductor quantum dot array," *Nature*, vol. 548, pp. 70–73, 2 2017.

[6] L. M. K. Vandersypen, H. Bluhm, J. S. Clarke, A. S. Dzurak, R. Ishihara, A. Morello, D. J. Reilly, L. R. Schreiber, and M. Veldhorst, "Interfacing spin qubits in quantum dots and donors - hot, dense and coherent," *npj Quantum Information*, vol. 3, p. 34, 12 2017.

[7] J. K. Cullum and R. A. Willoughby, *Lanczos Algorithms for Large Symmetric Eigenvalue Computations Volume 1*. 2002.

[8] J. I. Cirac and P. Zoller, "Goals and opportunities in quantum simulation," *Nature Physics*, vol. 8, pp. 264–266, 4 2012.

[9] A. Noiri, K. Kawasaki, T. Otsuka, T. Nakajima, J. Yoneda, S. Amaha, M. R. Delbecq, K. Takeda, G. Allison, A. Ludwig, A. D. Wieck, and S. Tarucha, "A triangular triple quantum dot with tunable tunnel couplings," *Semiconductor Science and Technology*, vol. 32, p. 084004, 8 2017.

A

Design and fabrication of capacitance spectroscopy devices

Here I describe design and nano-fabrication details for the devices used for the capacitance spectroscopy measurements of **Chapter 3**. Note that different designs (and corresponding recipes) have been used in order to fabricate either devices with a single global top gate or two gates: a grid gate and a uniform global top gate. I start by providing the step-by-step fabrication details for one double gate design in particular, which should serve as an example from which the steps required for the others can be deduced. Background considerations in fabrication and differences to other device designs are discussed thereafter. Furthermore, our experiences in iteratively improving the heterostructure design itself are outlined.

Detailed fabrication recipe

- **Ohmic contacts**

  Spin PMMA 495K A8 resist at 6000 rpm - bake 15 min at 175 °C (400 nm) - lithography - development 60 s in 1:3 MIBK/IPA - wet etch of 180 nm in diluted Piranha - evaporation of 5/150/25 nm Ni/AuGe/Ni - lift-off in acetone and IPA rinse - anneal 60 s at 440 °C in forming gas.

- **Mesas**

  Spin PMMA 495K A8 resist at 6000 rpm - bake 15 min at 175 °C (400 nm) - lithography - development 60 s in 1:3 MIBK/IPA - wet etch of 700 nm in diluted Piranha - sputtering 700 nm of SiO_2 - lift-off in acetone and IPA rinse.

- **Bridges**

  Spin PMMA 495K A8 resist at 6000 rpm - bake 15 min at 175 °C (400 nm) - lithography - cross-link PMMA strips through electron beam overdose at 25 mC/cm^2.

- **Connection pads and markers**

  Spin PMMA 495K A8 resist at 6000 rpm - bake 15 min at 175 °C (400 nm) - lithography - development 60 s in 1:3 MIBK/IPA - evaporation of 10/50 nm Ti/Au - lift-off in acetone and IPA rinse.

- **Grid gate**

  Spin CSAR 62.04 resist at 5000 rpm - bake 3 min at 150 °C (72 nm) - lithography - development 70 s pentylacetat and 60 s 1:1 MIBK:IPA - evaporation of 20 nm Al - lift-off in NMP at 70 °C using soft ultrasound excitation for 4 hrs and subsequent acetone and IPA rinse - oxidation in 20 min at 200 °C at 100 mTorr and 300 W RF power using the remote plasma of an ALD machine.

- **Top gate**

  Spin PMMA 495K A8 resist at 6000 rpm - bake 15 min at 175 °C (400 nm) - lithography - development 60 s in 1:3 MIBK/IPA - evaporation of 50 nm Al - lift-off in acetone and IPA rinse.

- **Bonding pads**

  Spin OEBR-1000 (200cp) lift-off resist at 3500nm - bake 30 min at 175 °C (500 nm) - spin PMMA 950K A2 resist at 2000 rpm - bake 10 min at 175 °C (90 nm) - lithography - evaporation of 50/200 nm Ti/Au - lift-off in acetone and IPA rinse.

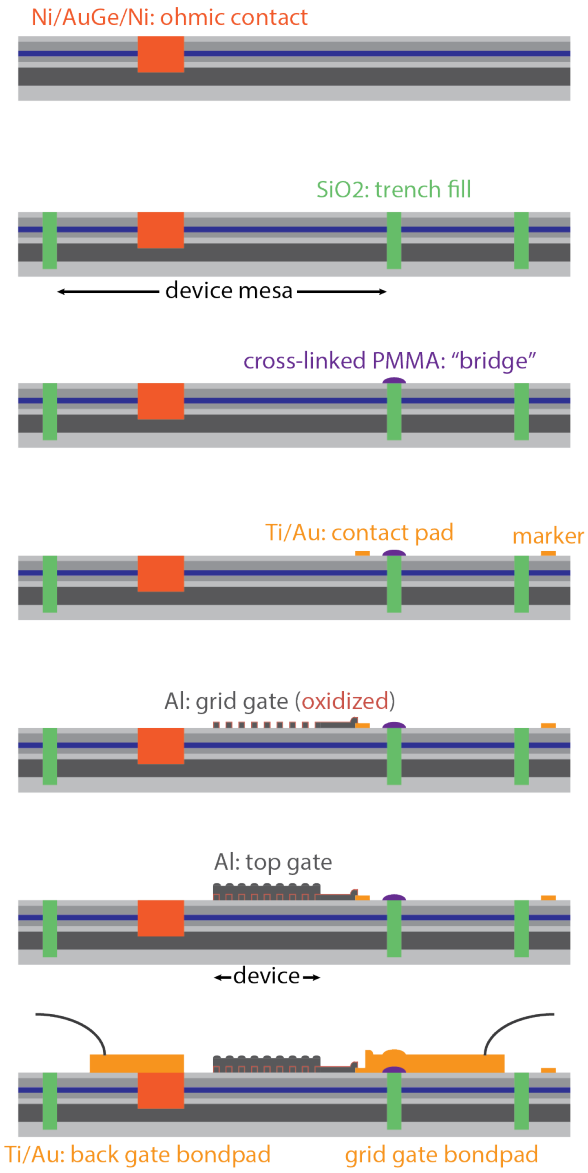

Figure A.1: Fabrication overview. Schematic side-view representation of nano-fabrication steps of a double gate device for capacitance spectroscopy, with overlapping metallic gates. Starting from a bare wafer (not shown), each figure indicates the result of a distinct lithography (and corresponding process) step. The bond pad for the top gate is not shown in this view.

Comments on the fabrication

A side-view of the device at the end of each of these steps is shown in Fig A.1. Note that the bridge sections are easily added features to make sure any remaining steps or gaps in the filled mesa can be crossed by the bond pad lead, and that we use thin layers of Ti/Au to be connected on two sides in order to make a robust electrical connection (typically several Ohm) between the Al gates and the Au bond pads.

Fabricating the grid gates (the only step with sub-micron features) is the critical step in the fabrication process. The requirement of small features clashes with that of homogeneity and strains both the lithography and the evaporation/lift-off process. Typical problems that arise in the lithography of such large, but detailed, features, are drift (typically several tens of nm/min) and stitching errors. We have gotten rid of these almost completely by direct programming of an iterative sequence that the e-beam follows in writing the grid (as compared to the conventional procedure of converting a design file using BEAMER software). This allows for an entire 200 µm x 200 µm grid to be written in under a minute and in a single main field. Furthermore, we add a 200 nm thin frame around the grids whose overdose is chosen to counter proximity edge effects (Fig A.2).

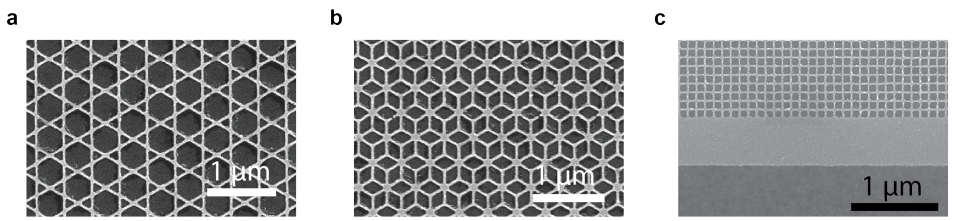

Figure A.2: Nano-fabricated grids. Electron micrographs of metallic (20 nm of Al, light) grid-shaped gates fabricated on GaAs (darker background). Besides square grids, kagome (**a**) and dice-shaped lattices can also be fabricated (**b**). Homogeneity at the edges is provided for by overdosing a thin frame at the edge, as shown in **c**.

The opposite requirements of high resolution and undercut required for lift-off are best met using a single layer CSAR62 resist. Note that with these fabrication details, we actually find feature size, yield and reproducibility to be limited by the grain size of the evaporated Al, instead of the resist mask or lithography process and contrary to what might be expected. As such, Ti/Au but especially Ti/AuPd gates were easier to fabricate than Al gates.

Different designs and considerations

The fabrication detailed above represents only one of the designs used throughout the work. First results were obtained on conducting wafers, where the ohmic contact could be made on the back side of the wafer. Single layer gate devices then only require a single lithography step to define the top gate. For double layer gate devices, though, this can cause issues. Because mesas cannot be defined by a shallow etch, bonding pads have to be placed on top of a thick dielectric layer in order to reduce stray capacitance [1].

Although this requires fewer steps, handling both sides of the wafer proved tricky, especially when detailed features (the grids) exist. Furthermore, it does not allow for the definition of mesas, and as such only works when the bonding pads of the grid and the top gate are placed on a thick dielectric layer to reduce the stray capacitance to the back gate. Adhesion issues of metal on GaAs can be bad enough, but adhesion of dielectrics on the wafer surface is even worse, and as such, bonding yield for such devices is unforgivably low (See Fig A.4 for some images of bonded devices).

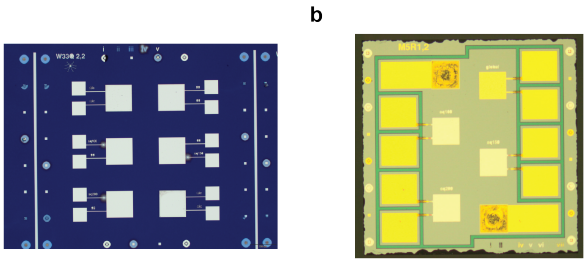

Figure A.3: Optical images of device cells. Of the 6 squares in the center, the top left and bottom right ones are the ohmic contacts to the back gate. The other four squares are devices. Connected pairs of outer metallic squares are the bonding pads, which in the case of a thick dielectric layer (**a**) can be placed directly on the dielectric (although one of the two requires a via through the dielectric to contact the grid gate), but which in absence of a dielectric layer (**b**) require dedicated bond pad mesas to be constructed (the SiO_2 that fills up the mesa etch shows up in green).

Heterostructure stack: wafers used and considerations

The general goal in varying the heterostructure design is to minimize the measured disorder levels and increase the ability to apply a periodic potential. The latter can be done either by reducing the back gate screening or by increasing the maximum voltage that can be applied to the wafer before leakage occurs. The table below shows the growth details of some of the wafers measured.

Initial wafer design was based on Dial [2], and grown on a conducting substrate (initial wafer W1 and W2, where the growth conditions itself were further optimized). We varied quantum well width and spacer layer thickness (both in the range from

15 to 30 nm), but none of these changed the disorder levels considerably. Furthermore, we varied capping layer (from 5 to 10 nm) and blocking barrier thickness (in the range from 40 to 70 nm, see M1 and W3). This also did not have a large effect on disorder levels, and changes the maximum voltages we could apply to our gates only slightly.

Instead, we found that increasing the tunnel barrier width (which has to be accompanied by a change in aluminum content to keep the tunnel frequency constant) does reduce disorder levels substantially, with the Landau fan diagram data shown in Chapter 3 measured on wafer M2.

Table A.1: Heterostructure details. Layer thicknesses and aluminum content of $Al_xGa_{1-x}As$ layers of several wafers used for the capacitance spectroscopy devices. Also noted are the tunnel frequency f_t and the minimum field B_0 at which Landau levels can be resolved, an indicator for disorder levels.

	W1	W2	M1	W3	M2
capping layer	GaAs 10 nm	GaAs 10 nm	GaAs 5 nm	GaAs 10 nm	GaAs 5 nm
blocking barrier	0.316 60 nm	0.316 60 nm	0.316 40 nm	0.315 60 nm	0.360 60 nm
quantum well	GaAs 23 nm	GaAs 23 nm	GaAs 23 nm	GaAs 23 nm	GaAs 23 nm
tunnel barrier	0.316 13 nm	0.316 13 nm	0.316 14 nm	0.315 14 nm	0.199 16 nm
spacer layer	GaAs 25 nm	GaAs 15 nm	GaAs 15 nm	GaAs 15 nm	GaAs 15 nm
back gate	GaAs n^{++} 800 nm	GaAs n^{++} 800 nm	GaAs n^{++} 400 nm	GaAs n^{++} 400 nm	GaAs n^{++} 400 nm
f_t at 0 T $n \approx 10^{11}$ cm^{-2}	1 MHz	200 kHz	2 kHz	30 kHz	100 kHz
B_0	3 T (at 4 K)	0.65 T	0.50 T	0.40 T	0.25 T
comments	n^{++} doped wafer	n^{++} doped wafer			

References

[1] C. Sanna, *Nanofabrication of Quantum Dot Arrays for Quantum Simulation*. MSc thesis, 2015.

[2] O. E. Dial, *PhD thesis*. 2007.

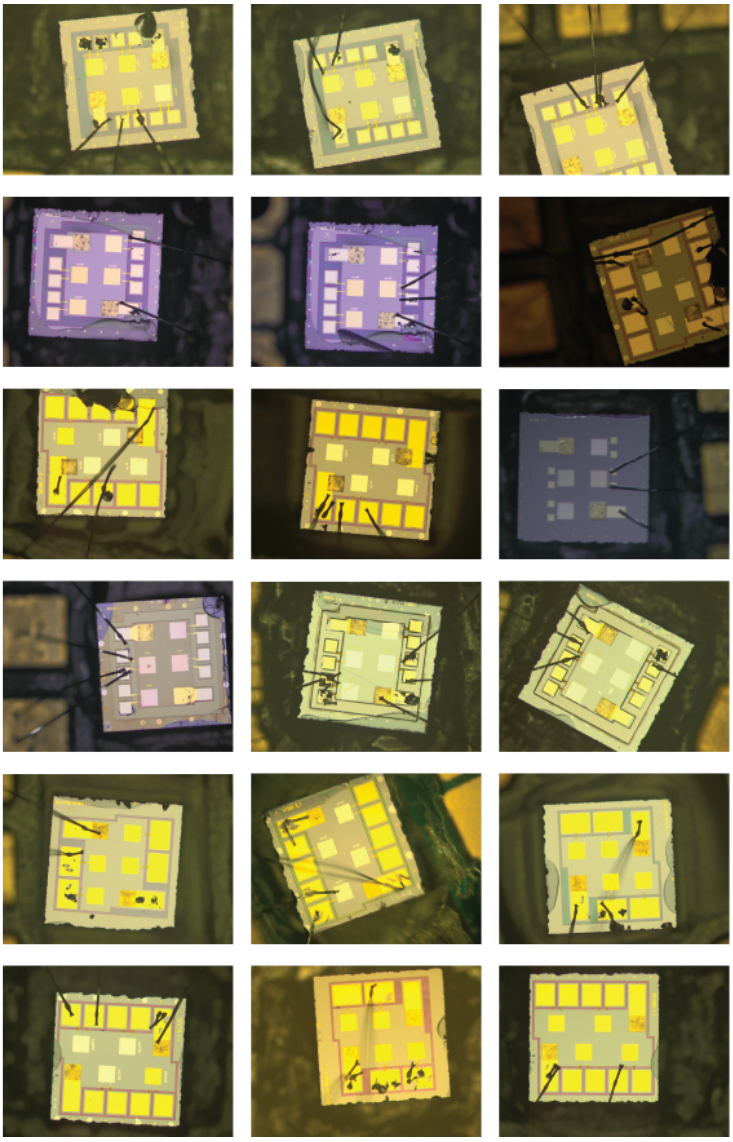

Figure A.4: The hassle of bonding. We found bonding on GaAs surfaces to be unreliable regardless of the metal (thickness) used for bonding pads: the resul of poor adhesion of the metal to the semiconductor surface and the brittleness of the GaAs wafers themselves. As adhesion for dielectrics is even worse, bonding pads on top of dielectrics are a bad idea. Really, just don't.

Summary

Novel technologies are often kick-started by the synthesis of materials with new properties. Actually, much of the technology we take for granted today relies in some way on semiconductor materials, which are well-understood using early last-century quantum physics and resulting advances in materials science. The employed material properties, however, amount to but the tip of the iceberg of what the underlying quantum physics allows for. Materials in which electrons build up strong correlations, for instance, represent a class of systems with the potential for novel emergent electronic and magnetic properties, that cannot be fully described and understood with classical methods alone.

In this thesis, conduction band electrons confined to an array of coupled sites, defined by a combination of semiconductor band engineering and gate electrostatics, so-called quantum dots, are shown to be able to emulate the physics of correlated electrons on a lattice. The underlying hope is that quantum dot arrays can be used to elucidate novel emergent magnetic and electrical properties of materials by realizing the underlying many-body physics. Disorder and inefficient control of the quantum dot properties, however, have previously made it hard to achieve accurate mapping over large phase spaces, as well as to scale up to larger arrays.

The Fermi-Hubbard model that underpins the many-body physics of electrons on a lattice is introduced first, to which the specific Hubbard model describing quantum dots is compared. Addition spectra are of importance, as they allow one to map a quantum dot system to the Hubbard model by focusing on the set of charge transitions that appear as function of changes in the control fields. Furthermore, the concept of emergent models is mentioned, as it allows us to understand system properties in certain parameter windows in a simpler picture. The emergent spin physics of the magnetic degree of freedom of the electrons, for instance, forms a platform for the realization of quantum processors.

Next, it is shown how the technique of capacitance spectroscopy can be used to measure electron addition, in particular the global density of states of a large two-dimensional electronic system, and how gates can be added to impose a lattice potential. The wafer disorder and device (in)homogeneity are assessed, with the first of these shown to limit the visibility of periodic effects and the formation of large arrays of quantum dots.

In an alternative approach, small arrays are defined using a set of electrostatic gates whose gate voltages allow for site-specific control. This control is typically inefficient due to gate cross-talk, non-linearities and initial disorder, but a toolbox of techniques is presented that allows for overcoming these issues to nonetheless orthogonally control single-particle energy offsets and inter-site tunnel couplings, as well as measure Coulomb-driven interaction energies.

The potential for such efficient control of the underlying potential landscape is shown as the physics of a small quantum dot array is mapped onto that of the interaction-driven Mott transition, highlighting how quantum dots can be used to emulate Fermi-Hubbard physics. A good agreement between Fermi-Hubbard theory and the measurement further validates the toolbox for Hamiltonian engineering. In the process, general metrics describing the remaining classical entropy and inhomogeneity are measured and discussed.

Lastly, an outlook is made on the types of experiments that can be done in the (near) future, keeping current limitations and expected advances for quantum dot arrays in mind. Despite the fact that we are already close to realizing quantum dot systems whose description using a full diagonalization of the underlying Hubbard model would be intractable, it is not a trivial problem to envisage how experiments in the near future can aid in the improved understanding of relevant many-body physics. Nonetheless, ideas for future experiments that focus on many-body localization and (doped) Mott insulators are presented, as well as the lessons learned in realizing this work that future experiments should keep in mind.

Toivo Hensgens

Samenvatting

Vooruitgang in de techniek is vaak afhankelijk van de synthese van materialen met nieuwe en gunstige eigenschappen. Zo leunen veel technologieën die we vandaag de dag als vanzelfsprekend beschouwen op chips van halfgeleiders, materialen die we goed begrijpen en kunnen realiseren met behulp van vroeg twintigsteeeuwse quantummechanica en verwante vooruitgang in de materiaalkunde. De eigenschappen van halfgeleiders, echter, vormen slechts het topje van de ijsberg van wat de quantummechanica allemaal toestaat. Materialen wiens elektronen sterke correlaties vertonen, bijvoorbeeld, vormen een klasse van systemen met de potentie voor nieuwe emergente elektrische en magnetische eigenschappen die niet kunnen worden beschreven en begrepen met enkel klassieke methodes.

Dit proefschrift laat zien dat elektronen uit de geleidingsband van een halfgeleider, gevangen in naburige potentiaalminima met behulp van elektrostatische gates en een zorgvuldig ontworpen bandenstructuur, zogenaamde quantum dots, de natuurkunde van gecorreleerde elektronen op een rooster kunnen nabootsen. De onderliggende verwachting is dat quantum dots licht kunnen schijnen op nieuwe emergente magnetische en elektronische eigenschappen van materialen door de onderliggende fysica in een gecontroleerde omgeving te realiseren. Een combinatie van wanorde en inefficiëntie in controle, echter, maken het lastig om zulke fysica correct na te bootsen over een grote faseruimte, zowel als om haar op te schalen naar grotere roosters.

Als eerste wordt het Fermi-Hubbard model geïntroduceerd, dat de veel-deeltjes fysica van elektronen op een rooster beschrijft. Additie spectra zijn belangrijk, daar ze ons toestaan om een quantum dot systeem direct te vergelijken met het Hubbard model door ladingstransities te volgen als functie van veranderingen in de elektrische velden waarmee de dots worden gecontroleerd. Ook wordt het concept van emergente modellen beschreven, die het toestaan om systeemeigenschappen in bepaalde situaties helderder te beschrijven. Zo vormt de emergente spin fysica van de magnetische vrijheidsgraad van de elektronen, bijvoorbeeld, een platform voor de realisatie van quantumprocessoren.

Hierna komt de techniek van capaciteitsspectroscopie aan bod, die kan worden gebruikt om de additie van elektronen, specifiek de globale toestandsdichtheid van een tweedimensionaal elektronengas, te meten, en hoe ontwerpen kunnen worden gerealiseerd die een roosterpotentiaal aanbieden. De intrinsieke wanorde in het materiaal en de (in)homogeniteit in de samples worden beoordeeld, waarbij het duidelijk wordt dat de materiaalswanorde de zichtbaarheid van effecten van het periodieke potentiaal verbergt en de formatie van grote roosters van quantum dots tegenhoudt.

In een alternatieve aanpak wordt een klein aantal quantum dots in een rij gevormd met behulp van een aantal metallische gates op het oppervlak van de halfgeleider, via wiens voltages dots individueel kunnen worden aangestuurd. Zulke controle is typisch inefficiënt vanwege kruistermen, niet-lineariteiten en initiële wanorde, maar een stel technieken wordt gepresenteerd die het toestaan om deze moeilijkheden het hoofd te bieden en individuele energieniveaus in dots en de tunnel koppelingen ertussen te controleren, zowel als om de Coulomb interactie energieën te meten.

Een demonstratie van deze technieken wordt gedaan door met behulp van een klein aantal dots de fysica van de interactie-gedreven Mott transitie na te bootsen. Dit dient als voorbeeld van de potentie voor quantum dots om het Fermi-Hubbard model te emuleren. Een goede overeenkomst tussen theorie en experiment valideert het succesvolle implementeren van de beoogde Hamiltoniaan. In het proces worden algemene metrieken van quantum dots aangestipt, zoals de eindige klassieke entropy en de homogeniteit.

Als laatste wordt een vooruitzicht gemaakt naar types experimenten die gedaan kunnen worden in de (nabije) toekomst, waarbij huidige beperkingen en verwachte vooruitgang in quantum dots worden meegenomen. Ondanks het feit dat huidige experimenten in de buurt komen van het regime waarin een volledige diagonalisatie van het onderliggende Hubbard model niet meer mogelijk is, is het geen triviale exercitie om te zien hoe toekomstige experimenten kunnen helpen om meer begrip te vergaren van relevante veel-deeltjes fysica. Desalniettemin worden toekomstige experimenten voorgesteld, die zich richten op interactie-en-wanorde gedreven localizatie effecten en (gedoteerde) Mott isolatoren, als ook de in dit proefschrift opgedane inzichten opgesomd, die relevant zijn voor toekomstig werk.

Toivo Hensgens

Acknowledgements

I am afraid that the number of people I fail to mention here will only be trumped by my inability to formulate clearly what those of you whose names can be found below have meant to me personally and have contributed to my work and life in the last couple of years.

It was you, **Pierre**, who first taught me the ways of the device physicist, how to combine physical insight with nuts-and-bolts level engineering as well as how to balance long-term ambition and day-to-day frustration. In those days, even though our group was considerably smaller than it is today, it was never a problem to find help, which was extended to me at any level by **Floris**, **Victor**, **Thibault** and **Mohammad**. Let me also thank you, **Pasquale**, whose friendliness and vividness knows no bounds, and you, **Erika**, whose fervor is unmatched. I am certain you will find your way nicely in the exciting playground of academia. The same applies to you, **Srijit**, you who has managed to transition from researcher to group leader whilst, in true Delft fashion, remaining the light of any party.

Tim, in your own dissertation you wish us much good fortune with the quadruple quantum dot you fabricated and ran experiments on yourself. A quick glance at this one, however, will show you that it is the triple dot set-up that I owe much of my own success to. The level of engineering you managed to achieve there is still unrivaled within our group, an indication of the success I am sure you currently enjoy as a research engineer. My real training in the ways of the *few*, however, came from you, **Takafumi**. It was a pleasure working with you, not only because you are the most incredibly bright and pleasant person, but also because you possess a certain thought-out calmness that combined with my personal creativity (lack of patience) to yield a very fruitful and innovative effort. And indeed, much of current work in the lab is aligned along converting the dark magic of your control of these quantum dot systems into well-understood and well-engineered things.

It was my pleasure to kick-start the research efforts of others. **Carla**, you have an energy and optimism about you that even the hard work I had you do in the cleanroom could not stifle, and which helped power me through a tough period of my work in Delft. And **Laurens**, whom I regard as the quintessential Delft student: organized, confident and independent - you have realized much of the data I put on display in this booklet, and I am sure you will excel in whatever your chosen field will be. And as history is known to repeat itself, I find myself describing you, **Udit**, as my final padawan. You have injected an unprecedented amount of energy and optimism into any of our joint efforts, mastering the art of cleanroom work and solving all manner of engineering problems in ways and timescales that have consistently made my head spin. You are awesome and you know it.

Talking about people whose endurance in fighting the fight in the trenches of nano-fabrication knows no bounds: **Nodar**. Let me thank you by trying to describe the indescribable, you, someone who combines the practical resourcefulness of a boy scout with a contagiously ironic wit and a contradicting stressed relaxedness - and all of this in a frame inside which one would not expect a physicist to be skulking. For the last half of my work, I could also always rely on you, **JP** and **Tom**, to help me out when help was needed and to provide some much-needed physics background to help contain my sometimes overly innovative ideas. You both exemplify the ideal post-doc: knowledgeable and approachable, organized and responsible.

I am happy to leave the group in the hands of the next generation of researchers. **Jelmer**, I am sure your sense for responsible initiative and confidence will keep this raft of an experimental group of ours somewhat organized whilst maneuvering in this ever-changing (post-)academic reef. As something of a child to this environment yourself, **Sjaak**, I am sure you will continue to use your pragmatic approach to get great work done. **Guoji**, it is nice to see how your efforts have materialized into successful work and the motivational boost it provides, both of which I am sure will only continue. The same can be said for **Stephan**, you driven and confident go-getter. **Xiao**, **Anne-Marije**, **Gabriel**, **Nima**, **Christian**, **Sergey** as well as **Pieter**, **Delphine** and **Kanwal**, I wish the best to you all.

The Qutech institute has clearly followed up on the former Quantum Transport group as a place that consistently manages to attracts a vibrant and colorful group of people. Listing the likes of **Michiel**, **Christian**, **Florian**, **Alex** and **James** as following in the footsteps of such peeps as **David**, **Vincent** and **Machiel** I find myself rethinking as to whether I want to leave this place. That being said, though, a moment's thought of a mere whiff of the smell of an intermittently reappearing concoction of a particular alcoholic beverage makes that choice somewhat easier. Thanks for the good times and all the best!

Furthermore, thanks to the many great and amicable people who have helped me here and there and can be relied upon to have a chat from time to time, people like you: **Suzanne**, **Julia**, **LaReine**, **Jasper** and **Iman**. The same applies to the support staff, in particular **Yuki** and **Marja**. I also very much enjoyed my interactions with the cleanroom technicians. Much of the stuff that works in this thesis can be boiled down to the efforts of you, **Arnold**, **Ewan**, **Marc** and **Marco**, whilst much that did not work can be boiled down to the experimental wandering of me and my peers.

As a research group as a whole but also as an individual researcher, I feel greatly indebted to our staff of technicians. In a way, I think the fact that not everyone recognizes how much you help out the group is a mere indication of just how good you are: the days of people constantly worrying about individual set-ups is a thing of the past. Most of the problems that do occur I often find to be the result of the fact that the decision making (as well as basic planning) is not left to you guys in the first place. **Jelle**, **Siebe** and **Mark**, you have helped us realize a new lab in which I am happy to leave my colleagues behind, and **Remco**, without your help neither could we have kept the older systems running. **Raymond**, you already

know that many students, myself included, would not have been able to accurately measure a resistor without your help, let alone realize world-class research. The vast amount of accrued knowledge between you, **Raymond**, **Marijn** and **Hans** is equaled only by the elegance with which you manage to thrive in such a hectic and needy group of young researchers.

Thanks also to **Vincent**, **Xiao** and **Sankar** for the sometimes much needed theory support. It is always a pleasure to find oneself working together efficiently and successfully with people with a different view, and this has definitely been the case with you.

For more than just keeping up with my power scream and the unsavory smell of my climbing shoes, I consider you, **Peter** and **Norbert**, to have become close friends. Apart from forming a power team in your own lab, your amicability, broad interests and quick wits means that also individually and outside the spheres of academia, you both present a force to be reckoned with.

Much has changed in these wings of the physics building since I started here. **LeoK**, you have made quantum in Delft continuously move forward, creating a dynamic that I feel fits you better than the isolationism that characterizes many other teams in academia, a push that is never easy but nonetheless commendable. What's in a name - I see a similar drive in you, **LeoDC**, creating a fast-moving and result-driven dynamic that propels all of Qutech labs forward. Ambition is also abundant in your case, **Ronald**, something which I am sure means that I will keep coming across many press releases of your group in the future. I furthermore would like to wish the best of luck to the new group leaders at Qutech, in particular **Giordiano**, whose relaxedness adds a brilliant Italian-Australian vibe to the spin qubit team, and **Atilla**, whom I still remember being startled to see being flipped like a burger in the bottom bunk of our shared bunk bed in the middle of the night during my first QT uitje. **Menno**, thanks a lot for many an interesting hallway conversation and in your organizational efforts in the spin qubit team as a whole. I am sure you will keep finding creative ways to mix interesting and open physics questions with the long-term view inherent to Qutech's activities.

Foremost, however, let me thank you, **Lieven**. Your leadership style combines a good judgment with a profound trust in those that work for you in a most inspirational manner. It has often amazed me how you can join a discussion on any topic without the detailed look of those of us laboring in the mud, and still get any of us to start focusing on the relevant items every time. I have learned a lot from your strive to have us understand everything to the point where we can explain it as simple as possible, and am most grateful for the opportunity to have been a part of your team these past years.

On to those who have kept me sane in these long years laboring in high school physics class and physics departments. To my **Bernardinus** buds, thanks for everything from childish fun to adolescent joy, but also for being sufficiently rowdy to have had me placed separate from you in maths class. Turns out the blond girl I got placed next to and I had a lot in common.. My friends of **198+**, you will be glad to hear that I am finally leaving these same gray corridors we first entered together in '09 behind - it has been a great ride! Thanks also to my dear friends **Diederik**, whom I wish all the success in the world in becoming a real-life dr, and **Lars** - it is my honor to have you join the defense as my paranymph. You are unquestionably bright and despite your resolute ambition and accompanying seriousness in many matters, you never fail to appreciate my often simple and rather cynically harsh jokes on a bunch of those. To my **MASt** physics buds at Cambridge, I will never forget our hectic but joint preparation for the general physics paper on an undergraduate program we did not attend, nor our unbridled relief of finishing such ordeals relatively unscathed. To my Wolfson crew of **Hilary**, **John** and **Tair**, I promise that even though we can no longer use the excuse of academic conferences to go visit one another, we will still find ways to keep in touch, as you guys are the best. And to the Utrecht Sunday morning **boulder crew**, I look forward to the prospect of sharing with you many more a lazy indoor climb or outdoors adventure.

Verder heb ik het goede geluk een **familie** te hebben die me loslaat, maar waar ik altijd op terug kan vallen. Daartoe beschouw ik ook jullie, **Jan**, **Annemieke** en **JW**. Jullie hebben me met open armen een onderdeel laten worden van jullie familie, geen vanzelfsprekendheid maar iets waarvoor ik erg dankbaar ben. En lieve **Hans** en **Tiny**, ondanks de fysieke afstand van de laatste jaren en het geringe contact, houden jullie altijd een speciale plek in mijn hart.

Chey, je bent een kanjer. Je hebt een hoeveelheid energie en een wilskracht die je niet bij veel mensen ziet, en bent er altijd voor me wanneer ik je nodig heb. Ik heb geluk met jou als broer.

Marij, jij en **Hub** hebben me van huis uit alles meegegeven wat ik nodig heb om mijn eigen weg te bewandelen. Je hebt me altijd de vrijheid en het vertrouwen gegeven om mijn dromen na te streven, een vertrouwen dat ik mijn hele leven mee zal nemen. Ik zal jullie trots blijven maken.

Lieve **Heleen**, ondanks het feit dat je mijn concentratie bij de wiskundeles enigszins teniet hebt gedaan, sta ik hier nu toch, voor geen klein deel dankzij jou. Want jij bent het die me vrolijk maakt na elke lange dag, die me naar de toekomst laat kijken en die mijn leven zin geeft. Je bent prachtig, gepassioneerd, ontdekkend, eigenwijs en intelligent, en houdt me altijd een spiegel voor wanneer dat nodig is. Ik hou zielsveel van jou.

List of Publications

5. *Capacitance spectroscopy of gate-defined electronic lattices*
   T. Hensgens[*], U. Mukhopadhyay[*], P. Barthelemy[*], R.F.L. Vermeulen, R.N. Schouten, S. Fallahi, G.C. Gardner, C. Reichl, W. Wegscheider, M.J. Manfra and L.M.K. Vandersypen,
   arXiv:1709.09058

4. *Een quantumschaalmodel*
   T. Hensgens
   Nederlands Tijdschift voor Natuurkunde **83**, 360-363 (2017)

3. *Quantum simulation of a Fermi-Hubbard model using a semiconductor quantum dot array*
   T. Hensgens, T. Fujita, L. Janssen, Xiao Li, C.J. Van Diepen, C. Reichl, W. Wegscheider, S. Das Sarma and L.M.K. Vandersypen,
   Nature **548**, 70-73 (2017)

2. *Double-stranded RNA under force and torque: Similarities to and striking differences from double-stranded DNA*
   J. Lipfert, G.M. Skinner, J.M. Keegstra, **T. Hensgens**, T. Jager, D. Dulin, M. Köber, Z. Yu, S.P. Donkers, F. Chou, R. Das and N.H. Dekker,
   Proc. Natl. Acad. Sci. **111**, 15408-15413 (2014)

1. *A force calibration standard for magnetic tweezers*
   Z. Yu, D. Dulin, J. Cnossen, M. Köber, M. van Oene, O. Ordu, B.A. Berghuis, **T. Hensgens**, J. Lipfert and N.H. Dekker,
   Rev. Sci. Instrum. **85**, 123114 (2014)

[*] These authors contributed equally.

Toivo Hensgens

May 6th, 1992 - Heerlen, The Netherlands

2003–2009 **Secondary School** (cum laude)
Bernardinuscollege Heerlen

2009–2012 **Bachelor of Science in Applied Physics** (cum laude)
Delft University of Technology

Undergraduate research project in the group of prof. dr. N.H. Dekker,
"The ABC of dsRNA and beyond: Elastic Properties and Structural Transitions under Force and Torque"

2012–2013 **Master of Advanced Studies in Experimental and Theoretical Physics** (with distinction)
University of Cambridge

Graduate research project in the group of dr. J.W.A. Robinson,
"All-Oxide Manganite/Cuprate Superconducting Spin-Valve"

Awarded the *Wolfson College Jennings Prize* and the *Cavendish Laboratory M.A.St. Prize*

2013–2017 **PhD in Experimental Quantum Physics**
Delft University of Technology

Doctoral research in the group of prof. dr. ir. L.M.K. Vandersypen,
"Emulating Fermi-Hubbard physics with quantum dots"